The Integument of Water-walking Arthropods: Form and Function

John W.M. Bush[a], David L. Hu[b] and Manu Prakash[c]

[a]*Department of Mathematics, MIT, Cambridge, MA, USA*

[b]*The Courant Institute of Mathematical Sciences, NYU, New York, NY, USA*

[c]*Center for Bits and Atoms, MIT, Cambridge, MA, USA*

ADVANCES IN INSECT PHYSIOLOGY VOL. 34
ISBN 978-0-12-373714-4
DOI: 10.1016/S0065-2806(07)34003-4

Abstract

We develop a coherent view of the form and function of the integument of water-walking insects and spiders by reviewing biological work on the subject in light of recent advances in surface science. Particular attention is given to understanding the complex nature of the interaction between water-walking arthropods and the air–water surface. We begin with a discussion of the fundamental principles of surface tension and the wetting of a solid by a fluid. These basic concepts are applied to rationalize the form of various body parts of water-walking arthropods according to their function. Particular attention is given to the influence of surface roughness on water-repellency, a critical feature of water-walkers that enables them to avoid entrapment at the interface, survive the impact of raindrops and breathe if submerged. The dynamic roles of specific surface features in thrust generation, drag reduction and anchoring on the free surface are considered. New imaging techniques that promise important insights into this class of problems are discussed. Finally, we highlight the interplay between the biology, physics and engineering communities responsible for the rapid recent advances in the biomimetic design of smart, water-repellent surfaces.

1 Introduction

Textured surfaces are known to play an important dynamical role for a number of swimmers and fliers (Bushnell and Moore, 1991; Fish, 1998, 2006); however, no creature depends more critically on its surface structure than do water-walking arthropods. Their surface roughness is critical in maintaining water-repellency, generating thrust as they strike the water surface, reducing drag as they glide across the surface and generating buoyancy and permitting respiration when they are submerged.

Water-repellency is generated in the same way in both plant and animal kingdoms (on plant leaves, animal fur and bird feathers) by presenting a textured waxy or oily surface that increases the energetic cost of wetting and so discourages fluid–solid contact. Lotus leaves are known to be both water-repellent and self-cleaning owing to their complex surface structure (Barthlott and Neinhuis, 1997; Neinhuis and Barthlott, 1997). Their surface is characterized by roughness on two scales (the smallest being sub-micron) and a waxy coating, which together render it superhydrophobic. When water drops strike it, instead of sticking, they roll off, taking with them any dust that might have collected on the plant. The rough piliferous integument of water-walking arthropods plays a similar role in maintaining water-repellency. Moreover, we shall see that it also plays a critical dynamic role in both thrust generation and drag reduction.

The interaction of fluid interfaces and solids arises in a wide range of problems in biology and industry. Much of the early work on fluid–solid interactions was motivated by the desire to optimize insecticides designed to coat their insect target while leaving the plant unharmed (Moore, 1921; English, 1928; Wilcoxon and Hartzell, 1931; O'Kane *et al.*, 1932; Hoskins, 1940; Pal, 1951), a task made all the more challenging by the fact that the two coverings are often virtually identical (e.g. Hadley, 1981; Farrell and Mitter, 1990; Barthlott *et al.*, 1994). Subsequently, the subject was reconsidered with a view to developing water-repellent textiles (Cassie, 1944; Cassie and Baxter, 1945; Bartell *et al.*, 1948). Most recently, the subtle water-proofing strategies of plants and insects have provided important guidance in the rapid advances in the development of superhydrophobic surfaces (Feng *et al.*, 2002; Wagner *et al.*, 2003; Callies and Quéré, 2005; Furstner *et al.*, 2005; Mock *et al.*, 2005; Liu *et al.*, 2006; Feng and Jiang, 2006). This new class of engineered biomimetic surfaces are finding a wealth of applications including self-cleaning, water-repellent windows (Blossey, 2003), corrosion protection (Kousik *et al.*, 2001), drag reduction (Ou *et al.*, 2004; Choi and Kim, 2006; Choi *et al.*, 2006), clean inkjet nozzle release (Yi and Kim, 2004) and devices for underwater breathing (Shirtcliffe *et al.*, 2006).

Water-walking arthropods have been evolving for over 100 million years, and so from a purely mechanical perspective represent a highly adapted, robust system. There are over 1200 species of water-walking insects and spiders (Andersen, 1982; Fig. 1) each of which depends critically on its ability to manipulate and control the air–water interface. Propulsive forces may be generated by striking or deforming the free

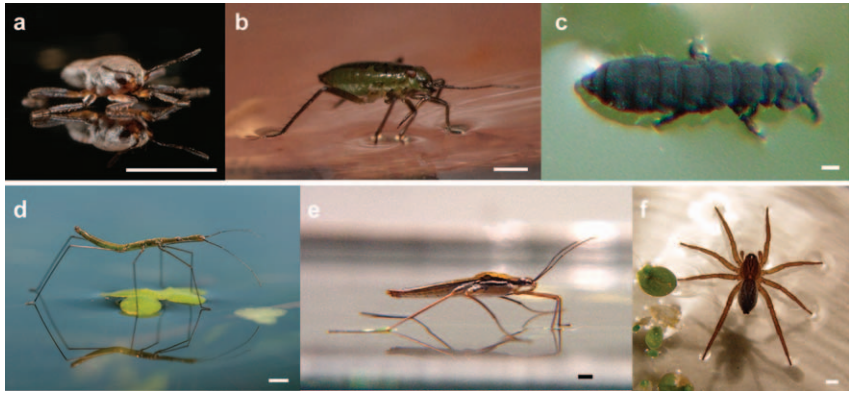

FIG. 1 Common water-walking arthropods, ordered roughly by size. (a) Broad-shouldered water strider *Microvelia*, (b) water treader *Mesovelia*, (c) springtail *Anurida maritima*, (d) water measurer *Hydrometra stagnorum*, (e) water strider *Gerris* and (f) fisher spider *Dolomedes triton*. Scale bars, 1 mm.

surface or by chemically altering the surface tension (Bush and Hu, 2006; see Section 3.3). The ability to manipulate the free surface depends critically on the creature's wetting properties; for example, without a water-repellent coating, insects cannot be sustained atop the interface by surface tension forces, but instead pass through it and sink. The vital role of the wetting properties of water-walking insects has long been recognized (Imms, 1906; Brocher, 1910; Hungerford, 1919; Baudoin, 1955, 1976). The goal of this review is to develop a coherent view of the form and function of the surface structure of water-walking arthropods by reviewing biological work on the subject in light of recent advances in surface science.

The arthropod integument has received attention from various fields of biology. Entomological material scientists have focused on the chemical structure of the surface layer, or cuticle (e.g. Vincent and Wegst, 2004); developmental entomologists have considered the changes prompted by growth of the cuticle (e.g. Wigglesworth, 1950, 1979) and comparative entomologists have contrasted the water-repellent properties of terrestrial, aquatic, and semi-aquatic arthropods (Heckman, 1983; Stratton *et al.*, 2004b; Perez-Goodwyn, 2007). This article is written from the perspective of a fluid mechanician rather than a biologist, but with a biological audience in mind. We shall thus devote considerable effort to reviewing the fundamental physical principles required to understand the static and dynamic interaction between water-walking arthropods and the free surface. Given our limited backgrounds in biology, we shall try to avoid the use (and probable misuse) of all but the most basic biological jargon, and to suppress any discussion of the ecology or philogeny of water-walkers. Instead, we take a purely mechanistic view of the subject of water-walking arthropods, and hope to highlight outstanding physical problems required to rationalize their existence and persistence at the interface.

In Section 2, we review fundamental concepts of surface tension and discuss its importance in both the statics and dynamics of water-walking arthropods. In Section 3, we discuss the fundamentals of wetting, giving particular attention to the impact of surface roughness on water-repellency. In Section 4, we review biological studies of the cuticle of water-walking arthropods. In Section 5, we attempt to understand the composition, morphology and stability of the cuticle on the basis of principles discussed in Sections 2 and 3. In Section 6, we review new imaging techniques that promise novel insights into the interaction between water-walking arthropods and the free surface.

2 Surface tension

We begin with a brief introduction to surface tension, then proceed to consider the capillary forces generated by objects residing at rest at an

air–water interface. In Section 2.1, we describe the role of surface tension in the weight support of small floating bodies. In Section 2.2, we describe the lateral forces that arise between two adjacent objects at a free surface. In Section 2.3, we demonstrate that the propulsive force of water-walking arthropods is typically the contact force generated by the driving leg striking the free surface.

Discussions of the molecular origins of surface tension may be found in Rowlinson and Widom (1982), Israelachvili (1992) and de Gennes *et al.* (2003). Molecules in a fluid feel a mutual attraction. Let us consider the free surface between air and water. A water molecule in the bulk is surrounded by attractive neighbours, while a molecule at the surface is attracted by a reduced number of neighbours and so in an energetically unfavourable state. The creation of new surface is thus energetically costly, and a fluid system will act to minimize its surface area. It is thus that small fluid bodies tend to evolve into spheres; for example, a thin water jet emerging from the kitchen tap will generally pinch off into spherical drops to minimize the total surface area (Plateau, 1873; Rayleigh, 1879).

If U is the total cohesive energy per molecule, then a molecule at a flat surface will lose $U/2$. Surface tension is a direct measure of this energy loss per unit area of surface. If the characteristic molecular dimension is R, its area scales as R^2; thus the surface tension $\sigma \sim U/(2R^2)$. Note that surface tension increases as the intermolecular attraction increases and the molecular size decreases. Surface tension σ has the units of force/length or equivalently energy/area. To create a surface of area A thus requires an energy σA. For a clean air–water interface, $\sigma = 72$ dynes cm^{-1}. Impurities will generally act to reduce the surface tension, so that in ponds or other standing bodies of water, $\sigma \sim 62 - 70$ dynes cm^{-1}. An exception to this rule is salt, which may act to increase surface tension slightly: at sea, surface tensions as high as $\sigma \sim 72$ dynes cm^{-1} have been reported (White, 1994).

Surface tension is a force per unit length acting everywhere tangent to the free surface. When an interface adjoins a solid, it applies a contact force per unit length σ along the contact line in a direction tangent to the interface. It is precisely these forces that enable water-walking arthropods to reside at rest on the free surface: by deforming the planar free surface, they generate contact forces that bear their weight (Fig. 2a). The influence of surface tension on an initially planar interface is two-fold. First, it resists the distortion of the interface and the associated increase in surface energy. This resistance may be expressed as a jump in normal stress (force/area) across an interface, termed the curvature pressure: $P_c = \sigma(R_1^{-1} + R_2^{-1})$, where R_1 and R_2 are the principle radii of curvature of the deformed interface (de Gennes *et al.*, 2003). Inside a spherical drop of radius R the pressure is higher than that outside by an amount $2\sigma/R$; hence the vigorous popping of surfacing champagne bubbles. Figure 3 illustrates a *Mesovelia*

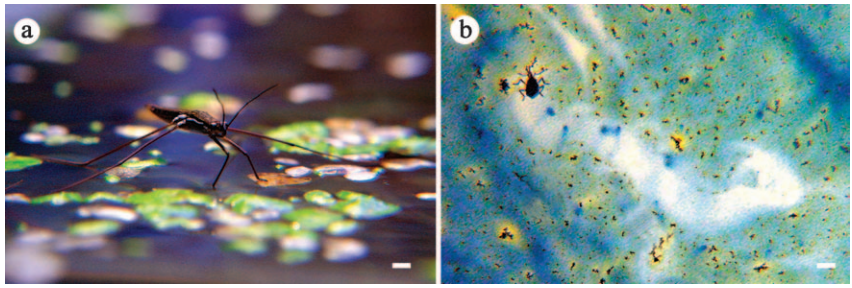

FIG. 2 Surface tension may be used by water-walkers for both weight support and propulsion. (a) A water strider's weight is supported by the curvature or contact forces generated by its deforming the free surface. (b) By releasing surfactants onto the free surface, *Microvelia* generates surface tension gradients that propel it forward. The surfactants reduce the surface tension, causing surface divergent motions that sweep the surface clear of the blue dye. Scale bars, 1 mm.

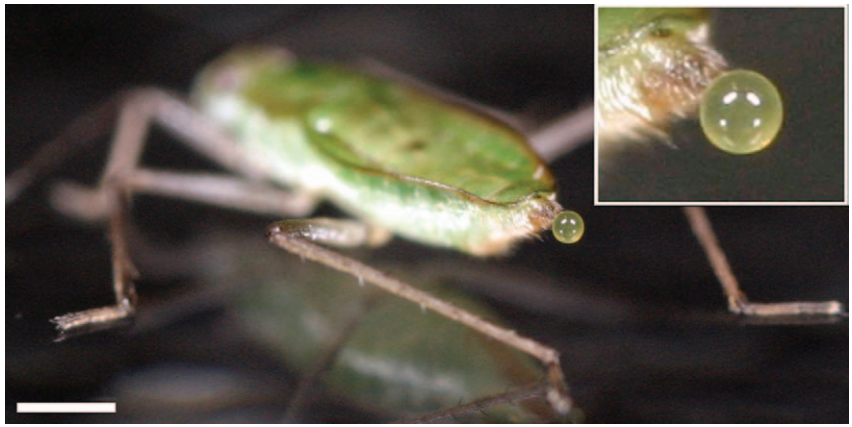

FIG. 3 Care must be taken by semi-aquatic insects to excrete liquid without compromising their water-repellency. Here, fluid is excreted from the anus of *Mesovelia*. A drop of size $R \sim 0.3$ mm requires an excess pressure of $P \sim 2\sigma/R = 0.004$ atm. Scale bar, 1 mm.

excreting liquid waste: the size of the droplet indicates excess extrusion pressures on the order of 0.004 atm.

Insofar as normal stresses are concerned, the surface tension makes the air–water interface behave like a trampoline. The second physical effect of surface tension accompanies gradients in surface tension, as may be generated by gradients in temperature or surface chemistry. Surface tension gradients correspond to tangential stresses at a free surface, and so necessarily drive flows known as Marangoni flows (Scriven and Sternling, 1970).

If an object floats on a free surface, and if the surface tension is diminished on one side relative to the other, the body will be propelled in the direction of increasing surface tension. This means of propulsion, termed Marangoni propulsion (Bush and Hu, 2006), is used as an escape mechanism by a number of water-walking insects, as well as beetles and terrestrial insects that accidentally fall onto the water surface (Fig. 2b). By releasing a lipid that reduces the surface tension, such creatures can propel themselves forward at peak speeds of order $20\,\mathrm{cm\,s^{-1}}$ (Schildknecht, 1976). When a pine needle falls into a lake or pond, it is similarly propelled across the surface since the resin at its base decreases the local surface tension.

While the world of humans is dominated by gravity, surface tension dominates that of water-walking arthropods. The relative magnitude of gravitational and capillary forces is made clear by considering a fluid drop of radius a placed on a substrate. Gravity acts to flatten the drop into a planar film, while surface tension acts to maintain its sphericity. The relative magnitudes of these two competing effects may be expressed as the ratio of the hydrostatic and curvature pressures, termed the Bond number: $Bo = \rho g a^2/\sigma$. These two pressures are comparable when $Bo = 1$, which arises at a length scale corresponding to the capillary length: $\ell_c = (\sigma/(\rho g))^{1/2}$. For an air–water surface, for example, $\sigma \sim 70$ dynes cm^{-1}, $\rho = 1\,\mathrm{g\,cc^{-1}}$ and $g = 980\,\mathrm{cm\,s^{-2}}$, so that $\ell_c \sim 2$ mm. Bodies of water in air are dominated by the influence of surface tension provided they are smaller than the capillary length. The capillary length prescribes the maximum size of raindrops, and of pendant drops that may hang from a ceiling. Note that as a fluid system becomes progressively smaller, surface tension becomes progressively more important relative to gravity.

Surfactants, or surface-active reagents, are molecules that have an affinity for interfaces; common examples include soaps and lipids. Owing to their molecular structure (often a hydrophylic head and hydrophobic tail), they find it energetically favourable to reside at the free surface. Their presence reduces the surface tension; consequently, gradients in surfactant concentration Γ result in surface tension gradients and concomitant Marangoni flows (Fig. 2b). There are many different types of surfactants, some of which are insoluble (and so remain at the interface), others of which are soluble in the suspending fluid and so diffuse into the bulk. Most organic materials are surface active; therefore, surfactants are ubiquitous in the natural aqueous environment. For a wide range of common surfactants, surface tension is a monotonically decreasing function of Γ until a critical concentration is achieved, beyond which σ remains constant (de Gennes *et al.*, 2003). Surfactants rarely reduce the surface tension of water to less than 30 dynes cm^{-1}, although superwetting agents have recently been introduced by Dow Corning that reduce it to 23 dynes cm^{-1}. It is noteworthy that the peril posed by surfactants to water-walking creatures does not result from the reduction in surface tension and so

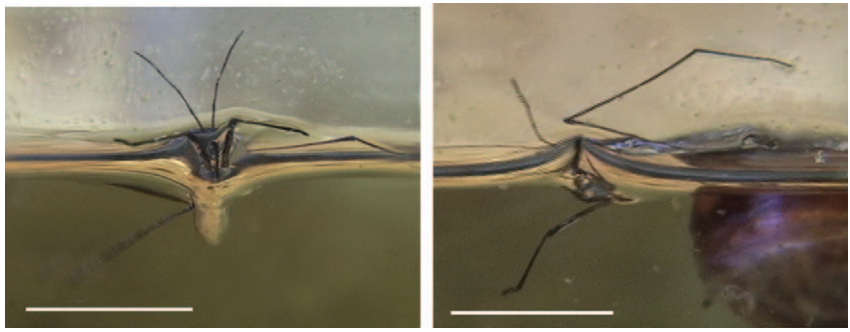

FIG. 4 Surface contamination presents a grave risk for water-walking arthropods. Here, a drop of soap on the water surface destroys the water-repellency of the water strider: water impregnates its hair layer, causing it to sink. Scale bars, 1 cm.

weight-bearing potential of the free surface: as we shall demonstrate in Section 2.1, the great majority of water-walking arthropods maintain a large margin of safety. Rather, surfactants such as soap or petroleum are a danger owing to their tendency to drastically alter the wetting properties of the insect cuticle (Sections 3 and 4), eliminating their water-repellency and so allowing them to pass through the interface. The perilous effect of a commercial soap on a water strider is evident in Fig. 4. Brown (1966) discusses the deleterious effects of surfactants on stream invertebrates.

2.1 WEIGHT SUPPORT

Archimedes principle states that the buoyancy force on a floating object is equal to the weight of fluid displaced by that object. It follows that bodies heavier than water sink, and bodies lighter than water float with a submerged volume prescribed by the relative magnitudes of the body and fluid densities. Water-walking arthropods are generally more dense than water, and so would sink unless sustained by surface tension forces. The statics of small floating bodies is well understood (Mansfield *et al.*, 1997; Keller, 1998; Vella *et al.*, 2006a) and may be applied directly to understand the vertical force balance on a creature residing at rest on the air–water surface.

Consider a body with density greater than that of water $\rho_b > \rho$ and mass M floating at the interface (Fig. 5a). Its borders will generally be adjoined by a meniscus, details of which will depend on the wetting properties of the solid, but whose lateral extent will correspond to the capillary length $\ell_c = (\sigma/(\rho g))^{1/2} \approx 2$ mm. The body weight must be supported by some combination of the buoyancy force, F_b, and contact force, F_c: $Mg = F_b + F_c$. The buoyancy force is deduced by integrating the hydrostatic pressure

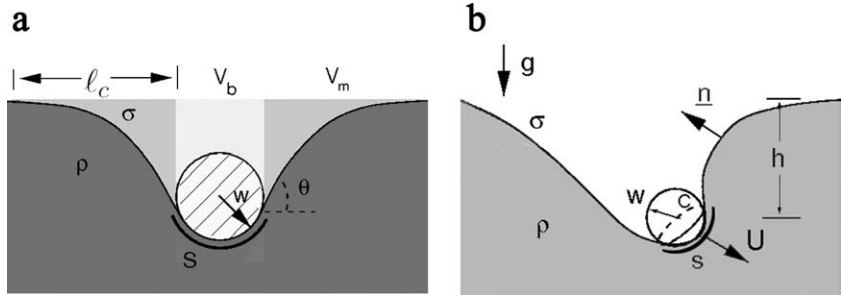

FIG. 5 Schematic illustrations of the leg of a water-walking creature in both static and dynamic states. n denotes the normal to the surface and σ the surface tension. (a) We consider the forces on a floating body of characteristic length w with a contact line C and wetted area S. Its weight is supported by a combination of buoyancy and curvature forces, whose magnitudes are prescribed by the weights of the fluid volumes displaced inside and outside the contact line, respectively V_b and V_m. (b) The body strikes the free surface obliquely at a speed U. Its motion is resisted by some combination of the forces enumerated in Eq. (2).

$p = \rho g z$ over the body surface S in contact with the water, and so is equal to the weight of fluid V_b displaced above the body and inside the contact line C. The contact force may be deduced by integrating the surface tension force along the contact line: for a two-dimensional (2D) body (Fig. 5a), the vertical contact force per unit length is $2\sigma \sin\theta$.

Mansfield *et al.* (1997) and Keller (1998) demonstrate that the contact force is precisely equal to the weight of fluid displaced outside the contact line, thereby generalizing Archimedes principle to the case where surface tension forces are important: the force acting on a floating body is equal to the total weight of the fluid displaced. The buoyancy and contact forces are equal to the weights of the fluid displaced by the meniscus, respectively, in- and outside the contact line. For long thin bodies such as insect legs, their relative magnitudes are thus prescribed by the ratio of the characteristic body size w to the capillary length ℓ_c.

$$\frac{F_b}{F_c} \sim \frac{V_b}{V_m} \sim \frac{w}{\ell_c} \tag{1}$$

Bodies small relative to the capillary length are supported primarily by surface tension and can be sustained even when they are more dense than the underlying fluid. As the leg diameter of most water-walking arthropods is $\sim 100\,\mu m \ll \ell_c$, one sees that they rely primarily on surface tension for their support: by deforming the free surface like a trampoline, they generate tensile forces that bear their weight.

The cuticle of water-walking arthopods significantly complicates the nature of their interaction with the free surface. In particular, the contact lines do not run smoothly along the tarsi in contact with the free surface;

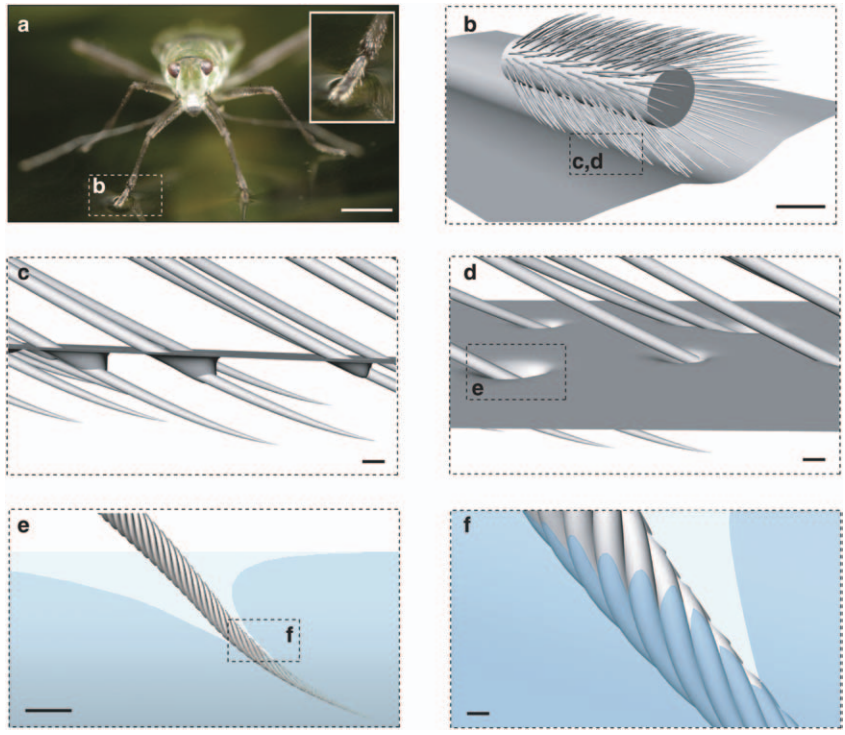

FIG. 6 The contact between the water treader *Mesovelia* and the free surface. (a) *Mesovelia* supports its weight by deforming the surface. Scale bar, 1 mm. (b) A schematic of a hairy leg. Scale bar, 100 μm. (c–d) Further zooms of individual hairs penetrating the surface. Scale bar, 1 μm. (e) A single hair penetrating the free surface. Scale bar, 1 μm. (f) The hairs are covered in nanogrooves that trap air when the hair is submerged. Scale bar, 0.1 μm.

rather, they correspond to loops along the individual hairs abutting the free surface (Fig. 6). Nevertheless, one can gain some insight by crudely thinking of their having contact with the free surface along the entire contact length P of their support legs. One can then define the maximum supporting curvature force available to such a creature as $F_s \sim \sigma P$. In Fig. 7, we plot the relation between F_s and the weight $F_g = Mg$ for various water-walking arthropods. Creatures above the line $\mathrm{Ba} = F_g/F_s = 1$ may be statically supported by surface tension; those below cannot. Assuming that the insects are isometric, with body proportions independent of their size (McMahon and Bonner, 1985), one anticipates that $M \sim L^3$ and $P \sim L$, so that $\mathrm{Ba} \sim L^2$ (Baudoin, 1955). The best fit for Fig. 7 is $F_s \sim F_g^{0.46}$, which indicates $\mathrm{Ba} = F_g/F_s \sim F_g^{0.5} \sim L^{3/2}$. This slightly weaker dependence of Ba on L may suggest that water-walker's legs grow proportionally longer

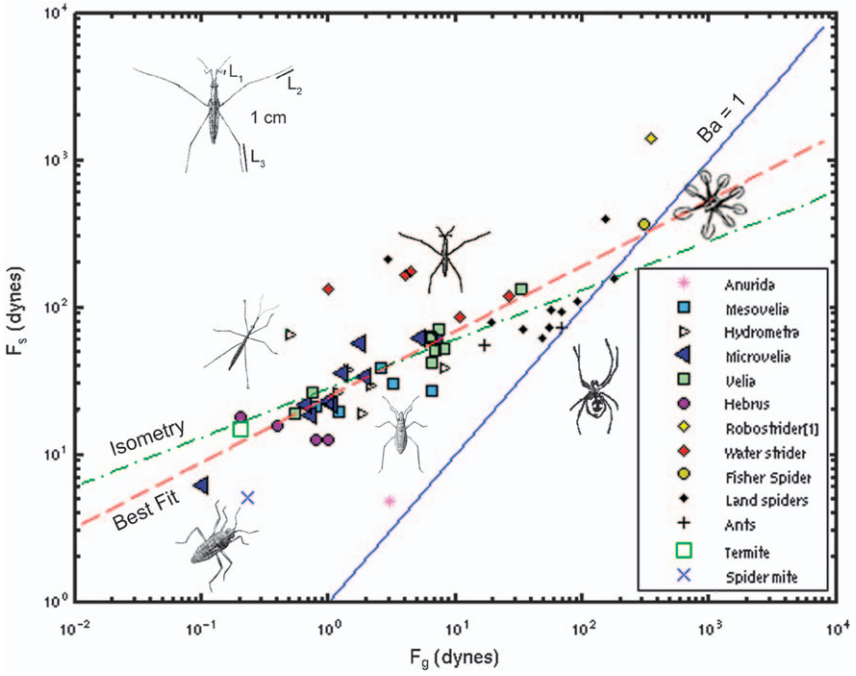

FIG. 7 The relation between the weight, $F_g = Mg$, and the maximum supporting surface tension force, $F_s = \sigma P$, for water-walking insects and spiders, where the contact perimeter $P = 4(L_1 + L_2 + L_3)$ (see inset top left). All water-walking arthropods fall above the line $Ba = 1$ and so may reside at rest on the water surface. Their margin of safety generally decreases with body size. Note that many terrestrial insects (such as the ants and spiders included here) can also be supported by surface tension if they are sufficiently water-repellent. Isometry would suggest $F_s \sim F_g^{1/3}$, a relation indicated by the dash-dotted line. The best fit to the data is given by $F_s \sim F_g^{0.46}$ (dashed line). Data reprinted from Hu and Bush (2008a) and Hu, Chan and Bush (2003).

with increasing body size; alternatively, it may indicate the significance of the microscale topology of the insect cuticle on weight support.

It is important to note that the surface deformation will in general depend on the surface structure of the floating object. For a smooth object, the curvature force will depend explicitly on the contact angle (see Section 3.1; Vella *et al.*, 2006a). Water-walking arthropods are covered in a complex layer of hair that traps air, thereby increasing the volume of fluid displaced and the concomitant force of buoyancy. As we shall see in Section 4, this trapped air layer may be a substantial fraction of the leg volume and so contribute significantly to the force of buoyancy (Fig. 6). Feng *et al.* (2007) examine the surface distortion generated by depressing a water strider leg. They found that, owing to its high contact angle, the leg was capable of

reaching depths as high as 4.8 mm before breaking through. Matsuda *et al.* (1985) used a shearing interferometer to measure the free surface deflections generated by stationary water striders, and found distortions of order 100 μm. The new imaging techniques discussed in Section 6 will provide new insight into the floatation of roughened bodies.

2.2 CAPILLARY ATTRACTION

An object floating at a free surface may be subject not only to vertical but also lateral forces. Fluid mechanicians (Nicolson, 1949; Gifford and Scriven, 1971; Chan *et al.*, 1981; Mansfield *et al.*, 1997; Kralchevsky and Denkov, 2001) have long known that lateral capillary forces exist between small floating objects, an effect responsible for the formation of bubble rafts in champagne and the clumping of Cheerios in a cereal bowl (Vella and Mahadevan, 2005). Recently, such capillary forces have been recognized as a means by which to promote self-assembly of microstructures at a free surface (Gryzbowski *et al.*, 2001; Whitesides and Grzybowski, 2002; Manoharan *et al.*, 2003; Lauga and Brenner, 2004; Zeng *et al.*, 2006). Understanding such forces is critical for rationalizing the ability of certain insects to propel themselves up menisci by surface deformation (Baudoin, 1955; Hu and Bush, 2005) and for assessing the stability of insect cuticle (Crisp, 1950).

Consider two objects floating on the free surface (Fig. 8). The total energy of the system as a function of distance of separation, x, can be expressed as the sum of the gravitational potential energy and the surface energy $\sigma A(x)$, where A is the difference in areas of the deformed and undeformed surfaces.

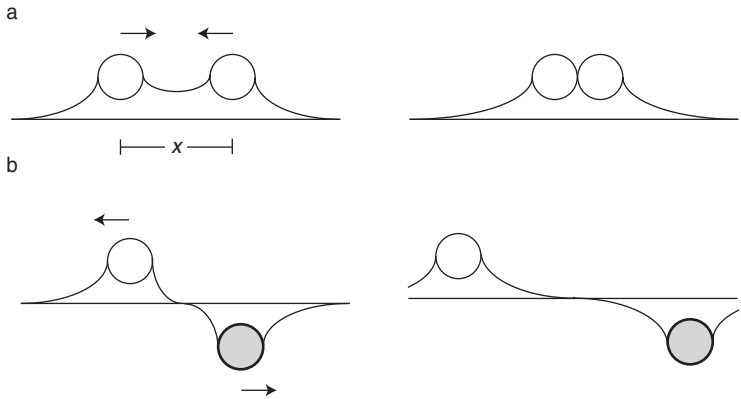

FIG. 8 Lateral capillary forces between small floating bodies initially separated by a distance x. (a) Two floating bubbles generate like-signed menisci and so are mutually attracted. (b) Two floating objects with opposite buoyancy generate opposite-signed menisci and so are mutually repelled. The range of these capillary forces is limited to the capillary length, $\ell_c \sim 3$ mm for an air–water interface.

If this total energy decreases with decreasing x, then the bodies will be subject to an attractive force. Such is the case when both bodies have the same density anomaly, that is, for a pair of bubbles (Fig. 8a) or for two relatively heavy particles. Conversely, if the total energy increases with decreasing x, a repulsive force is felt. Such is the case between two floating objects with opposite density anomaly (Fig. 8b). The range of such forces is prescribed by the lateral extent of the surface deformation, specifically, the capillary length. Their magnitude is prescribed by the rate of change of total energy (surface plus gravitational potential energy) with separation distance. Finally, we note that such forces also depend not only on the buoyancy of the objects, but on their wettability (Whitesides and Grzybowski, 2002), a matter to be discussed in Section 3.

Baudoin (1955) first reported that some insects may climb menisci without moving their limbs. Wetting creatures, such as the beetle larve, are circumscribed by a contact line; consequently, by arching their backs, they generate menisci at their nose and tail and an associated lateral capillary force that drives them up menisci (Fig. 9a). Their ascent is best understood in terms of energetics: if the surface energy they create through arching their backs exceeds the gravitational potential energy gained through their

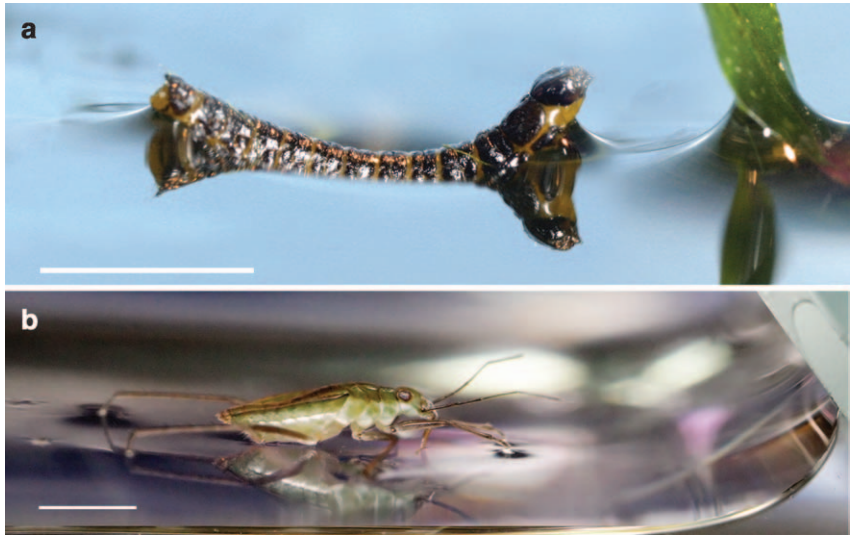

FIG. 9 Meniscus climbing by wetting and non-wetting insects. (a) The beetle larva *Pyrrhalta* is circumscribed by a contact line and so may generate menisci simply by arching its back. The resulting lateral capillary force (Fig. 8a) propels it towards the leaf. (b) The water treader *Mesovelia* has a water-repellent body, but uses the hydrophilic claws (or ungui) at its leg tips to clasp the free surface (see Figs. 22 and 35), and so generate the capillary force that drives it up the meniscus at right Hu and Bush (2005). Scale bars, 3 mm.

ascent, they will be drawn up the meniscus by capillary forces (Hu and Bush, 2005). Baudoin (1955) performed a simple experiment to demonstrate that floating metal rectangles, when arched slightly, will ascend menisci just as do wetting climbers. The manner in which water-walking insects, which are generally water-repellent, are able to clasp the free surface and so climb menisci will be discussed in Section 5.3.

The lateral capillary forces between bodies at an interface are also of critical importance in the maintenance of the water-repellency of water-walkers. As we shall see in Section 4.3, an air layer is maintained between the insect surface and the water by cuticle hairs lying roughly tangent to the interface. Provided these hairs deform the interface, there will be a capillary force acting between them. Crisp (1950) pointed out that such forces, if not matched by the hair's resistance to bending, may destabilize the hair layer: the clumping of hairs in one region will necessarily lead to bald patches into which water more readily intrudes. The elastocapillary stability of insect cuticle at an interface will be further considered in Section 4.3.

2.3 PROPULSION

The hydrodynamics of water-walking creatures were reviewed in Bush and Hu (2006), where the relevant equations are presented and discussed in greater detail. They present the first dynamic classification of all water-walking creatures by grouping them according to their primary source of thrust. Consider a smooth object of characteristic scale w striking the free surface above water (density ρ, dynamic viscosity μ, kinematic viscosity $\nu = \mu/\rho$, surface tension σ) at an impact speed U (Fig. 5b). Its motion will be resisted by some combination of hydrostatic, contact and hydrodynamic forces. The buoyancy force arises from the hydrostatic pressure (that increases with depth z as $\rho g z$) acting on the wall of the cavity against which the water-walker strokes (Glasheen and McMahon, 1996a,b). Contact forces act along the contact lines and have characteristic magnitude σw. The form drag results from the dynamic pressure generated by the impact, that scales as ρU^2. An estimate for the viscous drag is obtained by integrating a characteristic viscous stress $\mu U/w$ over the contact area $A \sim w^2$ of the body. Finally, an added mass force arises from the acceleration of fluid by the impacting body (Daniel, 1984; Glasheen and McMahon, 1996c).

The net force exerted on the impacting body may thus be roughly expressed as

$$|\mathrm{F}| \sim \underbrace{\rho U^2 w^2}_{\text{form drag}} + \underbrace{\rho g h w^2}_{\text{buoyancy}} + \underbrace{\rho V \frac{dU}{dt}}_{\text{added mass}} + \underbrace{\mu U w}_{\text{viscosity}} + \underbrace{\sigma w}_{\text{curvature}} - \underbrace{\nabla \sigma w^2}_{\text{Marangoni}} \tag{2}$$

The relative magnitudes of the six force components are prescribed by five dimensionless groups, the Reynolds *Re*, Weber *We*, Bond *Bo*, Strouhal *St* and Marangoni *Ma* numbers, defined, respectively, by

$$Re = \frac{Uw}{\nu} = \frac{\text{inertia}}{\text{viscous}} \qquad We = \frac{\rho U^2 w}{\sigma} = \frac{\text{inertia}}{\text{curvature}}$$

$$Bo = \frac{\rho g h}{\sigma / w} = \frac{\text{buoyancy}}{\text{curvature}} \qquad St = \frac{fw}{U} = \frac{\text{added mass}}{\text{inertia}}$$

$$Ma = \frac{\nabla \sigma}{\sigma / w} = \frac{\text{Marangoni}}{\text{curvature}}$$

The magnitudes of these dimensionless groups for representative water-walkers were assessed by Bush and Hu (2006), who show that the motion of the great majority of water-walking arthropods is characterized by $Re > 1$, $We < 1$ and $Bo < 1$. The principal force resisting their driving legs, and so the principal propulsive force, is thus the curvature force. By deforming the free surface, they generate contact forces that propel them forward.

We note that this macroscopic picture of the dynamics of water-walking creatures needs to be revised in light of the fact that the driving legs of arthropods are not smooth cylinders, but rather roughened hydrophobic surfaces. As will become clear in Section 3, each of the components of the hydrodynamic force listed in Eq. (2) is directly affected by the form of the surface roughness. These issues notwithstanding, the revised estimates for the relative magnitudes of these force components still indicate the dominance of contact forces in the propulsion of water-walking arthropods. The dynamic role of arthropod cuticle will be considered in Section 5.4.

3 Wetting

Wetting arises when a liquid–gas interface comes into contact with a solid (Dussan, 1979; Adamson, 1982; de Gennes, 1985). The degree of wetting is in general determined by both the material properties of the solid and fluid phases, and the topography of the solid surface. In Section 3.1, we consider the classic scenario of water wetting a flat solid surface, then in Section 3.2 proceed by describing the influence of surface roughness. The important concept of contact angle hysteresis is discussed in Section 3.3. The conditions required for a surface to be water-repellent are enumerated in Section 3.4. Our discussion follows that presented in de Gennes *et al.* (2003).

3.1 THE CONTACT ANGLE

Just as a fluid–fluid interface has an associated energy per unit area (or equivalently, a surface tension, σ), so do solid–fluid interfaces. For the case of a liquid–gas interface with tension σ in contact with a solid, the relevant surface energies are those of the solid–liquid and solid–gas interfaces, respectively, γ_{SL} and γ_{SG} (Fig. 10). The tendency of the liquid to wet the solid depends on the relative magnitudes of σ, γ_{SL} and γ_{SG} through the spreading parameter (Ross and Becher, 1992)

$$S = \gamma_{SG} - (\gamma_{SL} + \sigma) \tag{3}$$

If $S > 0$, the surface energy of the solid is lower wet than dry, so the liquid spreads completely into a thin film. Such is the case for oils spreading on most solids, including glass. Conversely, when $S<0$, it is energetically favourable for the solid to stay dry, so the fluid remains in the form of a droplet with a finite chemical (or equilibrium) contact angle θ_e. The fluid is then said to partially wet the solid. Given σ, γ_{SL} and γ_{SG}, one can calculate the contact angle θ_e by considering the horizontal force balance at the contact line or triple junction (Fig. 10)

$$\sigma \cos\theta_e = \gamma_{SG} - \gamma_{SL} \tag{4}$$

known as Young's relation (Young, 1805). This may alternatively be derived by considering the change in energy $\mathrm{d}W$ associated with the contact line moving a distance $\mathrm{d}x$

$$\mathrm{d}W = \mathrm{d}x(\gamma_{SG} - \gamma_{SL}) - \mathrm{d}x\ \ \sigma\cos\theta_e \tag{5}$$

At equilibrium, $\mathrm{d}W/\mathrm{d}x = 0$, and Young's relation (Eq. (4)) again emerges.

Consider the case of interest: an air–water interface in contact with a solid. Complete wetting arises only if $\theta_e = 0$; otherwise, the normal situation of partial wetting obtains. The solid is said to be hydrophilic if $\theta_e \leq 90^\circ$,

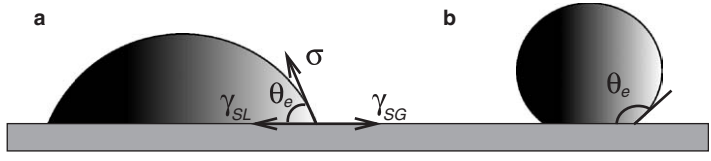

FIG. 10 The wetting of a solid by a liquid drop. The system is characterized by the surface energies per unit area of the liquid–gas interface, σ; solid–liquid interface, γ_{SL} and solid–gas interface, γ_{SG}. The horizontal force balance at the contact line yields the equilibrium contact angle θ_e in terms of σ, γ_{SL} and γ_{SG} via Young's relation (Eq. (4)). For a water drop, a surface is (a) hydrophilic if $\theta_e < 90^\circ$ and (b) hydrophobic if $\theta_e > 90^\circ$. Here, drops are assumed to be sufficiently small that gravity is negligible, so the drops assume the form of spherical caps.

hydrophobic if $\theta_e \geq 90^\circ$ and superhydrophobic if $\theta_e \geq 150^\circ$ (Fig. 10). Water is totally wetting on perfectly clean glass, but partially wetting on most solids. The equilibrium contact angles for water on a number of naturally occuring and manufactured substrates are listed in Table 1.

A liquid rises or falls in a vertical capillary tube piercing a horizontal interface according to whether θ_e is greater or less than 90°. The rise height is prescribed by a balance between curvature and hydrostatic pressures just beneath the interface. A fluid column of density ρ within a capillary tube of radius R will rise to a height h

$$h = \frac{2\sigma \cos\theta_e}{\rho g R} \tag{6}$$

provided $R \ll h$ (de Gennes *et al.*, 2003). The rise height increases with increasing surface tension and decreasing radius. Most notably, the sign of h changes with contact angle: hydrophilic tubes ($\theta_e < 90^\circ$) draw water upwards, while hydrophobic tubes ($\theta_e > 90^\circ$) oppose the impregnation of water. This simple model has important implications for the wetting of rough surfaces: fluid that is not predisposed to wetting ($\theta_e > 90^\circ$) is even less likely to enter pore-like intrusions. Finally, we note that if the tube is tilted by an angle α relative to the vertical, the rise height remains the same, but the intrusion distance along the tube increases by a factor of $1/\cos\alpha$.

3.2 SURFACE ROUGHENING

If a solid surface is not smooth, the chemical contact angle θ_e will generally differ from that observed on a macroscopic scale, specifically, the apparent contact angle θ^* (Fig. 11). Moreover, the energetic cost of wetting will depend not only on the surface chemistry (which prescribes γ_{SG} and γ_{SL}), but also the surface roughness. The influence of surface roughness may be incorporated by reconsidering Eq. (5). If we define the roughness r to be the real surface area per planar area of the surface, then the energetic cost of contact line motion becomes

$$dW = r\ dx(\gamma_{SG} - \gamma_{SL}) - dx\ \sigma\cos\theta^* \tag{7}$$

The equilibrium condition, $dW/dx = 0$, when taken in conjunction with the Young's relation Eq. (4) then yields the relationship between the apparent and microscopic contact angles

$$\cos\theta^* = r\cos\theta_e \tag{8}$$

a result known as Wenzel's (1936) relation. If a surface is hydrophilic ($\theta_e < 90^\circ$), roughening will generally make it more so: the additional surface area exposed through roughening will make the surface all the more

TABLE 1 Contact angles in nature and technology

Substrate	Contact Angle θ_e	Advancing Angle θ_A	Receding Angle θ_R	Reference
Natural materials				
Human skin	91 +/−4			Elkhyat *et al.* (2004)
Beeswax	97			Pal (1951)
Human hair		103 +/−4		Lodge and Bhushan (2006)
Chitin (composes the insect cuticle)	105			Holdgate (1955)
Plants				
Water lily *Nymphaea*		68		Fogg (1948)
Wax palm (carnuba wax, same wax as lotus)		74 +/−8		Cheng and Rodak (2005)
Surface of a common weed *Plantago lancelota*		74		Holloway (1970)
Cherry laurel evergreen shrub *Prunus laurocerasus*		75		Fogg (1948)
Pine needles	105–115			Cape (1983)
with wax removed	79			Cape (1983)
Various plant waxes (from uroslic acid to *n*-Alkanes C_{18}–C_{36})	89–109			Holloway (1970)
Wild mustard plant *Sinapis arvensis*		96		Fogg (1948)
Isolated wax of a common weed *Plantago lancelota*		102		Holloway (1970)
Eucalytpus leaf *Eucalyptus globulus*, isolated wax		105		Holloway (1970)
surface		170		Holloway (1970)
Wheat germ *Triticum vulgare*		141		Fogg (1948)
Lotus leaf	160			Cheng and Rodak (2005)
Indian cress	180			Otten and Herminghaus (2004)
Birds				
Duck feather material, smooth		90	65	Cassie and Baxter (1945)
with roughness included	150			Cassie and Baxter (1945)
Uropygial gland oil (in aquatic birds)		90	60	Rijke (1970)
Mallard, breast		137	121	Elowson (1984)
Reed cormorant, breast		133	130	Elowson (1984)
feather shaft		155	146	Elowson (1984)
Insects				
Aquatic				
Water boatman *Notonecta glauca*, adult, wings		30		Pal (1951)
dorsal		180		Pal (1951)

Water bug *Naucoris cimecoides*, prothorax		90	56	Holdgate (1955)
Great diving beetle *Dytiscus marginalis*, elytra		90	10	Holdgate (1955)
Water scavenger beetles *Hydrobius*		87	0–50	Holdgate (1955)
Water scorpion *Ranatra linearis*, elytra		62	0	Holdgate (1955)
Emperor dragonfly *Anax imperator*, aquatic nymph		45	0	Holdgate (1955)
Damselfly *Coenagrion puellam*, aquatic nymph		35	0	Holdgate (1955)
Water bug *Naucoris cimicoides*, larva	110			Pal (1951)
Terrestrial				
Tick *Ornithodorus moubata*, dorsal		43–95		Pal (1951)
Aphid *Aphis*	62			Pal (1951)
Orb weaving spider *Mangora placida*, legs	74			Stratton *et al.* (2004a,b)
Cockroach *Periplaneta americana*, legs		67		Pal (1951)
ventral		77		Pal (1951)
dorsal		83		Pal (1951)
wings		85		Pal (1951)
elytra		106	91	Holdgate (1955)
Mealworm *Tenebrio molitor*, adult, elytra		107	92	Holdgate (1955)
Potato aphid *Macrosiphum*	106			Pal (1951)
Grain weevil *Calandra granaria*, larva	107			Pal (1951)
Spitting spider *Scytodes*, legs	100–112			Stratton *et al.* (2004a,b)
Common jumping spider *Phidippus audax*, legs	145			Stratton *et al.* (2004a,b)
Flying				
Blowfly *Calliphora erthrocephala*		175	155	Holdgate (1955)
Variable damselfly *Coenagrion puellam*, adult		175	170	Holdgate (1955)
Locust *Locusta migratoria*, prothorax, flanks		128	104	Holdgate (1955)
forewings		107	89	Holdgate (1955)
Garden tiger moth *Arctia caja*, dorsal, single hair	97			Pal (1951)
array	180			Pal (1951)
Mediterranean flour moth *Ephestia kuhniella* Zell	85			Pal (1951)
House mosquito *Culex pipiens*, *larva*, dorsal		180		Pal (1951)
ventral		180		Pal (1951)
legs		75		Pal (1951)
wings		95		Pal (1951)
Semiaquatic				
Whirligig beetle *Gyrinus marinus*		105	90	Holdgate (1955)

TABLE 1 (*Continued*)

Substrate	Contact Angle θ_e	Advancing Angle θ_A	Receding Angle θ_R	Reference
Fisher spider *Dolomedes triton*, legs	147			Stratton *et al.* (2004a,b)
Water strider *Gerris lacustris*, legs	168			Gao and Jiang (2004)
Larvae				
Cutworm *Polia oleracea*	18			Pal (1951)
Housefly *Musca domestica*	48–65			Pal (1951)
Cabbage moth *Mamestra brassicae*	18			Pal (1951)
Man-made materials				
Plexiglass (Polymethyl methacrylate)		63	41	Taylor *et al.* (1998)
Glass	42 +/−4			Slodowska *et al.* (1999)
Candle wax (parrafin), smooth	105–110			Pike *et al.* (2002)
rough	110–140			Zisman 1964
Teflon		120	118	Sabbatovskii *et al.* (2004)
Alkylketene dimer, smooth	109			Onda *et al.* (1996)
rough	174			Onda *et al.* (1996)
Fluorosilanated silicon, smooth		118	100	Bico *et al.* (1999)
Fluorosilanated silicon, decorated with holes		138	75	Bico *et al.* (1999)
stripes (parallel to motion)		143	125	Bico *et al.* (1999)
stripes (perpendicular to motion)		165	132	Bico *et al.* (1999)
spikes		170	155	Bico *et al.* (1999)
Fluoroalkylsilanated silicon, smooth	114			Yoshimitsu *et al.* (2002)
rough	153			Yoshimitsu *et al.* (2002)
Methylchlorosilanated silicon (Lichau's surface)	180	180	180	Gao and McCarthy (2006)

Note: On rough surfaces, the values correspond to the apparent contact angle θ^*. Measurement techniques are detailed in the accompanying references. Contact angles in each category are listed in roughly increasing order. Among the insects, contact angles are highest for the semi-aquatic creatures, then in turn for their flying, terrestrial and aquatic counterparts. Note that contact angle generally varies with body region. Data reproduced from Elkhyat *et al.* (2004), Pal (1951), Lodge and Bhushan (2006), Cheng and Rodak (2005), Holloway (1970), Fogg (1948), Cape (1983), Otten and Herminghaus (2004), Cassie and Baxter (1945), Rijke (1970), Holdgate (1955), Stratton *et al.* (2004a), Gao and Jiang (2004), Taylor *et al.* (1998), Slodowska *et al.* (1999), Pike *et al.* (2002), Sabbatovskii *et al.* (2004), Onda *et al.* (1996), Bico *et al.* (1999), Yoshimitsu *et al.* (2002), Zisman (1964) and Gao and McCarthy (2006).

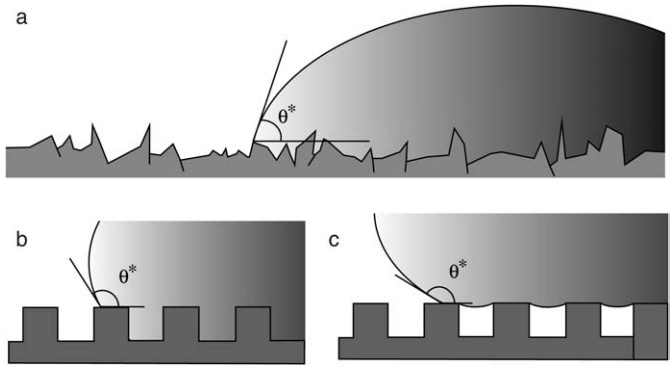

FIG. 11 Roughening a surface will amplify its wetting tendencies. In the randomly roughened surface in (a), the microscopic contact angle remains θ_e, but the observed contact angle on the macroscopic scale is θ^*. The two generic states of wetting, the Wenzel and Cassie states, are shown schematically in (b) and (c). In the Wenzel state (b), the pores are impregnated by fluid, increasing the fluid–solid contact. In the Cassie state (c), air pockets are trapped by the overlying fluid, reducing the fluid–solid contact.

attractive to the spreading liquid. Similarly, a hydrophobic surface ($\theta_e > 90^\circ$) will become all the more so when roughened (Cassie, 1948). This is a critical point when considered in the context of water-walking arthropods and their elaborate covering of micron scale hairs: if the surface of the insect cuticle had a contact angle $\theta_e < 90^\circ$, insects would be hydrophilic rather than hydrophobic. As we shall see in Section 4, their waxy surface coating generally ensures that $\theta_e > 90^\circ$ (Holdgate, 1955), so that their surface roughening encourages rather than discourages their water-repellency.

If the surface is sufficiently rough, air pockets are trapped between the liquid and solid and the Wenzel picture of wetting no longer applies. This scenario is described by the Cassie–Baxter model for a planar but chemically heterogeneous surface (Fig. 11c). We consider a planar surface tiled with two materials characterized by respective areal fractions f_1 and f_2 and contact angles θ_1 and θ_2. The motion of the contact line by an amount dx brings about a change in surface energy

$$dW = f_1(\gamma_{SG} - \gamma_{SL})_1\, dx + f_2(\gamma_{SG} - \gamma_{SL})_2\, dx - \sigma \cos\theta^* dx \qquad (9)$$

The equilibrium condition, in conjunction with Young's relation applied to both materials, yields the Cassie–Baxter relation

$$\cos\theta^* = f_1 \cos\theta_1 + f_2 \cos\theta_2 \qquad (10)$$

The apparent contact angle on such a surface is the mean of the contact angles in each region weighted by their areal fractions. If the tiled material

designated as 1 is air (contact angle $\theta_1 = 180^\circ$), the Cassie–Baxter relation yields

$$\cos\theta^* = -1 + f_S(1 + \cos\theta_e) \tag{11}$$

where f_S is the exposed area fraction of the solid substrate and θ_e is the contact angle of water on a planar solid substrate. The validity of this equation for fluid drops on a number of patterned surfaces was demonstrated by Bico *et al.* (1999). Note that as the area fraction of the solid $f_S \to 0$, the apparent contact angle approaches 180°. As we shall see in Sections 4 and 5, this Cassie–Baxter model is appropriate for describing the wetting by water of rough insect cuticle.

de Gennes *et al.* (2003) and Carbone and Mangialardi (2005) present criteria for the trapping of an air layer by a rough surface. In their 2D model, fluid contacting a rough surface characterized by sinusoidal undulations of amplitude a and wavelength $\lambda = 2\pi/k$ (Fig. 12) will remain in a Cassie–Baxter state provided

$$a > \frac{1}{2\pi}\lambda\tan\theta_e \tag{12}$$

where θ_e represents the equilibrium contact angle. In the limit of small amplitude roughness, $ka \ll 1$, the roughness is given by $r = 1 + \frac{1}{4}(ka)^2$, and the critical roughness beyond which trapping occurs is simply expressed

$$r_T = 1 + \frac{1}{4}\tan^2\theta_e \tag{13}$$

We note, however, the importance of three-dimensional (3D) effects on the wetting of corrugated surfaces in the presence of a gravitational field. Shuttleworth and Bailey (1948) considered the spreading of a liquid over a corrugated solid, specifically, a surface with a field of 2D grooves. By analogy with the case of a closed capillary tube, if $\theta_e < 90^\circ$, fluid will be drawn into the grooves with a force that increases inversely with the groove

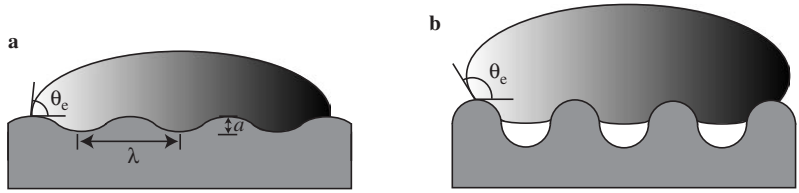

FIG. 12 Wetting on a sinusoidally varying surface with wavelength λ and amplitude a. (a) In the limit of small amplitude roughness, fluid fills the troughs of the sinusoid and a Wenzel state obtains. (b) If the roughness exceeds a critical amplitude defined by Eq. (13), air is trapped in the troughs, resulting in a Cassie–Baxter state.

width. Conversely, if $\theta_e > 90^\circ$, fluid will be expelled from the grooves, and complete wetting of the corrugated surface will be discouraged. A detailed investigation of rough wetting is presented by Bico *et al.* (2001).

The two different modes of wetting have been observed in both the plant and animal kingdoms. For reasons to be discussed in Section 3.4, the maintenance of a Cassie–Baxter rather than a Wenzel state (Fig. 11) is generally required for water-repellency. The water-repellent nature of the lotus leaf is attributed to its surface roughening (Barthlott and Neinhuis, 1997). Similar surface structures have been reported on a number of other plant leaves, including the rice plant (Feng *et al.*, 2002) and the lady's mantle (Mock *et al.*, 2005; Otten and Herminghaus, 2004) and in the animal kingdom on butterflies (Wagner *et al.*, 1996), beetles (Parker and Lawrence, 2001) and cicadae (Lee *et al.*, 2004). The common feature to most of these naturally occuring water-repellent surfaces is hierarchical roughness on two or more scales, the smallest being the sub-micron scale.

Bico *et al.* (1999) examine how surface roughening can be exploited to produce large contact angles on synthetic materials. Onda *et al.* (1996) produced a synthetic hydrophobic surface from an alkylketene dimer film that exhibited a static contact angle of 174°. The surface took a complex fractal-like form with several scales of roughness; owing to the heightened roughness of such surfaces, the cost of wetting can be enormous and the contact angle correspondingly high. The authors were able to rationalize the observed contact angles on the basis of the Cassie–Baxter relation (Eq. (11)) in conjunction with the theoretical predictions of Hazlett (1990) for the hydrophobicity of fractal surfaces. Herminghaus (2000) argues that roughness beyond a second scale is vital in the hydrophobicity of plant leaves. Indeed, he demonstrates theoretically that fractal roughness may generate water-repellency on solids with any finite contact angle, a conjecture demonstrated experimentally by Feng *et al.* (2003). de Gennes *et al.* (2003) note, however, that hydrophobic states generated by complex surface texturing of hydrophilic material are only metastable. It is worth noting that such engineered superhydrophobic surfaces generally rely on complex surface topography such as sharp corners (Oliver *et al.*, 1977; Carbone and Mangialardi, 2005) that are not typical of the piliferous cuticle of water-walking insects. Finally, the most water-repellent man-made surface is the recently developed 'Lichao's surface' (Gao and McCarthy, 2006), composed of a tangled network of 40 nm fibers that exhibits a static contact angle of 180°.

3.3 CONTACT ANGLE HYSTERESIS

While the concept of an equilibrium contact angle is useful conceptually, it is important to note that, for a given solid–fluid combination, a range of

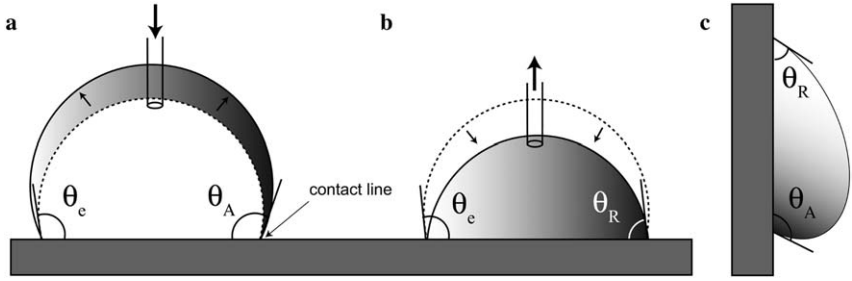

FIG. 13 Contact angle hysteresis. A drop of fluid at rest on a solid may exhibit a range of contact angles. (a) If a drop is filled with a pipette, it swells while remaining pinned at the contact line until the contact angle reaches a critical value, θ_A, at which the contact line advances. (b) If fluid is withdrawn from the drop, its contact angle decreases progressively until it reaches θ_R, after which the contact line recedes. The difference $\theta_A - \theta_R$ is known as the contact angle hysteresis. (c) Contact angle hysteresis is responsible for suspending drops on vertical windows. The largest drop that can be so supported is prescribed by Eq. (15).

static contact angles may be observed (Dettre and Johnson, 1964; Johnson and Dettre, 1964). Consider a drop of fluid emplaced on a solid. If the drop is filled, it will grow, and its contact angle increase progressively until reaching a critical value, θ_A, at which the contact line begins to advance (Fig. 13). If conversely, fluid is withdrawn from the drop, its contact angle will decrease progressively until reaching a critical value, θ_R, at which the contact line begins to recede. Observed static contact angles θ may thus lie anywhere within the range $\theta_A > \theta > \theta_R$, bounded above and below by the advancing and receding contact angles. This finite range is associated with microscopic surface imperfections that distort the advancing interface, thereby resisting contact line motion (Joanny and de Gennes, 1984; Nadkarni and Garoff, 1992).

The finite range of static values for a given three-phase system is referred to as the contact angle hysteresis

$$\Delta\theta = \theta_A - \theta_R \tag{14}$$

An important consequence of this hysteresis is that there is a concomitant force of retention F_r that causes droplets to adhere to surfaces: differences in the contact angle around the perimeter of a drop may result in a net contact force that resists its motion (Dussan, 1979; Extrand and Gent, 1990). For example, raindrops may stick to window panes because of the difference in the contact angles on their upper and lower edges (Fig. 13c; Dussan and Chow, 1983). For droplets with circular contact lines the retention force may be approximated by (Extrand and Kumagai, 1995).

$$F_r = \frac{\pi}{2} D \ \sigma (\cos\theta_R - \cos\theta_A) \tag{15}$$

where D is the diameter of the contact region. There is thus a maximum droplet size that can be supported by the retention force: drops bigger than a critical size (comparable to the capillary length) will roll down the windowpane under the influence of gravity. Values of $\Delta\theta$ for water on a number of naturally occuring and man-made substances may be computed from Table 1 via Eq. (14).

The dependence of contact angle hysteresis $\Delta\theta$ on surface roughness is subtle (Johnson and Dettre, 1964) and depends on whether a Wenzel or Cassie–Baxter state is obtained (Bico *et al.*, 1999, 2002; Lafuma and Quéré, 2003). In the Wenzel state arising at low surface roughness, surfaces exhibit high advancing contact angles and low receding angles relative to those on a flat surface; consequently, $\Delta\theta$ is greatly increased. On rougher surfaces in a Cassie–Baxter state, both advancing and receding contact angles are higher; the contact angle hysteresis is moderately reduced relative to that on a smooth surface, and greatly reduced relative to that in the Wenzel state. The maintenance of a Cassie–Baxter state is thus critical in reducing the force of adhesion, F_r, of water droplets on rough solids, and so is considered as important a criterion for water-repellency as a high contact angle.

Öner and McKarthy (2000), Extrand (2003) and Gao and McCarthy (2007) examine the influence of importance of surface architecture on the contact angle hysteresis. Extrand (2002) considers a uniform array of pillars of width d and spacing δ tilted at an angle ω relative to the surface normal (Fig. 14a), and argues that the contact angle hysteresis for such a surface may be simply expressed as the weighted mean

$$\Delta\theta = \frac{d}{\delta}(\Delta\theta_0 + \omega) \tag{16}$$

where $\Delta\theta_0$ is the contact angle hysteresis on a planar surface. Note that the contact angle hysteresis and so the force of retention may be decreased by

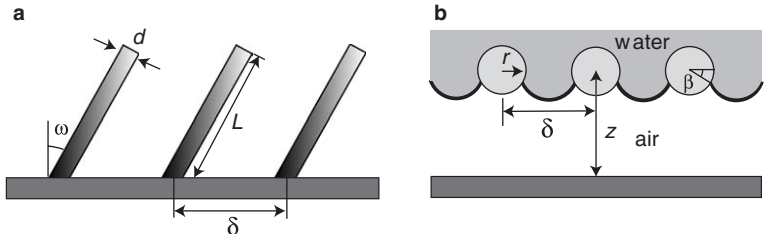

FIG. 14 Two geometries considered for the water-repellent hair pile. (a) A regular square array of cylindrical posts (either rectangular or cylindrical) of length L, width d and spacing δ are tilted at an angle ω relative to the vertical. (b) A regular array of horizontal cylinders of diameter r, spacing δ and height z above a horizontal substrate. The curved menisci, which intersect the hairs at a contact line lying at an angle β relative to the horizontal, protect the air layer from impregnation by the overlying water.

decreasing the size to spacing ratio of the pillars, and increased by increasing the tilt angle of the pillars. The dependence of the retention force on the topology of the substrate will be further discussed in the context of water-repellency in Section 3.4.

The contact angles of water on various plants and arthropods are listed in Table 1. The highest contact angles in the animal kingdom arise on water-walking arthropods, with θ ranges from 150° to 170°. The second group are the flying insects, whose survival depends on their ability to avoid or deflect raindrops; they exhibit contact angles between 90° and 170°. Third are terrestrial insects, with θ between 20° and 145°. Finally, aquatic insects prefer to remain wet when they surface and typically exhibit contact angles between 10° and 90°. We note that insect larvae do not generally have a waxy coating and so exhibit particularly low contact angles (Wigglesworth, 1950). In terms of contact angles, the integument of water-walking arthropods compares favourably with the most hydrophobic manufactured surfaces. Only Lichao's surface (Gao and McCarthy, 2006) achieves the ideal limit of perfect water-repellency $\theta_A = \theta_R = \theta^* = 180°$.

3.4 WATER-REPELLENCY

Water-repellency is a necessary adaptation for water-walkers. A creature of characteristic length L whose leg lies beneath the water surface can apply a maximum force that scales as L^2 (Alexander, 1985). If acting along its leg perimeter, the surface tension force that resists its leg crossing the interface scales as L, so the ratio of available muscular to curvature forces scales as L. Water striders are capable of penetrating the free surface (Perez-Goodwyn and Fujisaki, 2007). However, smaller creatures may be too weak to overcome curvature forces and it becomes a matter of survival that they do not wet, specifically, that they maintain a Cassie–Baxter state.

For a surface to be water-repellent, it must have two properties. First, it must resist impregnation of water. Second, it must exhibit minimal drop retention, so that when droplets strike the surface, they roll off rather than adhering. The wetting properties of rough solids have been shown to be hysteretic in a variety of settings. The hydrophobicity of certain plant leaves can be lost if the plant is submerged in water for an extended period (Herminghaus, 2000), and the same has been observed for a number of insects (e.g. Holdgate, 1955). Once the surface roughness has been impregnated with water, in the absence of evaporation it will remain so indefinitely unless subjected to high pressures. Owing to contact angle hysteresis, the required evacuation pressure generally exceeds the impregnation pressure (Adam, 1948). These observations make clear the importance of the insects remaining in a Cassie–Baxter rather than Wenzel state: the transition from one to the other is accompanied by a transition

from hydrophobic to hydrophilic states. Clear observational evidence of the air layer trapped in the integument of water-walking insects will be provided in Section 6.

For a rough solid to resist fluid impregnation, the curvature pressures generated by the interface that spans its roughness elements must be larger than any applied pressures. The magnitude of such curvature pressures depends critically on the geometry of the surface roughening (Lafuma and Quéré, 2003). A number of simple geometries have been considered experimentally. Patankar (2004) considers the influence of the weight of a dropet on its transition from a Cassie–Baxter to a Wenzel states when placed on a square array of rectangular posts. Journet *et al.* (2005) considered flow in the vicinity of a surface covered with a carbon nanotube forest, a regular array of vertical cylinders rolled from sheets of carbon atoms (Lau *et al.*, 2003). They demonstrate that the intrusion into a substrate with characteristic roughness scale δ by a surface with tension σ and equilibrium contact angle θ_e can be forced by a pressure of characteristic magnitude

$$\Delta P \sim \frac{2\sigma}{\delta}\cos\theta_e \tag{17}$$

with a slight correction required to account for the finite amplitude of the roughness. Note that this observation may be understood on the basis of Eq. (6) by viewing the space between the roughness elements as simple capillary tubes. Reyssat *et al.* (2006) and Bartolo *et al.* (2006) considered forced wetting of a surface decorated with pillars of height h spaced a distance δ apart, and demonstrated that when $h/\delta \ll 1$, the impregnation pressure is reduced by a factor of h/δ.

With the wetting of insect cuticle in mind, Thorpe and Crisp (1947a) and Crisp and Thorpe (1948) calculate the impregnation pressures required to force fluid through various arrangements of cylinders on a horizontal surface. They first considered a square array of vertical cylinders of diameter $d=2r$ and uniform spacing δ tilted at an angle ω relative to the vertical (Fig. 14a). Not surprisingly, they concluded that the impregnation pressure is maximized by decreasing the spacing of the array. Moreover, they found that impregnation pressures increases with ω: by reducing the free space between the cylinders, tilting the pillars serves to promote water-repellency. A similar conclusion was drawn by Extrand (2004) in his calculation of the impregnation pressure of a square array of square pillars: tilting the pillars enhances water-repellency. Thorpe and Crisp (1947a) and Crisp and Thorpe (1948) also considered a horizontal array of cylinders (Fig. 14b), and concluded that such an arrangement of may provide water-proofing for any $\theta_e > 0$. The horizontal arrangement of cylinders provides greater resistance than the tilted array: fluid impregnation between the horizontal cylinders requires the production of maximum surface area

and so maximum surface energy. For any such arrangement of cylinders (vertical, tilted or horizontal), the smaller the scale of the surface structure, the greater its effect on water-repellency: the impregnation pressure is generally inversely proportional to a characteristic length scale of the hair pile. Extrand (2006) notes that while tilting the pillars increase a rough surface's resistance to fluid impregnation, according to Eq. (16) it simultaneously increases the force of drop retention. Moreover, for a fixed spacing δ, while increasing the pillar size increases the surfaces resistance to impregnation, it increases the force of retention that acts along the drop perimeter.

4 Insect cuticle

As detailed in Section 3.2, the degree of wetting of a solid by a liquid is determined by both the material properties and the topography of the solid surface (de Gennes *et al.*, 2003). Surface roughening has long been used as a means of rendering a solid effectively non-wetting (Cassie, 1944, 1948; Adam, 1963): through increasing the contact area, one increases the energetic cost of wetting, and so encourages a non-wetting situation. We proceed by describing the form of insect integument to rationalize its water-repellent properties and elucidate its role in propulsion.

4.1 COMPOSITION

Wigglesworth (1979, 1984) and Hadley (1981) review studies of the form and function of insect cuticle, the outermost layer adjoining the epidermal cells. Insect cuticle is composed of a chitin–protein complex, and covered with a layer of epicuticular wax that serves to discourage the penetration of water. Insect cuticle consists of three layers, each with a distinct function. The bulk of the cuticle is the innermost endocuticle, which allows for the flexibility and extensibility required for movement, and the increases in bulk that accompany feeding. A hard exocuticle provides rigidity to some regions, such as the head. The outermost layer, the waxy epicuticle, is responsible for waterproofing and the prevention of dessication. Reviews of the chemistry of insect waxes are provided by Blomquist and Jackson (1979) and Howard (1993).

Holdgate (1955) reports the presence of a 0.25-μm-thick waxy or greasy layer (lipids such as hydrocarbons and esters) on the insect cuticle, and estimates its effect on the wetting of the cuticle by applying wax solvents that dissolve the layer. The presence of this waxy layer has long been known (Kühnelt, 1928; Wigglesworth, 1933) and Wigglesworth (1945) demonstrated its importance not only in water-proofing the insect, but in

water-retention: removing the wax layer of insects lead to their rapid dessication. The asymmetry of insect cuticle with respect to water permeability was considered by Hurst (1941, 1948), who concluded that the cuticle provides a greater impediment to outgoing than incoming water, a critical feature for desert beetles (Hadley, 1978, 1979). Beament (1945, 1948) reports that the wax layer thickness is remarkably constant, 0.2–0.3 μm for a great many insects, and suggests that this is the minimum thickness capable of providing maximum water-proofing. The wax layer can be removed by gently rubbing with an abrasive dust; if the insect is then exposed to dry air, it quickly dies; if exposed to moist air, the insect can secrete a fresh layer of wax and so restore its waterproofing. Wigglesworth (1984) reported that the wax layer of burrowing insects is so worn that they cannot survive in dry air.

The cuticle typically has numerous irregular structures such as hairs, scales and regions of varying curvature, all of which make the contact angle highly variable (Pal, 1951). Pal (1951) and Holdgate (1955) conducted comparative studies of the wetting properties of many terrestrial, semi-aquatic and aquatic insects, and concluded that terrestrial insects are generally hydrophobic and lipophilic (wetted by oil), while the aquatic species are often both hydrophilic and lipophilic. Key exceptions include plastron-bearing aquatic creatures such as the backswimmer *Notonecta* (Fig. 28) to be considered in Section 5.2. Contact angle hysteresis was documented; moreover, the contact angle was found to be a function of humidity, time after moulting and time after submergence in water. Pal (1951) noted the dependence of wetting properties on body part: generally, the legs and antennae are more wettable than the wings. Pal (1951) also measured the contact angles on individual insect hairs by spraying them with microdroplets generated by an atomizer. He demonstrates that the hairs of some terrestrial and aerial insects are sufficiently flexible to be drawn together by drops of water clinging to them. The flexibility of the cuticle of water-walking insects has only recently been confirmed experimentally (Bush and Prakash, 2007) and will be further discussed in Section 4.3. The contact angles of water on many terrestrial and aquatic insects are listed in Table 1.

4.2 MORPHOLOGY

Dufour (1833) was the first to note the importance of the microstructure of the leg-coating for water-walking insects: 'their legs are covered with a very fine velvet that is impermeable and gives these insects the ability to stand or run on water without getting wet.' The characteristics of the hair layer of many water-walking arthropods have been established using macrophotography and scanning electron microscopy. Some qualitative features of the

insect cuticle and its interaction with the free surface can be elucidated with macrophotography. The legs, bodies and antennae of the water-walkers are covered with hairs that reflect light to provide a colourful glossy sheen (Fig. 1; Gu *et al.*, 2003). The hair mats of *Mesovelia* and *Microvelia* are apparent in Fig. 15, while that of the fisher spider is evident in Fig. 16. Close-up images show that when a water-walking arthropod resides at rest on the free surface, its leg hairs appear as spokes whose tips abutt the free surface; therefore, a Cassie state is maintained.

Traditional microscopy techniques can be used to image the interaction between water droplets and the cuticle of water-walking arthropods. Stratton *et al.* (2004b) assessed the wetting properties of 25 species of terrestrial and semi-aquatic spiders by examining the contact angle of water microdroplets on individual hairs and on the hair pile. They found that the Fisher spider, which spends the bulk of its life on the water surface, exhibits substantially higher apparent contact angles θ^* than do its terrestrial counterparts, owing to its relatively large hair densities and chemical contact angles (Fig. 17). A number of their observations concerning the morphology of spider cuticle are reported in Tables 1 and 2.

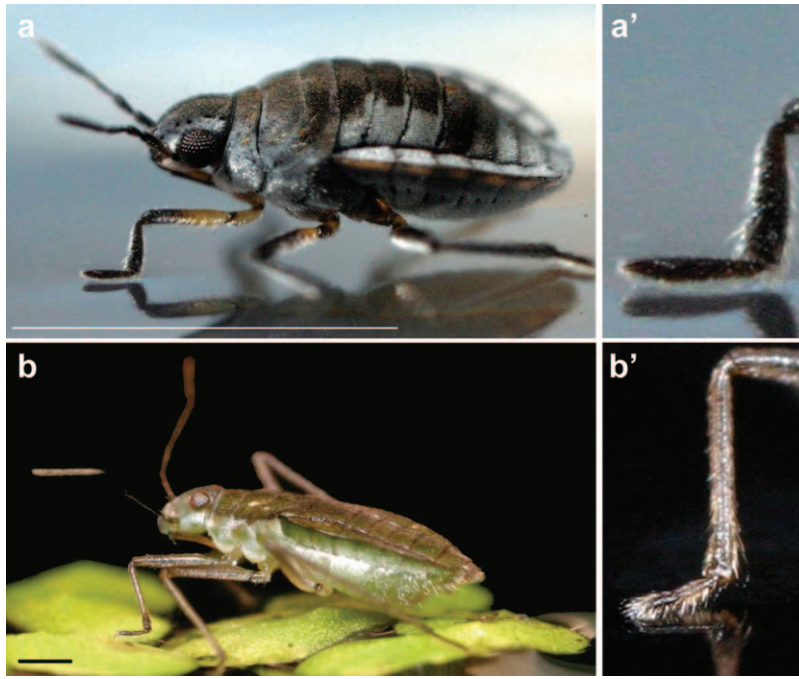

FIG. 15 The dense hair layer of two water-walkers: (a) *Microvelia* and (b) *Mesovelia*. Close-up images of their driving legs are given at right. Scale bars, 1 mm.

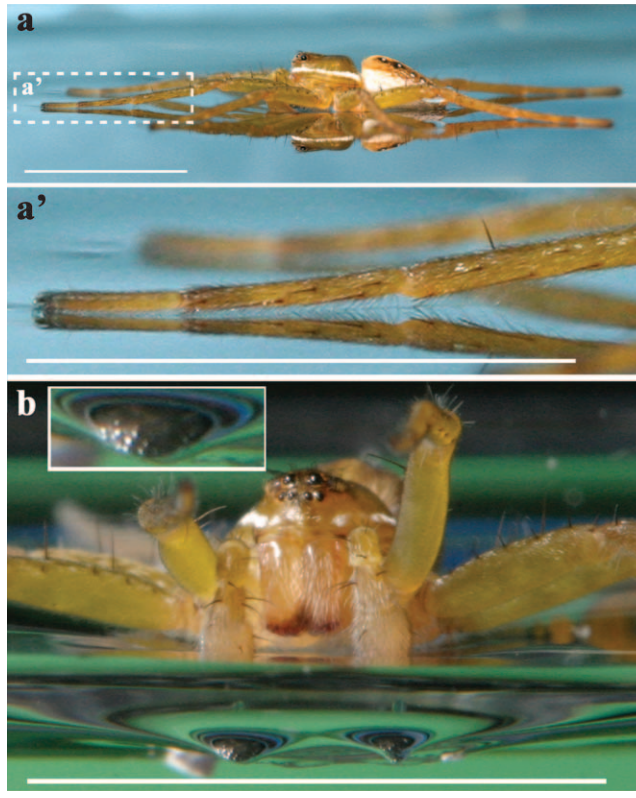

FIG. 16 The fisher spider on the free surface. (a) Hairs protrude from the leg and abut the free surface. In (b), the inset shows a magnified view of the dimpled surface deformation generated by the array of hairs. Scale bars, 1 cm.

Scanning Electron Microscopy (see Section 6.1) was first used to image the cuticle of water-walking insects by Cheng (1973), who considered freshwater and marine water striders. Subsequently, Andersen (1977, 1982) examined a wide range of semi-aquatic bugs under an electron microscope and provided detailed characterizations of their hair cover. Their studies provide fine detailed images of the hair pile, as well as the orientation and microstructure of the individual hairs. A hair map of the water strider is presented in Fig. 18; close-ups at locations numbered 1–6 are provided in Figs. 19–21. Fig. 19 depicts Scanning Electron Microscope (SEM) images of a water strider head, forelegs, flank and leg joint, virtually all of which are covered in hair.

Figure 20 indicates the form of the water strider's leg hair. The hairs are typically 30 μm long, tapering to a point from a 1-μm-diameter base,

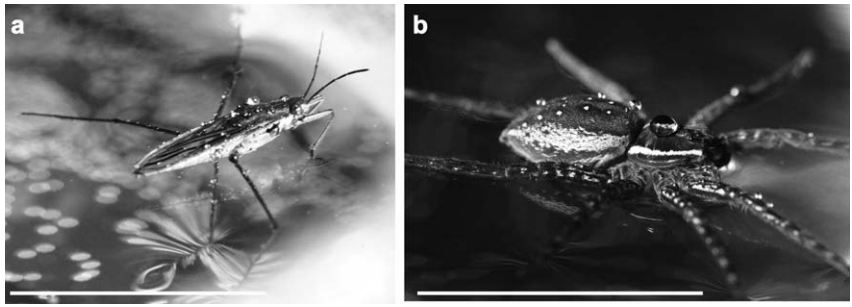

FIG. 17 Pearl drops generated by a fine water spray impinging on (a) the water strider and (b) the fisher spider. Their dense hair carpet is water repellent as indicated by the high contact angle of the droplets. Once wet, the water strider may dry itself by grooming or flipping over on its back: failing that, it can wait for the droplets to evaporate. Scale bars, 1 cm.

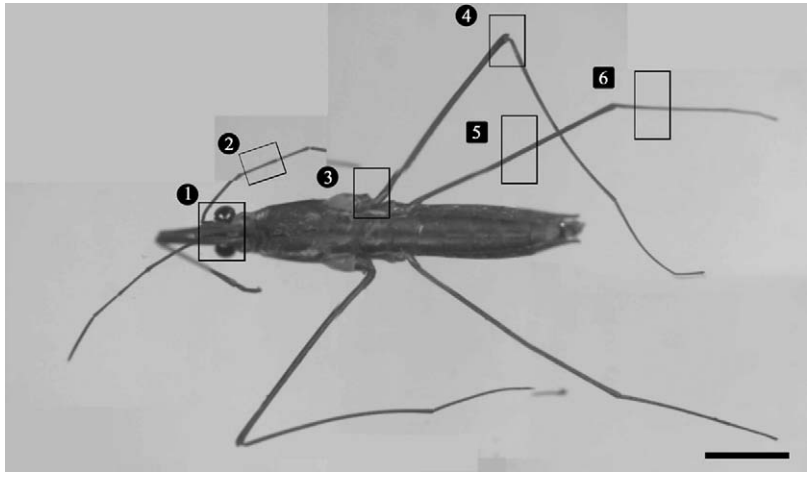

FIG. 18 A composite of photomicrographs of the adult water strider: a map indicating the origins of the SEM images presented in Figs. 19–21. Close-ups of regions 1–4 are displayed in Fig. 19 and of 5–6 in Fig. 20. Scale bar, 2 mm.

and inclined at an angle of $\sim 30^{\circ}$ to the underlying leg surface, forming a layer 10 μm thick. These hairs, termed macrotrichia, point in the direction of the leg tip, and bend inwards at their tips so as to lie roughly tangent to the leg and water surface. The hair density varies along the leg: the density is 4–6000 hairs mm^{-2} on the front tarsus, 12–16 000 mm^{-2} on the middle tarsus and 8–10 000 mm^{-2} on the hind tarsus (Andersen, 1977). The higher density on the middle tarsus might be anticipated on the grounds that it is

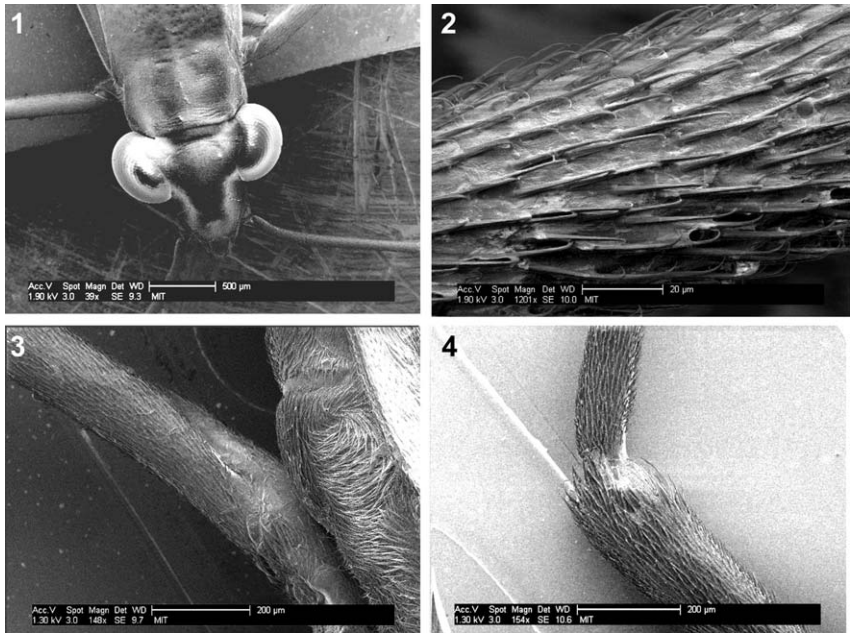

FIG. 19 Scanning electron microscope images of the water strider's (1) head, (2) antenna, (3) flank and (4) leg joint at locations indicated on Fig. 18. The great majority of the strider's body is covered with hair to repel water.

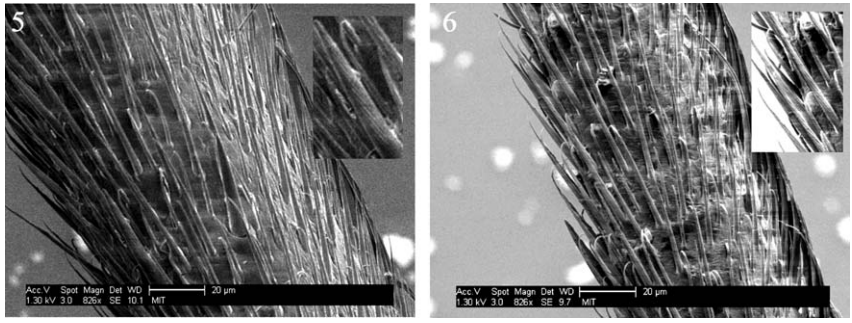

FIG. 20 Scanning electron microscope images of the strider's leg at locations (5) and (6) indicated on the hair map (Fig. 18). The insets reveal the nano-grooves on the hair surface (for a closer look, see Fig. 21). Note that the hair tips are bent inwards towards the leg, which discourages their piercing the water surface.

used for rowing and must therefore sustain higher dynamic pressures than the front and hind tarsi. Individual macrotrichia are covered in nano-grooves, roughly 400 nm wide and 200 nm deep, aligned with the direction of the hair (Andersen, 1977; Gao and Jiang, 2004; Fig. 21). On the thorax,

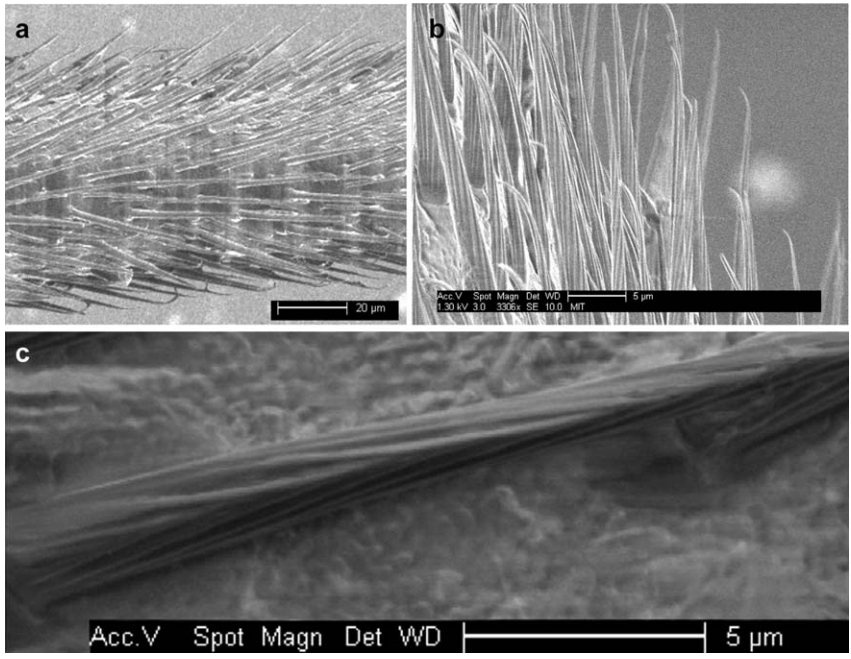

FIG. 21 SEM images of the hair layer of the water strider leg. (a) While the leg has thickness comparable to that of a human hair, it resembles a brush, whose thick carpet of hairs are tilted at $\sim 30^\circ$ relative to the leg surface. Hairs are typically 30 μm long, 1–3 μm thick at the base and tapered; their density is 12 000–16 000 hairs mm^{-2}. (b) A closer view of the hairs shows that their tips are bent inwards, towards the leg; moreover, each hair is patterned with grooves of characteristic width 400 nm that run its length, (c). Note that the leg surface at the roots of the hairs, evident in (c), is patterned with isotropic roughness reminiscent of plant cuticle.

in addition to the macrotrichia, there is an inner layer of microtrichia (Cheng, 1973; Andersen, 1977; Andersen and Cheng, 2004), whose purpose is to trap a layer of air and so permit respiration in case of submergence (see Section 5.2). While these are not as orderly as the macrotrichia, Cheng (1973) notes that for the sea-going Hemiptera, these hairs are also curved at their tips to lie tangent to the free surface. Andersen (1977) notes that their disorder and tangling may provide structural support against hydrostatic pressures during times of submergence. Finally, Fig. 22a depicts the smooth hydrophilic ungue present at the water strider leg tip.

Holdgate (1955) measured the static contact angle of water on cuticle wax, finding a value of $\theta_e = 105^\circ$. Gao and Jiang (2004) measured the static contact angle of water on a water strider leg, and report a value of $\theta^* = 167^\circ$. This large value was explained by considering the two scales of roughness on the strider leg; specifically, the 20-μm-scale roughness

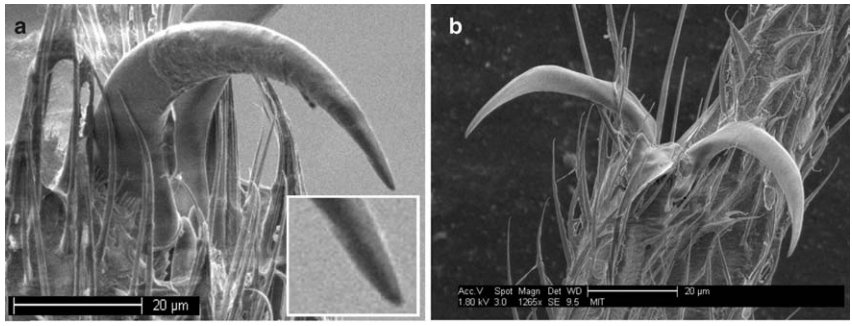

FIG. 22 The ungui at the leg tips of (a) the water strider and (b) *Microvelia*. Water striders may use their ungui to anchor themselves on the free surface against the wind. *Microvelia* use their ungues to grasp and lift the free surface to generate the lateral capillary forces used to climb menisci (Fig. 9b). The inset shows that, unlike the grooved hairs (Fig. 21), the ungui are smooth.

associated with microsetae, and the 100-nm-scale roughness associated with the nanogrooves on the microsetae. On the basis of the Cassie relation (Eq. (11)), the authors inferred that the solid fraction on the rough strider surface is merely $f = 3.14\%$. Feng *et al.* (2007) apply Cassie's Law to estimate 120° for the static contact angle required on smooth microsetae to rationalize the high apparent contact angle of $\theta^* = 167°$. Again using Cassie's relation, and the geometry of the nanogrooves (characteristic width and depth of, respectively, 400 and 200 nm), they find that the inferred 120° is consistent with the $\theta_e = 105°$ measured by Holdgate. They thus conclude that not only the microsetae but their nanogrooves are critical to achieving the high apparent contact angle on water strider legs.

We also conducted equivalent SEM imaging studies of *Microveia*, whose body hair is responsible for its sheen (Figs. 1a and 15b). The characteristic smooth, tapered horns of the two-pronged ungui are evident at the leg tip (Fig. 22b). The images in Fig. 23 depict the form of the body hair present on the tarsi and thorax. 20-μm-long hairs tilted at $\sim 45°$ are apparent on the tarsus (Fig. 23a). The hair density is significantly less than that on water strider legs. As on the strider, two distinct hair types are evident on the thorax: the relatively long and thick macrotrichia, and the inner layer of microtrichia (Fig. 23b). The macrotrichia are typically 20 μm long, 1 μm wide and curved so that their tips are roughly parallel to the body surface. The microtrichia are typically 2 μm long, 100 nm wide and more randomly oriented. Note the peg plates (that cover the spiracles through which the insect breathes) nestled in the microtrichia (Fig. 23c). Our scans also reveal the first evidence of nanogrooves on the macrotrichia of *Microvelia*, of characteristic width 200 nm and depth 50 nm (Fig. 23b). This new

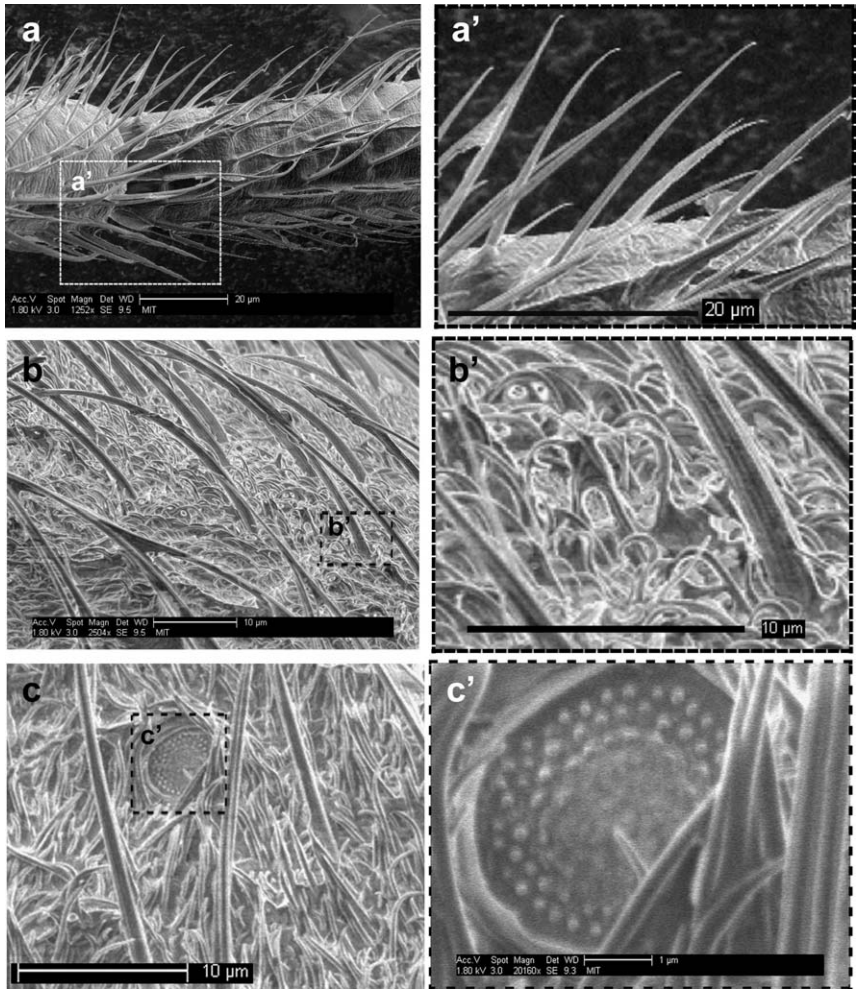

FIG. 23 SEM images of the hairy surface of the water treader *Microvelia*. (a) Leg hairs. In the magnified view (a′), the hair tips are bent inwards, which again discourages their penetrating the water surface. Evident in (a′) is the roughness of the leg surface to which the hairs adjoin, which may also play a role in water-repellency. (b) Body hairs: macrotrichia emerge from a tangle of microtrichia. (b′) Makes clear the grooves on the macrotrichia. The smaller-scale microtrichia twist and bend around one another for support (Andersen, 1977). (c) Among the microtrichia are the peg plates (c′) that cover the spiracles through which the insects breathe. Note that the surface of the peg plate has bumps reminiscent of the isotropic roughness on the lotus leaf.

observation indicates that these grooves are not peculiar to the water strider but may instead be a common feature on the macrotrichia of water-walking arthropods. Figure 6 is a cartoon depiction of the surface structure of *Mesovelia*.

The characteristics of the hair piles of other water-walking arthropods are reported in Table 2. The geometry of the hair layer is similar in nearly all water-walkers, but the hair density η varies among species, with the faster species generally having higher hair density. Included in Table 2 are estimates of the contact widths w_c along the tarsi of various water-walkers. The insect's weight is supported by the surface forces that act around the contact lines on its individual hairs. w_c corresponds to the width of the contact region required for the contact forces on the hairs to support the insect's weight: $w_c \sim 2\mathrm{Ba}/(\pi\eta d)$. Note that the contact width decreases with increasing hair density and tarsi length, but increases with insect weight. The extent of the observed contact widths of several water-walking arthropods will be rationalized in Section 6.2.

4.3 STABILITY

An important aspect of the insect cuticle is its stability (Crisp, 1950): if the hair is sufficiently flexible, it may bend or twist under the combined influence of curvature, van der Waals or electrostatic forces. Hair distortion will necessarily lead to gaps in the hair covering, which represent points of weakness in terms of fluid impregnation. Crisp (1950) studied the stability of an air layer bound by uniformly spaced horizontal hairs on a horizontal surface (Fig. 14b) and subjected to a uniform external pressure. He found that if the spacing is varied, hairs in regions with greater spacing may be deflected downwards by the pressure gradient. Moreover, he found that the force of capillary attraction between adjacent hairs (see Section 2.3) may lead to an instability characterized by the clumping of hairs. In the absence of a resistance to bending that maintains the positions of the hairs, the air layer would thus be intrinsically unstable. Thorpe and Crisp (1946, p. 262) considered the stiffness of the hairs, and so assessed their stability to buckling. For the case of *Alphelocheirus*, the air layer is observed to collapse through wetting when subjected to a pressure of 3 atm corresponding to a depth of 30 m. Thorpe and Crisp (1947a) suggest that this collapse results from the buckling of the hairs; however, Hinton (1976) calculates that the hairs should be stable to buckling at 40 atm, advocating the physical picture of effectively rigid cuticle hairs.

The maximum curvature force that can exist between two hairs will arise if they are spanned by a capillary bridge (Rabinovich *et al.*, 2005), in which case a capillary force per length 2σ will draw them together (Fig. 24). van der Waals forces are known to be responsible for strong dry adhesion of gecko setae to smooth surfaces (Autumn *et al.*, 2002) and bundling in carbon nanotube forests (Liew *et al.*, 2005). At nanometre length scales, van der Waals forces become relevant and can be responsible for the sticking of dust particles on the hair surface (Persson, 2003). Electrostatic forces arising from the development of friction-induced charges on the cuticle of honey

TABLE 2 Properties of common water-walking insects and their hair coats

				Strider		*Mesovelia*		*Hydrometra*	*Microvelia*	Fisher Spider
I Macroscopic properties	M	Mass	mg	4.5		3.2		1.8	0.1	350.0
	U	Leg speed	$\mathrm{cm\,s^{-1}}$	37.0		15.9		9.7	10.3	35.0
	w	Leg width	μm	102		68		52	41	1500
	h	Rowing leg length	cm	1.40		0.60		0.80	0.80	0.50
	P	Leg contact perimeter	cm	2.5		0.4		0.5	0.1	10.0
		Hair type		Macro	Micro	Macro	Micro	Macro	Macro	Macro
II Microscopic properties	η	Hair density	$\mathrm{hairs\,cm^{-2}} \times 10^5$	14.0	800.0	4.0	600.0	2.5	5.0	2.5
	d	Hair width	μm	1.5	0.6	5.0	0.5	5.0	1.5	6.5
	L	Hair length	μm	30	7.0	15	3.0	15	25	300
	ω	Tilt angle	degrees	30–50	NA	50	NA	90	50	NA
	δ	Hair spacing	μm	7.0	0.5	10.8	0.8	15.0	14.3	13.5
III Dimensionless groups	$Re_\delta = U\delta/v$	Reynolds		2.6	0.2	1.7	0.1	1.5	1.5	4.7
	$We_\delta = \rho U^2\delta/\sigma$	Weber	$\times 10^2$	1.3	0.1	0.4	0.03	0.2	0.2	2.3
	$Bo_\delta = \rho g h\delta/\sigma$	Bond	$\times 10^{-3}$	2.9	1.1	4.1	0.4	5.4	0.2	4.4

	$Ba = Mg/(\sigma P)$	Baudoin		0.02	NA	0.12	NA	0.05	0.02	0.49
	$r = (1+\eta\pi DL)$	Roughness		3.0	11.6	1.9	3.8	1.6	1.5	16.3
	$G = d^3/(32L^2L_e)$	Elasticity/curvature		12	14	1736	43	1736	NA	NA
IV Calculated values	$P^* = 1+\sigma/\delta$	Impregnation pressure	atm	1.10	2.37	1.07	1.90	1.05	1.05	1.05
	$U_w = (2\sigma \cos \theta_e/(\rho\delta))^{1/2}$	Wetting speed	cm s^{-1}	223	818	179	662	152	156	160
	$Z_w = \sigma\cos \theta_e/(\rho g\delta)$	Wetting depth	cm	25	342	16	224	12	12	13
	$w_c = 2Ba/(\eta\pi d)$	Predicted contact width	μm	0.76	0.03	3.67	0.24	2.39	1.34	19.26

Note: These measurements are gathered from our own SEM study, Hu and Bush (2008a,b), Andersen (1976, 1977, 1982) and Stratton *et al.* (2004a). In general, the fastest creatures have the highest hair density: the water strider has the highest hair density and is the most water-repellent. In II–IV, both types of body hair are considered, the macrotrichia present over the bulk of the body, and the microtrichia present on the thorax. The pressures, speeds and depths sustainable by the cuticle are reported for each of the insects, along with the inferred contact width required for their weight support. In these calculations, θ_e was taken as 105°.

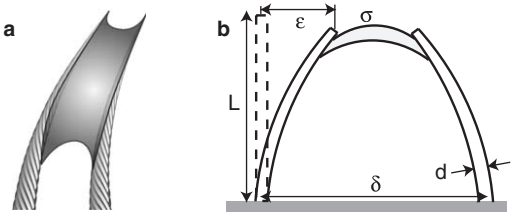

FIG. 24 (a) A schematic illustration of a capillary bridge between two flexible hairs. The resulting contact force will draw the hairs together, jeopardizing the water-repellency of the insect. (b) Definitions of the simple theoretical model of a capillary bridge between elastic rods. The cylindrical rods have diameter d, undeformed length L and are displaced a distance ε at their tips due to the capillary bridge.

bees have been shown to enhance transfer of pollen grains from the flower (Vaknin *et al.*, 2000). Grooming, as is commonly used by most water-walking insects to clean themselves, can generate static-electric charges on the insulating body surface of the insects, resulting in electrostatic repulsion or attraction between hairs.

The following relations provide the relative magnitude of characteristic van der Waals and electrostatic forces to capillary forces expected to arise on insect cuticle:

$$\frac{\text{van der Waals}}{\text{capillary}} \sim \frac{Hd}{\sigma\delta^3} \sim 10^{-12} \tag{18}$$

$$\frac{\text{electrostatic}}{\text{capillary}} \sim \frac{Kq_0^2 d^2 L^2}{\sigma\delta^3} \sim 10^{-13} \tag{19}$$

where d and L are the hair diameter and length, δ the average distance between hairs, $H = 10^{-20}$ J the Hamaker constant, $K = 9 \times 10^9$ Nm^2 C^{-2} the Coulomb force constant and q_0 the average electrostatic charge per unit area on the hair. Choosing typical values for the width, length, hair distance from Table 2 ($d \sim 1\,\mu$m, $L \sim 30\,\mu$m, $\delta \sim 10\,\mu$m) and a charge per unit area of $q_0 = 10^{-8}$ cm^{-2} (the maximum charge sustainable by a bumble bee in flight; Vaknin *et al.*, 2000), indicates that the leg hairs are dominated by curvature forces.

The greatest danger posed to the regular array of hairs comprising the insect cuticle are thus the curvature forces generated by capillary bridges spanning the hairs (Fig. 24). The stability of the hair layer will thus be determined by the relative magnitudes of the hair's resistance to bending and these destabilizing curvature forces.

$$G = \frac{\text{elastic resistance}}{\text{capillary}} \sim \frac{1}{32}\frac{d^3}{L^2\ell_e} \tag{20}$$

where $\ell_e = \sigma/E$ is the elastocapillary length and E the Young's modulus (Bico *et al.*, 2004). Substituting values for the width, length and Young's modulus ($E \sim 10^{11}$dynes cm^{-2}) of the insect hair (Hinton, 1976) suggests $G \sim 10$. The calculation of torsional stiffness is similar and has been examined by Dechant *et al.* (2001).

This crude scaling argument would seem to bring into question the conclusion of Hinton (1976) that the hairs are effectively rigid under the influence of capillary forces. If the hairs become sufficiently long and thin, capillary forces may pose an appreciable danger to the stability of the cuticle. Note that the hairs taper at the tip, where curvature forces are thus likely to cause appreciable deformation. Bico *et al.* (2004) and Kim and Mahadevan (2006) considered the capillary clumping of a series of elastic threads or sheets hanging through a horizontal free surface, and deduced criteria for the resulting elastocapillary instability. The authors define an elastocapillary length, $\ell_e = \sigma/E$ at which capillary forces become comparable to elastic forces. Using the value suggested by Hinton (1976) and Dechant *et al.* (2001) for the Young's modulus of insect cuticle, $E = 10^{11}$dynes cm^{-2}, indicates an elastocapillary length of 10^{-2} nm. While one thus does not expect the clumping of cuticle hairs poking through the surface, hair flexure may still arise. Figure 30 illustrates the interaction of the driving leg of a water strider and a 500 μm droplet moving along its length. Note that individual hairs are deflected by the contact forces associated with the advancing interface, then snap back into position once it has passed (Bush and Prakash, 2007). As we shall see in Section 7, the flexibility of the insect cuticle poses not only dangers but benefits to water-walking arthropods.

5 Function

We proceed by describing the principle functions of insect cuticle, in an attempt to rationalize its form. In Section 5.1, we consider the two types of body hairs discernible on water-walking creatures, respectively, macro- and microtrichia and their distinct roles in maintaining water-repellency. In Section 5.2, we consider the plastron, the air layer trapped on the body surface when an insect is submerged. In Section 5.3, we consider the ungui, the hydrophilic leg tips present on many water-walkers. Finally, in Section 5.4, we discuss the dynamic role of the insect cuticle in thrust generation and drag reduction.

5.1 WATER- AND RAIN-PROOFING

As we noted in Section 3.4, there are in general two criteria for water-repellency. The first is resistance to fluid impregnation while the second is

the resistance to adhesion by droplets. Thorpe and Crisp (1947c, 1949) distinguished between the two in the context of water-faring insects, and referred to them as, respectively, water- and rain-proofing.

To be waterproof, the insect cuticle must maintain a layer of trapped air, thereby retaining a Cassie–Baxter state. Doing so requires that the curvature pressures exceed all fluid pressures acting to cause impregnation. Of particular interest to water-walking arthropods are the hydrostatic pressures that they face if submerged and the dynamic pressures generated by their leg stroke or the impact of raindrops. The fluid pressure in a standing body of water in a static fluid increases with depth from the surface z as $P_0 + \rho g z$, where P_0 is atmospheric pressure, ρ the density of water and g the acceleration due to gravity. Roughly speaking, the hydrostatic pressure $\rho g z$ increases by 1 atm every 10 m. For a submerged hydrophobic body to stay in the Cassie–Baxter state, the curvature pressures generated along its surface must be sufficient to overcome the hydrostatic pressures. If the surface roughness is characterized by a single length scale δ (e.g. hairs of length and radius δ with a spacing δ), then, according to Eq. (17), the water-repellency may be preserved down to a critical depth, the wetting depth Z_w, defined by the balance: $\rho g Z_w \sim \sigma \cos\ \theta_e/\delta$. For $z > Z_w = \sigma \cos\theta_e/\rho g \delta$, an air layer trapped on the surface of an insect will collapse under the influence of hydrostatic pressures. For example, the wetting depth for cuticle with roughness $\delta \sim 1\,\mu m$ is $\sim 10\,m$.

When there is relative motion U between a solid and fluid, dynamic pressures within the fluid (of order $P_d \sim \frac{1}{2}\rho U^2$) may cause wetting. The transition from the Cassie–Baxter to Wenzel states will arise when the dynamic pressure exceeds the characteristic curvature pressure across the roughness, i.e. $P_d > \sigma \cos\theta_e/\delta$, that is for speeds $U > U_w = (2\sigma\cos\theta_e/\rho\delta)^{1/2}$. To avoid the transition to a Wenzel state, the insect must not exceed either the wetting speed U_w or the wetting depth Z_w. The criteria for the preservation of a Cassie–Baxter state for insect cuticle may thus be expressed in terms of surface Bond and Weber numbers

$$Bo_\delta = \frac{\text{buoyancy}}{\text{curvature}} = \frac{\rho g z \delta}{\sigma \cos\theta_e} < 1, \quad We_\delta = \frac{\text{inertia}}{\text{curvature}} = \frac{\rho U^2 \delta}{\sigma \cos\theta_e} < 1 \qquad (21)$$

Figure 25 is a regime diagram indicating the values of Bo_δ and We_δ for a number of semi-aquatic creatures. For all water-walking arthropods considered, $(Bo_\delta, We_\delta) \ll 1$: the curvature forces generated by fluid impregnation are more than sufficient to counter typical hydrostatic and hydrodynamic pressures generated by their leg strokes. Conversely, for large, diving creatures such as the otter, water-repellency is not critical: the air layer initially trapped in their fur is evacuated at depth by hydrostatic pressures.

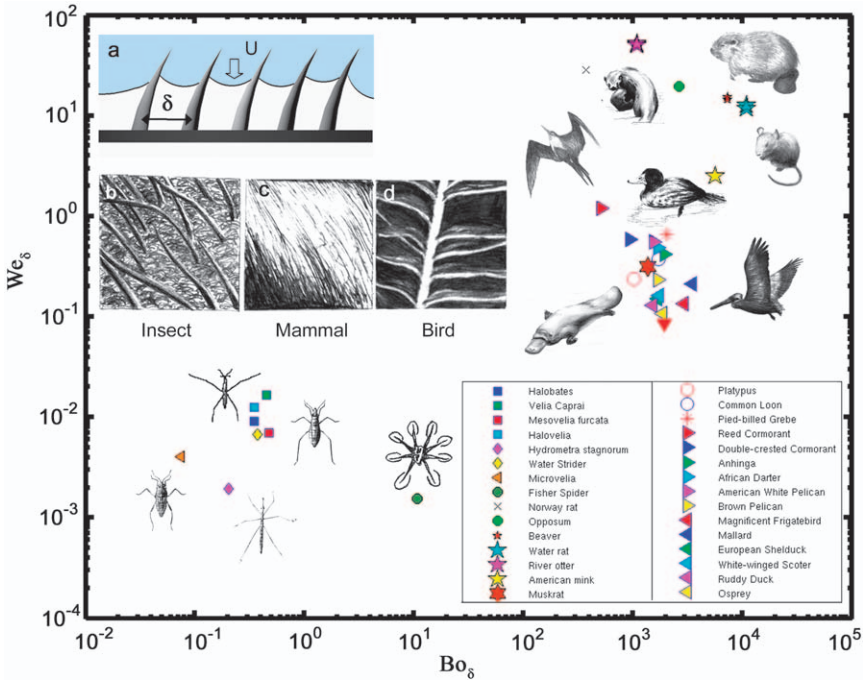

FIG. 25 Weber $We_\delta = \rho U^2 \delta/\sigma$ and Bond $Bo_\delta = \rho g h \delta/\sigma$ numbers characterizing the hair layers of 47 semi-aquatic creatures. (a) A schematic of the hair layer. Here U represents the peak leg speed, δ the inter-hair spacing and h the leg length. Definitions differ from Eq. (21) through omission of the contact angle dependence, owing to uncertainties in θ_e. (b–d) Sketches of water-repellent insect hairs, marine mammal fur and bird feathers (drawn from Dyck (p. 8, 1985) and Grant (p. 25, 1995)). Henceforth we shall refer to the barbs of the bird feather as their "hair". There is a clear division between two types of creatures. The first are water-walking arthropods for which maintenance of hydrophobicity is critical for their survival; the second are the semi-aquatic mammals and birds. The insects are characterized by low Weber number, indicating that their driving legs remain in a Cassie state as they propel themselves on the water surface (Fig. 11c). Conversely, semi-aquatic mammals and birds are characterized by high Bond and Weber numbers, indicating that air trapped in their hairs is forced out by dynamic pressures generated during their driving stroke or by hydrostatic pressures when they dive. Data is taken from Table 2 and collected from Mordvinov (1976), Andersen (1977), Elowson (1984), Fish (1984), Allers and Culik (1997), Fish *et al.* (1997, 2002), Fish and Baudinette (1999), Johansson and Norber (2001), Stratton *et al.* (2004b) and Ribak *et al.* (2005). Illustrations courtesy of Christina Sielert.

Wetting speeds and depths for a number of common water-walking arthropods are listed in Table 2. The impregnation pressure is greatest for the water striders, nearly 2.4 atm, indicating that they can dive to depths of 14 m before the air layer trapped by their microtrichia collapses. Insects

specialized for sub-surface breathing can typically ascend to greater depths (Vogel, 2006), and will be discussed in Section 5.2. The wetting speed for the strider is given by $U_w \sim 300\ \mathrm{cm\ s^{-1}}$, approximately three times the peak speed of its driving leg. We note that the arthropods most susceptible to wetting by hydrostatic or hydrodynamic pressures are generally the slowest moving.

Another fluid pressure that may cause impregnation of a rough solid is the curvature pressure inside small droplets adhering to the surface. McHale *et al.* (2005) studied the evaporation of water drops on superhydrophobic surfaces consisting of pillar-like structures fabricated using photolithography. Zhang *et al.* (2006) examined the so-called fakir transition from a Cassie–Baxter to a Wenzel state for water drops on the lotus leaf and biomimetic polymer surfaces. Contact line motion for evaporating drops in the Wenzel and Cassie–Baxter states differs drastically. A drop in the Wenzel state has a pinned contact line: evaporation occurs with no contact line movement. Conversely, for a drop in the Cassie–Baxter state, evaporation involves discrete de-pinning events at the contact line: the contact line recedes in discrete steps of a magnitude prescribed by the geometry of the surface roughness. Eventually, as evaporation proceeds, a fakir transition occurs, and the drop fluid impregnates the rough solid (Quéré, 2002). McHale *et al.* (2005) report that the transition occurs suddenly and is independent of drop size; however, a criterion for wetting in this situation is suggested by the study of Reyssat *et al.* (2006). In Section 6.1, we report experimental observations of this fakir transition on the legs of water striders.

As we saw in Section 3.4, while both water- and rain-proofing are encouraged by rigid, hydrophobic hairs, they benefit from qualitatively different hair morphologies. Water-proofing benefits from large amounts of solid–liquid contact, while rain-proofing benefits from minimizing this contact so that droplets can most easily escape the body (Extrand, 2006; Gao and McCarthy, 2007). Moreover, rain-proofing benefits from topologies that minimize the length of advancing or retreating contact lines (Joanny and de Gennes, 1984; Yoshimitsu *et al.*, 2002). Thorpe and Crisp (1947c, 1949) postulate different roles for the two hair layers on the thorax: the relatively long and stiff mesotrichia play the role of rain-proofing, while the inner layer of microtrichia play the role of water-proofing in the case of submergence. This two-tiered architecture has been reported in Hemiptera (Cheng, 1973; Andersen and Cheng, 2004), and various other semi-aquatic bugs (Andersen, 1977) including the water strider and *Microvelia* (Fig. 23), and so may be taken as a general feature of water-walking arthropods. According to the considerations of Section 3, the microtrichia's dense packing favours water-resistance. Moreover, they are often curved (Cheng, 1973) so as to arrive tangent to the free surface,

thus further enhancing resistance to fluid impregnation (Crisp and Thorpe, 1948; Section 3.4).

If the corrugations on the macrotrichia are in the vicinity of an interface, one expects on the basis of Eq. (6) that air will intrude to a considerable depth beneath the surface via the equivalent of capillary rise (Shuttleworth and Bailey, 1948). Such corrugations will thus necessarily trap air, thereby decreasing the force of retention of drops that come into contact with the insect cuticle. Moreover, one expects the grooves on the hairs to be beneficial in terms of structural rigidity, increasing the area moment of inertia of the hair without substantially increasing their weight (e.g. Crandall *et al.*, 1978). The dynamical role of the microgrooves will be considered in Section 5.4.

Rain-proofing is generally considered a measure of the ability of a surface to rid itself of small water droplets. For water-walking arthropods, however, the term must be taken more literally: the impact of a raindrop poses a potentially lethal threat. The impact of drops on a hydrophobic surface have been considered by Reyssat *et al.* (2006) and Bartolo *et al.* (2006), who deduced impalement criteria consistent with Eq. (21). Since the terminal velocity of a raindrop may be as large as $U_r \sim 10\ \mathrm{m\ s^{-1}}$, the associated impregnation pressures generated during impact, $\rho U_r^2 \sim 0.8$ atm, may exceed those generated during the leg stroke by two orders of magnitude. It is not entirely surprising that insects have been reported to seek refuge beneath overhanging vegetation, dive beneath the surface or leap vertically during rainstorms, presumably to reduce their exposed target area. Simply put, raindrops have terminal velocities that may exceed the wetting speed of insect cuticle (Table 2), and so pose a real threat to water-walking arthropods. As we shall see in Section 6, however, the wetting of their integument is not fatal: the cuticle dries via evaporation on the timescale of a minute.

The water-resistence of a hair pile will always be determined by its weakest point, for example, a gap in the hair pile. The maintenance of the order of the hairs of the insect cuticle is thus critical for ensuring their water-repellency. Kovac and Maschwitz (1999) discuss the role of grooming in maintaining the hydrophobic properties of various terrestrial beetles, while Stratton *et al.* (2004b) noted the same behaviour in terrestrial and semi-aquatic spiders. The grooming behaviour of a number of water-walking insects is apparent in Fig. 26.

5.2 PLASTRON RESPIRATION

A number of water-walking arthropods cross the surface during the course of their lives. Female water striders may submerge completely while laying

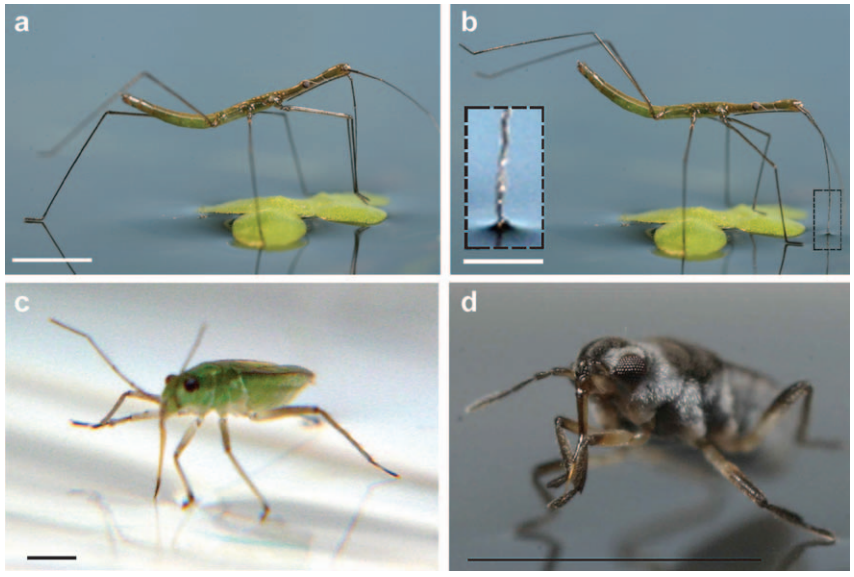

FIG. 26 Grooming of water-walking arthropods. (a) *Hydrometra* grooms its antenna with its forelegs. (b) *Hydrometra* grooms its hind legs by leaning forward, and anchoring with its antenna (see inset). (c) *Mesovelia* leans on its proboscis as it grooms its forelegs. (d) *Microvelia* grooms its proboscis. Scale bars, 1 mm.

eggs (Andersen, 1976) and the resulting strider nymphs hatch from eggs beneath the surface, swimming awkwardly to the surface before puncturing the interface (Fig. 27). Torre-Bueno (1907) reports that Veliidae can submerge completely, and Andersen and Polhemus (1976) report that sea-going water striders also dive to avoid pursuit. Spence *et al.* (1980) report several accounts of subsurface activity in the water strider. The water spider *Argyroneta aquatica* is known to submerge and fish beneath the surface with a bubble that serves as an air supply, periodically replenished from an underwater air-filled bell of silk (Lamoral, 1968). Finally, Kellen (1956) reports that certain intertidal species, such as *Halovelia*, remain submerged at high tide, enclosed in air pockets within porous volcanic rocks. It is also inevitable that water-walking arthropods be accidentally submerged, either by the impact of raindrops, crashing waves or attack from a predator. The hair layer is thus necessary not only in minimizing direct contact with the free surface, but in enabling these creatures to breath if accidentally submerged.

When submerged, many bugs and beetles appear to have shiny coatings owing to a thin layer of air trapped by their hair coating (Noble-Nesbitt, 1963; Rovner, 1986; Hebets and Chapman, 2000; Fig. 28). The term ‘plastron’ for this air layer was coined by Brocher (1909, 1912a,b,c, 1914),

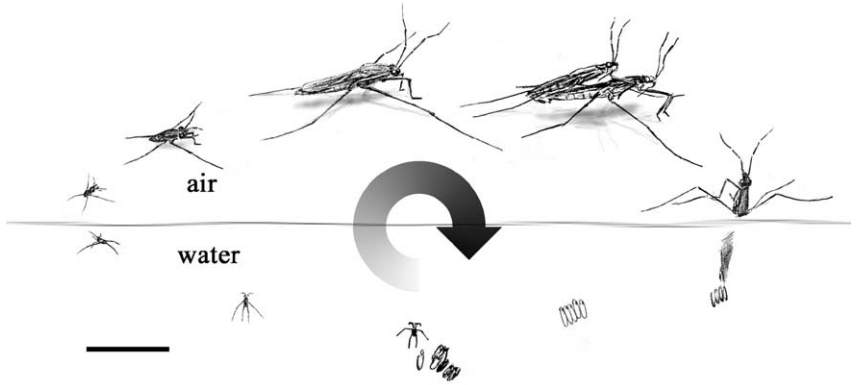

FIG. 27 The life cycle of the most common water-walker, the water strider. Other water-walking insects have a similar cycle involving underwater birth and several stages of growth. Gravid female water striders penetrate the free surface to lay their eggs underwater. The first-instar water striders that emerge from these eggs swim awkwardly towards then puncture the water surface, where their wet cuticle is dried via evaporation (see Fig. 32). Once atop the water surface, they moult several times before reaching adulthood. During mating, the larger female supports the weight of the male. Illustration courtesy of Brian Chan. Scale bar, 1 cm.

who recognized its importance in providing the buoyancy required for the insects to resurface. The importance of the plastron in respiration was first recognized by Straus-Durckheim (1828) and Dutrochet (1837). de Ruiter *et al*. (1951) provide an excellent review of studies of plastron respiration. The viability of plastron respiration was discussed in the context of various aquatic Hemiptera by Dogs (1908), Hagemann (1910) and Hoppe (1911); however, it was Ege (1915) who first provided the theoretical rationale for plastron respiration.

Plastron respiration was examined in a series of papers by Thorpe and Crisp (1947a,b,c, 1949) and Thorpe (1950), and found to be of critical importance to a number of semi-aquatic insects. The plastron is maintained by an array of hairs that lie roughly parallel to the body (Vogel, 2006; Fig. 14b). The ambient hydrostatic pressure is opposed by the curvature pressures generated as the water attempts to impregnate the gas film. The submerged insect breathes the air in the plastron through its spiracles (Fig. 23c), the orifices distributed regularly along its thorax. As the oxygen supply in the plastron is exhausted, oxygen is absorbed across the bubble surface from the ambient water. The plastron thus functions as an external gill: owing to the large surface area to volume ratio of the plastron, it presents an effective means of oxygen uptake from the water. The resulting plastron respiration is effective provided the bubble maintains a critical size, whose limiting value is prescribed by the initial volume of nitrogen

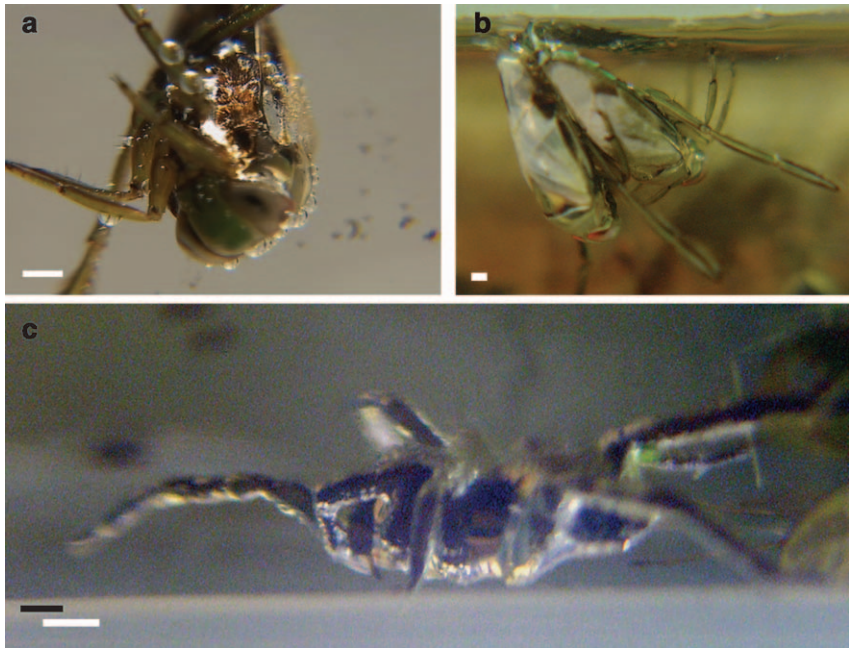

FIG. 28 Plastrons of (a–b) the backswimmer *Notonecta glauca* and (c) the fisher spider, visible as a silver envelope around the body and legs. Oxygen diffuses into these air layers, permitting underwater breathing. Formation of the plastron for the backswimmers begins as individual bubbles that are redistributed into a uniform sheet via vigorous grooming. The fisher spider generates a plastron simply by walking down emerging vegetation to cross the interface, a process documented by Brocher (1910). Scale bars, 1 cm.

in the bubble. Plastron respiration was considered by Vlasblom (1970), and models of gas exchange in a number of diving insects were developed by Rahn and Paganelli (1968), Gittelman (1975), Hinton and Jarman (1976) and Chaui-Berlinck *et al.* (2001). Philip *et al.* (2006) examined the plastron respiration of the backswimmer *Anisops*. By measuring the oxygen partial pressure within the beetle's captured bubble, they confirmed the conjecture of Miller (1964) that it maintains both oxygen levels and buoyancy via exchange with its haemoglobin. Experiments (Thorpe and Crisp, 1947a) indicate that for most insects, the collapse of the plastron typically arose at ambient pressures between 1 and 5 atm, corresponding to depths between 10 and 50 m.

Comstock (1887) and Harpster (1944) noted that certain diving insects actively drive flow over their trapped bubbles by flapping their limbs in 'respiration' movements. Stride (1955) noted that flow past the plastron may enhance the oxygen intake, a theory further discussed by Vogel (2006).

Brown (1987) describes plastron breathing in riffle beetles that live in aerated streams. While Ege (1915), Thorpe and Crisp (1947a) and Hinton (1976) assume that there is no substantial pressure jump across the interface, such will not generally be the case when flow speeds are high, or at great depth, where hydrostatic pressure will bow the plastron interface. Flynn and Bush (2008) note that while a closely packed hair lattice favours water-repellency, it reduces the area across which the insect breathes. By coupling the plastron chemistry and interfacial mechanics, they calculate the range of conditions over which plastrons can function. Shirtcliffe *et al.* (2006) created a biomimetic plastron consisting of a hydrophobic sol-gel foam material. The submerged chamber had a volume of 2.5 cm^3 and an external surface area of about 18 cm^2, and was supplied with oxygen from the water at a constant rate. They suggest that such a device, if scaled up to a sphere of 3 m diameter, might provide enough oxygen to support the oxygen requirements of a human.

Finally, we note the importance of plastron respiration in a number of terrestrial spiders, larvae (Krivosheina, 2005) and insect eggs (Hinton, 1969). During times of flooding, terrestrial insect eggs maintain a plastron via their textured hydrophobic surface, thereby surviving the deluge (Hinton, 1976). The silk nests of terrestrial spiders play a similar role, allowing their inhabitants to survive 10 times longer than in its absence (Rovner, 1986). Krantz and Baker (1982) examine the plastrons of certain species of mites that inhabit aquatic habitats.

5.3 CLASPING THE FREE SURFACE

While virtually all water-walkers have a rough surface coating to render them hydrophobic, many also have hydrophilic body parts that may be used to manipulate the free surface to various ends, including propelling themselves up menisci, launching themselves off the free surface, attracting mates, detecting prey, balancing and anchoring. Nutman (1941), Baudoin (1955) and Noble-Nesbitt (1963) pointed out that many water-walkers have hydrophilic claws or 'ungui' at the ends of their hydrophobic tarsal leg segments that they may use to penetrate or raise the free surface. The curved, conical ungui of the water strider and *Microvelia* are apparent in Fig. 22. Janssens (2005) (see also Thibaud, 1970) describes the ungui of *Anurida* as a three-sided prism, two sides being hydrophobic and the third hydrophylic, and argued the utility of this arrangement for their dynamic stability. The critical importance of ungui in meniscus-climbing by water-walking insects was first suggested by Baudoin (1955).

Figure 9b illustrates the posture assumed by *Mesovelia* during the ascent of a meniscus. The insect pulls up on the free surface with the ungui on its front legs, thus generating a lateral capillary force that draws it up the

meniscus (Section 2.2). The torque balance on the insect requires that it pull upwards with its hind legs. Finally, the vertical force balance requires that its central pair of legs bear its weight in addition to the vertical forces applied by its front and hind legs. Hu and Bush (2005) applied this simple physical picture to account for the ascent rates observed in their experimental study. Both Miyamoto (1955) and Andersen (1976) reported that certain species of insects assume laterally asymmetric, tilted body postures during their ascent. Hu and Bush (2005) rationalized this tilting behaviour by demonstrating that, depending on the relative leg lengths of the insect, tilting may be advantageous in maximizing the capillary propulsive force.

Wigglesworth (1950), Nutman (1941), Baudoin (1955) and Noble-Nesbitt (1963) report that certain surface-dwelling springtails, for example *Podura aquatica* and *Anurida maritima*, have a wetting ventral tube vessical that allows them to locally raise the free surface. Assuming the posture indicated in Fig. 29a allows the springtail to quickly escape aquatic predators: by releasing its grip on the free surface, it is propelled upwards by the curvature forces acting on its nose and tail. This posture also enables them to attract neighbours over a distance comparable to the capillary length (approximately their body length) and so provide capillary stabilization to their floating colony (Fig. 29b). Bounds on the maximum size of such colonies may be inferred from the study of Vella *et al.* (2006b), who develop equilibrium conditions for multiple floating bodies. We note that such capillary forces are presumably responsible for the novel crystal-like packings observed in floating mosquito larvae (Saliternik, 1942).

Many flying insects such as flies (West, 1982; Gorb, 1998) and mosquitoes (Wu and Kong, 2007) have specialized foot pads for anchoring themselves on solids using a variety of adhesion mechanisms (Gorb, 2008). Similarly, many water-walking insects, for example, Collembola (Janssens, 2005), are able to secure themselves to the free surface by way of hydrophilic ungui on their leg tips (Fig. 22). The ungui thus provide water-walking arthropods with a means of anchoring themselves to the surface.

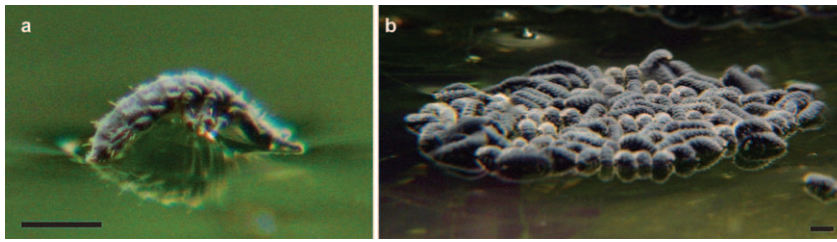

FIG. 29 Capillary attraction of Anuridae. (a) By arching its back and pulling up with its wetting ventral tube, Anurida forms a meniscus that will attract nearby partners. (b) Mutual capillary attraction facilitates the aggregation of an entire colony. Scale bars, 3mm.

The maximum capillary force that can be generated in such a fashion is $F_A \sim \pi D\sigma$, where D is the ungue diameter. For a water strider, $D \sim 30$ μm, so $F_A \sim 1$ dynes is comparable to its weight. It is noteworthy that a characteristic aerodynamic force on such a creature generated by a wind of magnitude $U \sim 1\ \mathrm{m\ s^{-1}}$, $F_a \sim \rho_a U^2 A \sim 1$ dyne (where A is the exposed area), has comparable order. Should a larger anchoring force be required, the creature may presumably wet some fraction of its leg cuticle to increase the contact forces acting thereon. In Fig. 26b, the antenna of *Hydrometra* is evidently being used as an anchor as it grooms its hind legs.

5.4 DRAG REDUCTION AND THRUST GENERATION

While the importance of the rough arthropod integument for water-repellency has been given considerable attention, its dynamical role has only recently been considered (Bush and Prakash, 2007). The role of superhydrophobocity in drag reduction is currently the subject of vigorous research (Cottin-Bizonne *et al.*, 2003; Choi and Kim, 2006; Choi *et al.*, 2006; Joseph *et al.*, 2006). When a rough surface advancing through a fluid is in its Cassie–Baxter state, that is, when much of its effective area is covered in air, the opposing viscous stresses are greatly diminished. Joseph *et al.* (2006) measured the velocity profiles of flow parallel to surfaces covered in carbon nanotube forests. For a surface in the Cassie–Baxter state, the net effect of the surface roughness is to reduce the tangential stresses felt at the boundary by an amount proportional to the ratio of the exposed solid area to the planar area. One thus expects that the rough surface of water-walking insects is important not only in maintaining their water-repellency, but in reducing their drag as they glide along the surface (Bush and Prakash, 2007).

The effects of anisotropic surface roughening on drag have also been considered. Patterning surfaces with microgrooves aligned with the flow may decrease drag by 5–10%, and is the basis of riblet technology (Walsh, 1990), which is finding applications in both aircraft and sailboat design (Choi *et al.*, 1996; Bechert *et al.*, 2000). For a surface with microchannels in the Wenzel state, Min and Kim (2004) demonstrate that the surface topography generally decreases hydrodynamic drag in the direction of the channels. Choi *et al.* (2006) examined the flow past superhydrophobic microchannels of characteristic width 200 nm in a Cassie–Baxter state. Drag was found to be reduced substantially in the direction of the grating owing to the air trapped in the grating. Conversely, the drag generated by flow perpendicular to the grating was enhanced relative to that on a smooth surface. We thus expect that both the orientation of the hairs and the presence of the nanogrooves on the macrotrichia will serve to reduce the drag on legs gliding along their length. Conversely, we expect these linear

features to enhance the resistance to the leg motion perpendicular to the direction of motion: the propulsive thrust generated in the driving stroke is thus maximized.

The water-repellency of a surface depends not only on a high contact angle, but on low drop adhesion (Gao and McCarthy, 2007). The force of retention depends not only on the contact angle hysteresis, but on the contact line geometry (Extrand, 2002, 2006). The influence of surface topography on the force of adhesion has been considered by Bico *et al.* (1999). Yoshimitsu *et al.* (2002) examined the force of adhesion that acts on water droplets suspended in a Cassie–Baxter state on surfaces decorated with grooves and pillars. They place a droplet on the surface and measure the critical tilt angle at which the force of gravity exceeds the force of adhesion, and the droplet rolls off the surface. Their experiments clearly demonstrate that drops roll with greatest ease in the direction of the grooves and with greatest difficulty perpendicular to the grooves; the case of square pillars being intermediate between the two. Their observations may be understood on the grounds that contact lines move with greatest difficulty in a direction normal to the line: imperfections existing even on a smooth surface cause the contact line to be caught, and the associated creation of surface area is energetically costly and so resists motion (Joanny and de Gennes, 1984; Nadkarni and Garoff, 1992). The experiments of Yoshimitsu *et al.* (2002) beautifully demonstrate the importance of the geometry of surface topography on adhesion; moreover, it allows us to rationalize the tilted hair orientation and grooved structures on the macrotrichia of water-walking insects.

For a water-walker on top of the free surface, the macrotrichia alone interact with the free surface. The nanogrooves on the macrotrichia reported on the water strider (Andersen, 1977; Gao and Jiang, 2004) and the *Microvelia* (Section 4) may be a generic feature of water-walking arthropods. When a hair slides in the direction of the grooves, the grooves minimize the extent of the advancing and retreating contact line (Yoshimitsu *et al.*, 2002), thereby reducing the contact force on the insect cuticle and associated drag on the insect. Conversely, when such a hair brushes the surface in a direction perpendicular to the grooves, relatively large contact forces will be generated. This would seem to be an important feature of the driving stroke: insects such as the water strider strike the surface perpendicular to the grooves, thereby generating large contact forces. Thereafter, they swing their legs through a 90° angle to align with the direction of motion, thereby reducing the contact force and allowing their legs to release from the free surface.

Water-walking arthropods rely on contact forces for both their weight support and propulsion; for both purposes, they benefit from maximum contact with the free surface. The maximum thrust is bounded by the total contact force sustainable by the cuticle during the driving stroke: if the

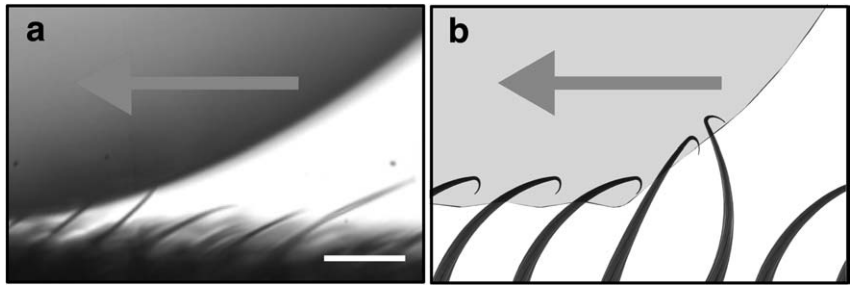

FIG. 30 Flexibility of insect cuticle caused by its interaction with a moving fluid interface. (a) The hairs on the driving leg of the water strider bend significantly when subjected to contact forces generated by a drop moving against the grain of the hairs. Once the drop has passed, the flexible hairs snap back into position. (b) A schematic illustration of the same.

applied force exceeds this value, the leg will detach from the free surface. By considering the geometry of the leg strike, one can thus rationalize the alignment of the leg hairs and nanogrooves on the macrotrichia, which both maximize the contact force felt by the driving leg. Contact forces are felt along each hair in contact with the free surface: moreover, they are amplified proportionally to every air-filled groove on the macrotrichia. To lift its legs following the driving stroke, the arthropod must detach from the free surface, and so overcome the contact forces acting on it (Fig. 30). This may be done most easily by withdrawing the leg along its length in a peeling motion, so that the contact force acts only across the wetted fraction of the hairs. Bush and Prakash (2007) thus argue that the variation in the contact force, as generated by the anisotropy of the insect cuticle in conjunction with the geometry of the leg stroke, is the basis for the propulsion of water-walking arthropods.

6 Imaging techniques

We proceed by reviewing microscopy techniques used in imaging solid–fluid interfaces, and highlighting the potential importance of these techniques in gaining insight into the dynamics of water-walking arthropods. In Section 6.1, we describe SEM imaging, giving particular attention to the advantages of wet-SEM over traditional SEM in imaging the interaction between insect cuticle and the free surface. In Section 6.2, we describe advances in optical imaging, including confocal imaging of 3D fluid interfaces, and interfacing with high-speed videography. We also describe a modified inverted confocal microscopy technique that enables one to study the dynamic interaction between live water-walking arthropods and the

free surface. In Section 6.3, we describe recent advances in scanning probe microscopy and its applications in imaging fluid interfaces at nanometric length scales. A discussion of recent advances in Particle Image Velocimetry (PIV) and micro-PIV techniques relevant to this class of problems is presented in Steinmann *et al.* (2006).

6.1 SCANNING ELECTRON MICROSCOPY

A huge advance in our understanding of the form of the insect cuticle accompanied the development of the SEM by Knoll (1935). The technique was improved upon until, by 1952, the instrument (built by Sir Charles Oatley) had achieved a resolution of 50 nm (Breton, 1999). Prior to the SEM, imaging small-scale objects relied on optical microscopy. An empirical limit, the Rayleigh criterion, yields the spatial resolution Δl (the minimum distance between two point objects that a microscope can clearly resolve) of a lens of diameter D and focal length f in terms of the wavelength λ of the light source: $\Delta l = 1.22 f\lambda/D$. This fundamental limitation was overcome by the invention of the SEM, which uses a beam of energized electrons instead of a light source. Modern SEMs yield resolutions of order 1–5 nm.

SEM is a scanning microscope, wherein a beam of electrons is focused at a narrow spot on the sample: electrons emitted from the sample are captured at the secondary electrodes. The main components of the microscope are the electron gun (for generating the high energy electron beam), electromagnetic lens assemblies (to focus and control the electron beam), low-pressure imaging chamber and a low-vibrational noise sample stage. The focused beam spot is scanned over an imaging area and the resulting intensity map (constructed from the current at the secondary electron electrode) is captured and stored as an image. Various parameters (e.g. pressure, gas composition, temperature and humidity) need to be precisely controlled inside the imaging chamber.

Most of the insights gained into the microstructure of the integument of water-walking arthropods reported in Section 4 were obtained via SEM. While traditional SEM provides very high-resolution images ($\sim 1-5$ nm resolution), the samples are subjected to extremely low vacuum pressures of order 10^{-9} atm. Such a vacuum is a harsh environment for biological samples, and may result in dehydration, crumpling and buckling of the sample. Moreover, only completely dry samples can be imaged effectively in this manner, thus precluding the possibility of studying the interaction between arthropod cuticle and fluid interfaces.

Various techniques have been developed to prepare biological samples for traditional SEM imaging. A common problem in SEM imaging of insulating surfaces (e.g. insect cuticle), charge build-up, may be averted by

coating the sample with a very thin layer (~ 1 nm) of a highly conducting surface, such as gold, platinum, graphite or tungsten (Reimer, 1998). A disadvantage of such coatings is that they modify the surface properties of the sample. Consequently, the sample cannot be used for studies where the surface chemistry is important, for example, to consider the interaction between water droplets and insect cuticle. Recent techniques for rapid freezing have made it possible to image fully hydrated biological samples using cryo-SEM (Walther and Muller, 1997; Craig and Beaton, 1996). While this method allows for imaging of delicate plant tissue and cells with no crumpling and buckling of the sample, its disadvantage is that ice crystals may form during cooling, damaging the sample and producing erroneous imaging artifacts.

A modification of traditional SEM techniques, wet or environmental SEM, provides a means of imaging samples with water vapour inside the imaging chamber (Donald, 2003). Jenkins and Donald (1999) and Stelmashenko *et al.* (2001) used wet SEM to directly measure contact angles and surface properties of partially wetting droplets on various substrates. In the context of insect cuticle, wet SEM allows for imaging without evaporation and dehydration of the sample. Moreover, it introduces the possibility of visualizing the interaction between the cuticle and the free surface in both static and dynamic settings. The technique relies on the exact control of three parameters inside the imaging chamber; temperature, pressure and water vapour pressure. Moreover, since no pre-treatment is required for imaging insulating substrates for wet-SEM, the surface properties are unmodified during the imaging procedure; this is crucial for studying the wetting properties of biological samples.

The principle difference between SEM and wet-SEM lies in the sample environment. In both cases, the electron gun is maintained at low pressure (1.3×10^{-9} atm). For the case of wet-SEM, the imaging chamber pressure can be as high as 10^{-2} atm. This is achieved by a differential pressure valve isolating the high- from the low-pressure regions. Thus the imaging chamber can be filled with various gases and water vapour, keeping the sample hydrated over an extended period. Since electrons colliding with gas molecules produce positive ions, no build-up of negative charge occurs on insulating samples. Moreover, a Peltier stage can be used to control condensation onto (or evaporation from) the sample. The resulting precise temperature, pressure and humidity control inside the imaging chamber is useful for studying structure-interface interactions in various experimental conditions.

The first biological application of wet-SEM was an examination of the interaction of droplets and the lotus leaf. Recent ESEM imaging demonstrates a fakir transition between Cassie–Baxter and Wenzel states for drops of a size comparable to the roughness scale (Cheng and Rodak, 2005). We here use wet-SEM techniques to image the interaction of the free

surface with the cuticle of water-walking insects; specifically, an XL30 ESEM from FEI Company was used to image wet samples of water strider legs. Legs from recently dead water striders were mounted on a silicon substrate and sprayed with a water mist to form a thin water film on the leg surface. Samples were then introduced into the imaging chamber, mounted inside the SEM on a three-axis stage. The chamber was carefully pumped up to 3×10^{-3} atm following the procedures of Stelmashenko *et al.* (2001) and Donald (2002), injecting water vapour from time to time to avoid complete dehydration of the sample. Figure 31 illustrates the fakir transition that accompanies the evaporation of an initially 10-μm-scale drop on a water strider leg using a conventional video microscope. Given the dangers inherent in such a transition, that transforms the cuticle from hydrophobic to hydrophilic, it bears further consideration in this biological context.

Figure 32 presents environmental SEM images of a thin water film that completely coats and wets the hairy surface of a water strider leg. Images of the film interface were taken at various beam energies as the water film evaporated. In the first image, the hairs are all coated with water, but are apparent as deformations of the free surface. In the second image, evaporation has reduced the mean film thickness and hairs have penetrated its surface. Note that the entire time taken for the wetted cuticle to dry via evaporation was ~ 30 s. This imaging technique is expected to yield valuable insight into the stability of the hair layer. We are currently performing a more extensive set of experiments to explore the nature of the interaction between insect cuticle and the air–water interface.

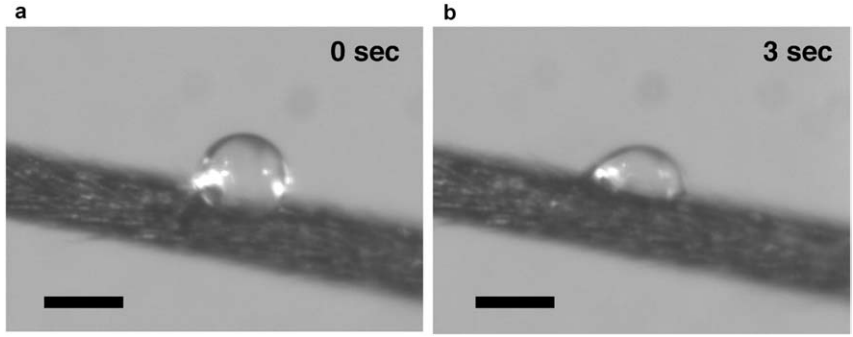

FIG. 31 The fakir transition of a water drop on a water strider leg. (a) A water drop initially deposited on the leg exhibits a high contact angle ($\sim 167^\circ$; Gao and Jiang, 2004), and is in a Cassie–Baxter state. (b) After evaporating for 3 s, its contact angle decreases dramatically to 60°, indicating a transition to a Wenzel state. Not shown: after 7 s, the drop has completely evaporated. Sequence photographed using a stereo microscope (STEMI Stereomicroscope by Zeiss). Scale bars, 200 μm.

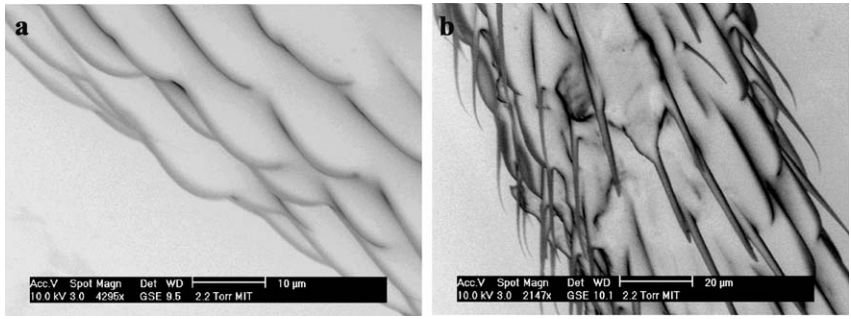

FIG. 32 The evolution of a thin film of water on the surface of a strider leg, as imaged via wet-SEM. (a) A fully wetted water strider leg: a water film covers the entire leg. The 10-μm-scale hairs generate indentations beneath the free surface. (b) After 10 s, the film has evaporated to the point that hairs poke through the free surface. Hairs are not visibly distorted by their interaction with the interface. The entire process of evaporative drying takes $\sim$30 s, and provides an important means of restoring the water-repellency of the cuticle following submergence.

6.2 OPTICAL MICROSCOPY

Even though SEM and wet-SEM imaging techniques provide unprecedented resolution and fine details of the interface-body interaction, the imaging environment is generally too harsh for live samples. This precludes the possibility of elucidating the dynamic interaction between a live insect leg and the free surface. We proceed by reviewing recent advances in optical imaging that make it possible to do so.

Laser-scanning-based confocal microscopy techniques provide a means to image dynamic 3D fluid interfaces with a resolution of order 1 μm. The underlying principles for confocal microscopy were first developed by Minsky (1953, 1988) to study the 3D structure of brain cells, and the technique was widely adopted in the biological community in the 1980s with the advent of commercial systems with multiple light sources and automated laser slicing. The technique uses an extremely thin focal plane and a laser as a light source. Images are taken through different slices, then later combined to construct a 3D map. Aarts *et al.* (2004) used confocal imaging to study the interfacial dynamics of a phase-separated colloid-polymer dispersion, observing thermal fluctuations on a fluid–fluid interface for the first time.

A conventional microscope configuration consists of an eyepiece and an objective above a sample holding stage with back or side illumination. An inverted microscope configures the light source on the top of a sample holding stage, while the objective and the eyepiece lie below the image sample plane. The inverted microscope is well suited to imaging the interface with live samples from below, yielding a resolution of order 2 μm.

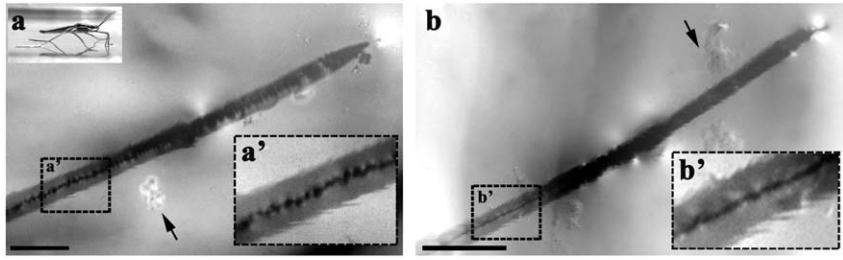

FIG. 33 Two views from below of the contact of a water strider leg with the underlying water. Only a single line of hairs intersects the free surface (rationalized in Table 2). The small white droplets of oil (indicated by the arrows) were shed by the leg. The photomicrographs were taken with an inverted microscope (Zeiss LSM Pascal) and a 20x and a 50x objective lense. Live insects were imaged as they moved freely on a water film above the microscope objective. Scale bars, 100 μm.

Bush and Prakash (2007) present a new inverted microscope technique that allows for both static and dynamic high-resolution imaging of the free surface and contact lines in water-walking arthropods. Our images yield new insight into the nature of the contact between water-walkers and the underlying fluid.

In Fig. 33, we present a series of inverted microscope images (Zeiss LSM Confocal microscope) of the contact of a live water strider leg with the free surface. The darker regions indicate the regions of contact with the surface. Note in Fig. 33 that only a small fraction of the leg, indicated by the thin dark line along the leg's centerline, is in contact with the surface: the weight-bearing section is narrow relative to the leg width. In Fig. 33a, the leg tip is marked by a bright white spot that results from the interaction of the hydrophilic ungue with the water surface. Small droplets of an oil-like substance released from the leg, perhaps cuticle wax, are apparent as white blobs floating on the surface.

Figure 34 is a series of inverted microscope images of a *Microvelia* standing on the water surface. The outline of the overlying insect body is clearly visible in the photomicrographs. The images depict *Microvelia* grooming; consequently, not all of its legs are in contact with the surface. The precise nature of the contact line on the insect cuticle may be observed by zooming in on the area of interest. Figure 34 depicts pinholes corresponding to individual hairs in contact with the water surface. The water strider needs only a single line of hairs to support its weight; conversely, since *Microvelia* has relatively shorter legs and a lower hair density, it requires a relatively broad swath of hairs to support its weight. The predicted values of w_c reported in Table 2 are thus consistent with those observed in Figs. 33 and 34. To the best of our knowledge, these images present the most detailed picture of the interaction between the

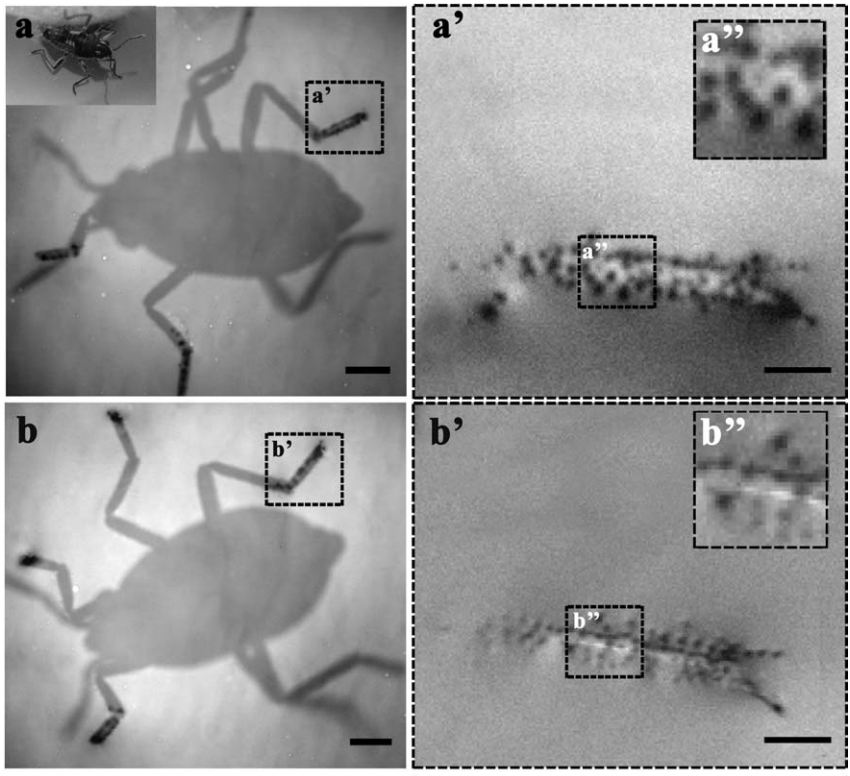

FIG. 34 The contact of *Microvelia*, as viewed from below. Its tarsi are shorter and less piliferous than those of the water strider leg, as can be seen by comparing Figs. 21a and 23a. Consequently, a contact region 5 hairs wide and 50 hairs long intersects the free surface, generating a pincushion-like deformation signature. The contact widths of various water-walking arthropods are rationalized in Table 2. The photomicrographs were taken as in Fig. 33. Scale bars, 20 μm.

interface and water-walking insects, and give clear evidence of the cuticle being in a Cassie–Baxter state.

Recent developments in high speed imaging provide insight into the fast interactions between solids and interfaces (e.g. Bergmann *et al.*, 2006). In Fig. 35, we show the interaction of a water strider leg tip with the free surface as imaged with a high-speed camera (Phantom V5, Vision Research). As we saw in Fig. 22, the ungui at the leg tips of water-walkers are smooth and hydrophilic. The leg of a dead water strider was mounted on a micro-positioner and brought down to the interface until its ungue just touched the interface. Thereafter, the leg was slowly extracted until the free surface was released by the ungue. The sequence of

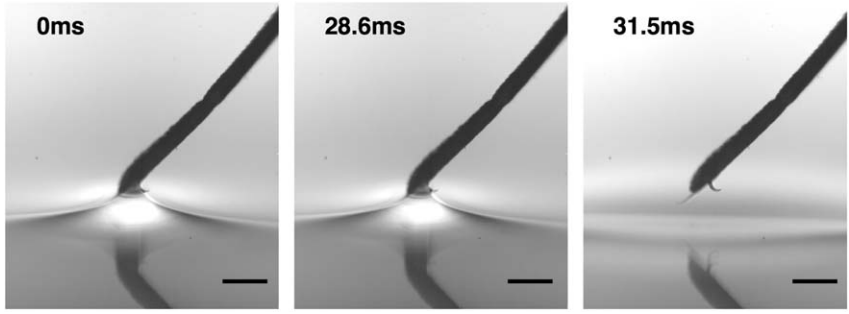

FIG. 35 A sequence of high-speed photomicrographs depicting the ungue of an adult water strider releasing the free surface. The initially wet ungue is slowly extracted from the water surface until the point of release. The sequence was taken using a high-speed video camera (Phantom V4). Scale bars, 100 μm.

images illustrates the rapid detachment of the free surface from the hydrophilic ungue.

Topographical imaging of fluid interfaces at such small length scales is a nascent field for which no quantitative high-speed imaging techniques have been developed. Techniques allowing reconstruction of the fast, microscopic distortions of fluid interfaces would greatly enhance our understanding of the dynamics of this class of problems.

6.3 SCANNING PROBE MICROSCOPY

In scanning probe microscopy, weak force interactions between a pointed tip and imaging substrate are utilized to image a sample. In essence, a mechanical, pointed probe (of diameter 10–100 nm) is scanned over the sample, and the deflection of the probe is measured optically or electronically. Since no light or particle source is used for illumination, this provides the highest resolution of any microscopic imaging technique, with resolutions on the order of molecular dimensions.

In Atomic Force Microscopy (AFM), a micro-scale cantilever is used to image a surface by scanning it over a given sample. Various interaction forces between the cantilever tip and the sample can be used, including contact, capillary, van der Waals, electrostatic and chemical forces. It is also possible to modify the tip geometry or chemistry to enhance the force being characterized. The deflection of the micro-scale cantilever during scanning operation is measured by an optical lever: by shining a laser beam onto the top surface of the cantilever.

Snyder *et al.* (1997) and Aston and Berg (2001) modified the AFM technique to image fluid interfaces at small length scales (a technique referred to as Fluid-Interface AFM). A polystyrene bead was attached to

the cantilever tip, and used to image an oil drop in water using a tapping mode. The capillary force of attraction between the bead attached to the cantilever tip and the oil–water interface was used to image the oil drop. Owing to the sensitivity of the AFM cantilevers, dynamic drop deformations due to particle–drop interactions can be imaged. Numerous authors (Lou *et al.*, 2000; Agrawal *et al.*, 2005; Agrawal and McKinley, 2005) have used AFM microscopy to image the spontaneous formation of nanometre-scale air pockets on hydrophobic surfaces. The ability to image dynamic interfaces on the nanometre scale using AFM will significantly enhance our understanding of fluid–structure interactions.

7 Discussion

It is ironic that workers in the subject water-repellency, first motivated by a desire to control the insect population, are now drawing their inspiration from this population. We have reviewed the modern theory of water-repellency and its relevance in understanding the integument of water-walking arthropods. We have seen that arthropod cuticle exhibits many of the characteristics of optimally hydrophobic surfaces. Moreover, we have noted the similarities and differences between the surface structure of plants and water-walking arthropods. The differences, in particular the anisotropic adhesive properties of the arthropod cuticle, have been rationalized in terms of their additional dynamical role.

The epicuticle of water-walking arthropods consists of a waxy substance that increases the contact angle beyond 90°; therefore, the addition of surface roughness renders the insect cuticle hydrophobic rather than hydrophilic, allowing the cuticle to remain in a Cassie–Baxter rather than a Wenzel state. Roughness arises in the form of an array of hairs, the form of which varies slightly from species to species and on different body parts of a given species. All water-walking insects and arthropods are covered in a layer of hairs that are tilted relative to the body surface so that they meet the free surface at an oblique angle, thus providing enhanced resistance to fluid impregnation (Crisp and Thorpe, 1948). This hair layer is most dense on the leg tips, where it precludes the impregnation of water under the influence of hydrodynamic pressures generated by the driving stroke. The outermost layer of macrotrichia is responsible not only for resisting impregnation pressures, but for channelling water droplets off the insect's surface (Thorpe and Crisp, 1949). On their thorax, most water-walking arthropods have a second relatively fine inner hair layer, microtrichia, that serves to preserve a plastron against hydrostatic pressures when the insect is submerged, thus enabling them to breathe underwater. In terms of wetting, the greatest risk to water-walking arthropods is the impact of raindrops.

In the case of fluid impregnation of the cuticle, recent experiments indicate that evaporation evacuates the cuticle in less than a minute.

The role of a second scale of roughness, specifically, grooves on the macrotrichia (as evident in our SEM images of the water strider and *Microvelia*), has only recently been considered. Gao and Jiang (2004) point out its importance in increasing the apparent contact angle of water on water strider cuticle; however, its dynamical significance has only recently been considered (Bush and Prakash, 2007). Feng *et al.* (2002) demonstrate that the anisotropic roughness on the hydrophobic rice leaf causes water droplets to roll parallel rather than perpendicular to the leaf edge. Yoshimitsu *et al.* (2002) clearly demonstrated that grooves of sufficient amplitude to maintain a Cassie–Baxter state act to dramatically reduce the force of adhesion in the direction of the grooves and to increase it in the perpendicular direction. This study suggests two dynamic roles of the nanogrooves. First, they reduce the force of retention parallel to the hairs, and so permit drops striking insects to more readily roll off them. Second, owing to the alignment of the hairs and the nanogrooves, the retention force experienced by a strider leg will be larger when the leg is aligned perpendicular than parallel to the flow. Bush and Prakash (2007) thus rationalize the form of the driving stroke of the water strider: the leg strike perpendicular to the direction of motion maximizes the propulsive contact force, while the alignment of the rear pair of legs with the direction of motion minimizes drag as they glide along the surface. The driving leg is extracted by lifting it along its length in a peeling motion; here again, the topology of the cuticle is beneficial, as the force of extraction is minimized by the grooved hairs. Finally, Bush and Prakash (2007) demonstrate that the leg cuticle exhibits unidirectional adhesion: fluid advances most easily towards the leg tip, and with greatest difficulty perpendicular to the leg. The implications of the unidirectionality of insect cuticle are currently under investigation.

Consideration of the flow on the scale of the insect cuticle requires that we revise the macroscopic view of both the statics and dynamics presented in Section 2. In terms of statics, the contact line is not the perimeter of the tarsus, but rather those around individual hairs (Fig. 6). Nevertheless, the total vertical curvature force available for weight-bearing is limited by the generalized Archimedes law: the total force on a floating body is precisely equal to the fluid displaced by the body. The air trapped in the cuticle displaces fluid, thereby enhancing the buoyancy force that bears the insect's weight. In considering the dynamics, the relevant length scale changes from the width of the driving leg to that of the hairs or perhaps even the nanogrooves on the hairs. Flows on this scale are characterized by $(Re, We) \ll 1$ and so dominated by fluid viscosity and surface tension. Moreover, we expect the surface roughness to affect all of the components of the propulsive force enumerated in Section 2.3. The physical picture that

emerges is thus one of a small-scale viscously dominated flow on the scale of the individual hairs combining to give rise to a bulk flow on the scale of the insect leg. Hu *et al.* (2003) and Hu and Bush (2008a) performed the first flow visualization studies of water-walking arthropods, and demonstrate that their wake is typically characterized by vortices that allow one to understand their propulsion in terms of momentum transfer. Consideration of the precise form of the contact between the arthropod and the water surface indicates that the vortices are generated by viscous interaction with the hairs on the driving legs.

A problem that has received very little attention is strategies of detachment from the free surface. Such strategies would seem all the more important given that the need to escape from an air–water surface is common to all insects: terrestrial insects must contend with capillary forces in times of heavy rain or flooding, and flying insects whenever they land on a body of water. While the contact perimeter may be reduced through the rough water-repellent cuticle, there are nevertheless contact forces that must be overcome to detach from the free surface, as arises with every step of a water-walker. The nanogrooves on the macrotrichia of the water strider and *Microvelia* suggest an interesting detachment mechanism. The grooves will tend to favour attachment through a single film of water whose thickness t is prescribed by the spacing between the nanogrooves. Tilting of the hair relative to the water surface will generate a film with a free edge that will necessarily retract under the influence of the surface tension force per length 2σ. Neglecting the effect of the body surface, one expects the sheet to retract at the Culick speed $U = (2\sigma/\rho t)^{1/2}$ that necessarily increases with decreasing sheet thickness t. Choosing $t = 500\,\text{nm}$ yields a retraction speed $U \sim 10\,\text{m}\,\text{s}^{-1}$. The details of this detachment mechanism are currently under investigation theoretically and experimentally.

One subject that certainly merits further investigation is the influence of elastic deformation of insect cuticle under the influence of capillary forces. While such deformation was proposed by Thorpe (1950) to set the maximum depth to which diving insects could descend, Hinton (1976) argued that the cuticle is effectively rigid at such pressures. Nevertheless, the recent study of Bush and Prakash (2007) indicates that the elastic deformation of arthropod cuticle is dynamically significant. Zheng *et al.* (2007) demonstrate that butterfly wings exhibit anisotropic adhesive properties: drops roll readily towards the wing's edge, but are pinned if they roll in the opposite direction. This directional adhesion was explained in terms of the wing's surface structure, which consists of a series of 50 μm scales themselves composed of a series of 500 nm bundles of tubes of diameter 100 nm aligned perpendicular to the wing's edge. From each of these bundles, one flexible tube protrudes. When drops roll towards the wing edge, the flexible tube is compressed and lies flush with its bundle. When they roll in the opposite direction, the tube tip is deflected away from its bundle, resisting drop

motion through the generation of surface energy. Bush and Prakash (2007) indicate that similar mechanisms arise on the cuticle of water-walking arthropods. The role of the flexibility of insect cuticle is currently being investigated both theoretically and experimentally.

Variable wetting properties are used by terrestrial insects to good effect. Certain bark-inhabiting bugs have hydrophilic body parts that are wetted by rain water so as to provide better camouflage against the backdrop of wet bark (Silberglied and Aiello, 1980). Just as water-walking insects maintain a thin layer of air with their hair layer, these creatures can preserve their camouflage by supporting a thin layer of water. The beetle *Stenorca* inhabits the Namib desert where it virtually never rains; thus, out of necessity, it has developed an ingenious means of condensing water from fog droplets in the 1–40 μm range (Parker and Lawrence, 2001). Its bumpy back consists of a series of hydrophilic peaks (of characteristic diameter 0.5 mm) in hydrophobic troughs: the fog drops thus stick to the peaks and grow by accretion until reaching a size that will allow them to be blown by the wind towards the insect's mouth. This technique is currently being investigated as a means of condensing water in inhospitable regions of the world.

Fundamental fluid mechanics problems are also suggested by this review. Recent studies have illustrated the importance of wetting properties on the form of the flow generated by bodies striking the free surface. Duez *et al.* (2007) examined a falling sphere impacting a free surface and found a surprising dependence on the sphere's wetting properties. In the high Re and We limits, where a smooth sphere makes no splash, a pronounced cavity and splash accompanied the roughened sphere. This study raises many interesting questions concerning the influence of water-repellency on water-walking arthropods. Through increasing the splash, hydrophobicity presumably increases the collapse time of the cavity, thereby granting the creature more time to withdraw its leg. The influence of water-repellency on impact in the small Bo limit of interest to water-walking arthropods is currently under investigation (Aristoff and Bush, 2008).

Finally, recent technological advances in microscopy, specifically, wet-SEM and inverted confocal microscopy, promise important insights into the interaction of insects and the water surface. Particular attention should be given to elucidating the detailed nature of the static and dynamic interactions between the interface and the micron-scale cuticle hairs. Coupling these microscopy techniques with high-speed videography is likely to yield unprecedented insights into dynamic wetting and optimal water-repellency. Providing the link between the micro- and macroscale dynamics will prove invaluable in rationalizing the locomotion of water-walking arthropods; moreover, it is likely to play a critical role in the engineering of smart surfaces, for example, those capable of self-cleaning, water-repellency and directional adhesion.

Acknowledgements

The authors thank David Quéré and two anonymous reviewers for their thoughtful comments on the manuscript; Mathilde Callies Reyssat for kindly forwarding an early version of her thesis; Robert Suter for generously sharing his data on the wetting properties of spiders and Lucy Mendel and Brian Chan for their assistance with illustrations. The authors gratefully acknowledge the financial support of the NSF: JB through grant CTS-0624830 and Career Grant CTS-0130465; DH through a Mathematical Sciences Postdoctoral Research Fellowship and MP through grant CCR-0122419. MP also acknowledges the microscopy resources at Center for Bits and Atoms, and thanks Jaebum Joo for assistance with the wet SEM.

References

Aarts, D. G., Schmidt, M. and Lekkerkerker, H. N. W. (2004). Direct visual observation of thermal capillary waves. *Science* **304**, 847–850.

Adam, N. K. (1948). Principles of penetration of liquids into solids. *Discuss Faraday Soc.* **3**, 5–11.

Adam, N. K. (1963). Principles of water repellency. In: *Waterproofing and Water-repellency* (ed. Moilliet, J. L.), pp. 1–23. New York: Elsevier.

Adamson, A. W. (1982). *Physical Chemistry of Surfaces*. New York: Wiley.

Agrawal, A. and McKinley, G. H. (2005). Nanobubble formation at the solid–liquid interface studied by atomic force microscopy. *Mater. Res. Soc. Symp. Proc.* **899**, 146–151.

Agrawal, A., Park, J., Ryu, D., Hammond, P., Russell, T. and McKinley, G. (2005). Controlling the location and spatial extent of nanobubbles using hydrophobically nanopatterned surfaces. *Nano Lett.* **5**, 1751–1756.

Alexander, R. M. (1985). The maximum forces exerted by animals. *J. Exp. Biol.* **115**, 138–231.

Allers, D. and Culik, B. M. (1997). Energy requirements of beavers (*Castor canadensis*) swimming underwater. *Physiol. Zool.* **70**, 456–463.

Andersen, N. M. (1976). A comparative study of locomotion on the water surface in semiaquatic bugs (Insects, Hemiptera, Gerromorpha). *Vidensk. Meddr. Dansk. Naturh. Foren.* **139**, 337–396.

Andersen, N. M. (1977). Fine structure of the body hair layers and morphology of the spiracles of semiaquatic bugs in relation to life on the water surface. *Vidensk. Meddr. Dansk. Naturh. Foren.* **140**, 7–37.

Andersen, N. M. (1982). *The Semiaquatic Bugs (Hemiptera, Gerromorpha): Phylogeny, Adaptations, Biogeography and Classification*. Klampenborg, Denmark: Scandinavian Science Press Ltd.

Andersen, N. M. and Cheng, L. (2004). Marine insect halobates (heteroptera: Gerridae): biology, adaptations, distribution, and phylogeny. *Oceanog. Mar. Biol. Annu. Rev.* **42**, 119–180.

Andersen, N. M. and Polhemus, J. T. (1976). Water-striders (Hemiptera: Gerridae, Veliidae, etc.). In: *Marine Insects* (ed. Cheng, L.), pp. 187–224. Amsterdam: North Holland Publication Co.

Aristoff, J. and Bush, J. W. M. (2008). Water entry of small hydrophobic bodies. *J. Fluid Mech*. submitted.
Aston, D. E. and Berg, J. C. (2001). Quantitative analysis of fluid-interface-atomic force microscopy (FI-AFM). *J. Coll. Interf. Sci.* **235**, 162–169.
Autumn, K., Sitti, M., Liang, Y. A., Peattie, A. M., Hansen, W. R., Sponberg, S., Kenny, T. W., Fearing, R., Israelachvili, J. N. and Full, R. J. (2002). Evidence for van der Waals adhesion in gecko setae. *Proc. Natl. Acad. Sci. USA* **99**, 12252–12256.
Bartell, F. E., Purcell, W. R. and Dodd, C. G. (1948). The measurement of effective pore size and of the water-repellency of tightly woven textiles. *Discuss Faraday Soc.* **3**, 257–264.
Barthlott, W. and Neinhuis, C. (1997). Purity of the sacred lotus, or escape from contamination in biological surfaces. *Planta* **202**, 1–8.
Barthlott, W., Riede, K. and Wolter, M. (1994). Mimicry and ultrastructural analogy between the semi-aquatic grasshopper *Paulina acuminata* (Arthropoda; Pauliniidae) and its foodplant, the water-fern *Salvinia auriculata* (Filicatae; Salviniaceae). *Amazoniana*, 47–58.
Bartolo, D., Bouamrirene, F., Verneuil, E., Beguin, A., Silberzan, P. and Moulinet, S. (2006). Bouncing or sticky droplets: impalement transitions on super-hydrophobic micropatterned surfaces. *Europhys. Lett.* **74**, 299–305.
Baudoin, R. (1955). La physico-chimie des surfaces dans la vie des Arthropodes aeriens des miroirs d'eau, des rivages marins et lacustres et de la zone intercotidale. *Bull. Biol. Fr. Belg.* **89**, 16–164.
Baudoin, R. (1976). Les insectes vivant a la surface et au sein des eaux. *Grassé Trait'e de Zool.* **8**, 843–926.
Beament, J. W. L. (1945). The cuticular lipoids of insects. *J. Exp. Biol.* **21**, 115–131.
Beament, J. W. L. (1948). The role of wax layers in the waterproofing of insect cuticle and egg-shell. *Discuss Faraday Soc.* **3**, 177–182.
Bechert, D. W., Bruse, M., Hage, W. and Meyer, R. (2000). Fluid mechanics of biological surfaces and their technological application. *Naturwissenschaften* **87**, 157–171.
Bergmann, R., van der Meer, D., Stijnman, M., Sandtke, M., Prosperetti, A. and Lohse, D. (2006). Giant bubble pinch-off. *Phys. Rev. Lett.* **96**, 154505 (4 pages).
Bico, J., Marzolin, C. and Quèrè, D. (1999). Pearl drops. *Europhys. Lett.* **47**, 220–226.
Bico, J., Roman, B., Moulin, L. and Boudaoud, A. (2004). Elastocapillary coalescence in wet hair. *Nature* **432**, 690.
Bico, J., Thiele, U. and Quere, D. (2002). Wetting of textured surfaces. *Colloids Surf. A* **206**, 41–46.
Bico, J., Tordeux, C. and Quère, D. (2001). Rough wetting. *Europhys. Lett.* **55**, 214–220.
Blomquist, G. J. and Jackson, L. L. (1979). Chemistry and biochemistry of insect waxes. *Prog. Lipid Res.* **17**, 319–345.
Blossey, R. (2003). Self-cleaning surfaces – virtual realities. *Nat. Mater.* **2**, 301–306.
Breton, P. (1999). From microns to nanometers: early landmarks in the science of scanning electron microscope imaging. *Scanning Microsc.* **13**, 1–6.
Brocher, F. (1909). Recherches sur la respiration des insectes aquatiques adultes. Les Dyticidés. *Ann. Biol. Lacustre* **4**, 383–398.
Brocher, F. (1910). Les phénomènes capillaires, leur importance dans la biologie aquatique. *Ann. Biol. Lacustre* **4**, 89–139.
Brocher, F. (1912a). Recherches sur la respiration des insectes aquatiques adultes. Les Elmides. *Ann. Biol. Lacustre* **5**, 136–179.

Brocher, F. (1912b). Recherches sur la respiration des insectes aquatiques adultes. Les Haemonia. *Ann. Biol. Lacustre* **5**, 5–26.
Brocher, F. (1912c). Recherches sur la respiration des insectes aquatiques adultes. L'Hydrophile. *Ann. Biol. Lacustre* **5**, 220–258.
Brocher, F. (1914). Recherches sur la respiration des insectes aquatiques adultes. Les Dyticidés (2me article), suivi d'une notice sur les mouvements respiratoires de l'Hydrophile. *Ann. Biol. Lacustre* **7**, 5–39.
Brown, H. P. (1966). Effects of soap pollution upon stream invertebrates. *Trans. Am. Microsc. Soc.* **85**, 167.
Brown, H. P. (1987). Biology of riffle beetles. *Annu. Rev. Entomol.* **32**, 253–273.
Bush, J. W. M. and Hu, D. L. (2006). Walking on water: Biolocomotion at the interface. *Ann. Rev. Fluid Mech.* **38**, 339–369.
Bush, J. W. M. and Prakash, M. (2007). Propulsion by directional adhesion. Submitted for publication.
Bushnell, D. M. and Moore, K. J. (1991). Drag reduction in nature. *Annu. Rev. Fluid Mech.* **23**, 65–79.
Callies, M. and Quéré, D. (2005). On water repellency. *Soft matter* **1**, 55–61.
Cape, J. N. (1983). Contact angles of water droplets on needles of Scots pine (*Pinus sylvestris*) growing in polluted atmospheres. *New Phytol.* **93**, 293–299.
Carbone, G. and Mangialardi, L. (2005). Hydrophobic properties of a wavy rough substrate. *Eur. Phys. J. E* **16**, 67–76.
Cassie, A. B. D. (1944). Physics and textiles. *Rep. Prog. Phys.* **10**, 141–171.
Cassie, A. B. D. (1948). Contact angles. *Discuss Faraday Soc.* **3**, 11–16.
Cassie, A. B. D. and Baxter, S. (1945). Large contact angles of plant and animal surfaces. *Nature* **155**, 21–22.
Chan, D. Y. C., Henry, J. D. J. and White, L. R. (1981). The interaction of colloidal particles collected at fluid interfaces. *J. Coll. Interf. Sci.* **79** (2), 410–418.
Chaui-Berlinck, J. G., Bicudo, J. E. and Monteiro, L. H. (2001). The oxygen gain of diving insects. *Respir. Physiol.* **128**, 229–233.
Cheng, L. (1973). Marine and freshwater skaters: differences in surface fine structures. *Nature* **42**, 119–180.
Cheng, Y.-T. and Rodak, D. E. (2005). Is the lotus leaf superhydrophobic? *Appl. Phys. Lett.* **86**, 144101–144103.
Choi, C.-H. and Kim, C.-J. (2006). Large slip of aqueous liquid flow over a nanoengineered superhydrophobic surface. *Phys. Rev. Lett.* **96**, 066001.
Choi, C.-H., Ulmanella, U., Kim, J., Ho, C.-M. and Kim, C.-J. (2006). Effective slip and friction reduction in nanograted superhydrophobic microchannels. *Phys. Fluids* **18**, 087105.
Choi, K. S., Prasad, K. K. and Truong, T. V. (1996). *Emerging Techniques in Drag Reduction*. London: Mechanical Engineering Publication Ltd.
Comstock, J. H. (1887). Note on the respiration of aquatic bugs. *Amer. Nat.* **21**, 577–578.
Cottin-Bizonne, C., Barrat, J. L., Bocquet, L. and Charlaix, E. (2003). Low-friction flows of liquid at nanopatterned interfaces. *Nat. Mater.* **2**, 237–240.
Craig, S. and Beaton, C. D. (1996). A simple cryo-SEM method for delicate plant tissues. *J. Microsc.* **182**, 102–105.
Crandall, S. H., Dahl, N. C. and Lardner, T. J. (1978). *An Introduction to the Mechanics of Solids*. New York: McGraw-Hill, Inc.
Crisp, D. J. (1950). The stability of structures at a fluid interface. *Trans. Faraday Soc.* **46**, 228–235.
Crisp, D. J. and Thorpe, W. H. (1948). The water-protecting properties of insect hairs. *Discuss Faraday Soc.* **3**, 210–220.
Daniel, T. L. (1984). Unsteady aspects of aquatic locomotion. *Am. Zool.* **24**, 121–134.

Dechant, H. E., Rammerstorfer, F. and Barth, F. (2001). Arthropod touch reception: stimulus transformation and finite element model of spider tactile hairs. *J. Comp. Physiol. A* **187**, 313–322.
De Gennes, P. G. (1985). Wetting: statics and dynamics. *Rev. Mod. Phys.* **57**, 827–863.
De Gennes, P. G., Brochard-Wyart, F. and Quéré, D. (2003). *Capillarity and Wetting Phenomena: Drops, Bubbles, Pearls and Waves*. Berlin: Springer.
Dettre, R. H. and Johnson, R. E. (1964). Contact angle hysteresis II. Contact angle measurements on rough surfaces. In: *Contact Angle, Wettability, and Adhesion* (ed. Fowkes, F. M.) Advances in Chemistry Series, Vol. 43, pp. 136–144. Washington, DC: American Chemical Society.
Dogs, W. (1908). Metamorphose der respirationsorgane bein *Nepa cinera*. *Mitth. Natur. Ver Neuv.* **40**, 1–55.
Donald, A. M. (2002). No need to dry – environmental scanning electron microscopy of hydrated system. *Mater. Res. Soc. Symp. Proc* **711**, 93–100.
Donald, A. M. (2003). The use of environmental scanning electron microscopy for imaging wet and insulating materials. *Nat. Mater.* **2**, 511–516.
Duez, C., Ybert, C., Clanet, C. and Bocquet, L. (2007). Making a splash with water repellency. *Nat. Phys.* **3**, 180–183.
Dufour, L. (1833). *Recherches Anatomiques et Physiologiques sur les Hémiptères, Accompagnées de Considèrations Relatives à l'Histoire Naturelle et à la Classification de ces Insectes*, pp. 68–74. Paris: Impr. de Bachelier, extrait des Mémoires des savans étrangers, tome IV.
Dussan, E. B. (1979). On the spreading of liquids on solid surfaces: static and dynamic contact lines. *Annu. Rev. Fluid Mech.* **11**, 371–400.
Dussan, E. B. and Chow, R. T. (1983). On the ability of drops or bubbles to stick to non-horizontal surfaces of solids. *J. Fluid Mech.* **137**, 1–29.
Dutrochet, M. H. (1837). *Memoires pour Servir à l'Histoire Anatomique et Physiologique des Végétaux et des Animaux: Du Mécanisme de la Respiration des Insectes*, pp. 486–491. Paris: Chez J.-B. Bailliére.
Dyck, J. (1985). The evolution of feathers. *Zool. Scripta* **14**, 137–154.
Ege, R. (1915). On the respiratory function of the air stores carried by some aquatic insects. *Z. Allg. Physiol.* **17**, 81.
Elkhyat, A., Courderot-Masuyer, C., Gharbi, T. and Humbert, P. (2004). Influence of the hydrophobic and hydrophilic characteristics of sliding and slider surfaces on friction coefficient: *in vivo* human skin friction comparison. *Skin Res. Tech.* **10**, 215221.
Elowson, A. M. (1984). Spread-wing postures and the water repellency of feathers: a test of Rijke's hypothesis. *Auk* **101**, 371–383.
English, L. L. (1928). Some properties of oil emulsions influencing insecticidal efficiency. *Bull. Ill. Nat. Hist. Surv.* **17**, 233–259.
Extrand, C. W. (2002). Model for contact angles and hysteresis on rough and ultraphobic surfaces. *Langmuir* **18**, 7991–7999.
Extrand, C. W. (2003). Contact angles and hysteresis on surfaces with chemically heterogeneous islands. *Langmuir* **19**, 3793–3796.
Extrand, C. W. (2004). Criteria for ultralyophobic surfaces. *Langmuir* **20**, 5013–5018.
Extrand, C. W. (2006). Designing for optimum liquid repellency. *Langmuir* **22**, 1711–1714.
Extrand, C. W. and Gent, A. (1990). Retention of liquid drops by solid surfaces. *J. Coll. Interf. Sci.* **138**, 431–442.
Extrand, C. W. and Kumagai, Y. (1995). Liquid drop on an inclined plane: the relation between contact angles, drop shape, and retentive force. *J. Coll. Interf. Sci.* **170**, 515–521.

Farrell, B. and Mitter, C. (1990). Phylogenesis of insect/plant interactions: have Phyllobrotica leaf beetles (Chrysomelidae) and the Lamiales diversified in parallel? *Evolution* **44**, 1389–1403.

Feng, L., Song, Y., Zhai, J., Liu, B., Xu, J., Jiang, L. and Zhu, D. (2003). Creation of a superhydrophobic surface from an amphiphilic polymer. *Adv. Mater.* **42**, 42–44.

Feng, X., Li, S., Li, Y., Li, H., Zhang, L., Zhai, J., Song, Y., Liu, B., Jiang, L. and Zhu, D. (2002). Super-hydrophobic surfaces: from natural to artificial. *Adv. Mater.* **14**, 1857–1860.

Feng, X.-Q., Gao, X., Wu, Z., Jiang, L. and Zheng, Q.-S. (2007). Superior water repellency of water strider legs with hierarchical structures: experiments and analysis. *Langmuir* **23** (9), 4892–4896.

Feng, X.-Q. and Jiang, L. (2006). Design and creation of superwetting/antiwetting surfaces. *Adv. Mater.* **18**, 3063–3078.

Fish, F. E. (1984). Mechanics, power output and efficiency of the swimming muskrat (*Ondatra zibethicus*). *J. Exp. Biol.* **110**, 183–201.

Fish, F. E. (1998). Imaginative solutions by marine organisms for drag reduction. In: *Proceedings of the International Symposium On Seawater Drag Reduction* (ed. Meng, J. C. S.), pp. 443–450. Arlington, VA: Office of Naval Research, Newport, Rhode Island.

Fish, F. E. (2006). The myth and reality of Gray's paradox: implication of dolphin drag reduction for technology. *Bioinsp. Biomim.* **1**, R17–R25.

Fish, F. E. and Baudinette, R. V. (1999). Energetics of locomotion by the Australian water rat (*Hydromys chrysogaster*): a comparison of swimming and running in a semi-aquatic mammal. *J. Exp. Biol.* **202**, 353–363.

Fish, F. E., Baudinette, R. V., Frappel, P. B. and Sarre, M. P. (1997). Energetics of swimming by the platypus *Ornithorhynchus*: metabolic effort associated with rowing. *J. Exp. Biol.* **200**, 2647–2652.

Fish, F. E., Smelstoys, J., Baudinette, R. V. and Reynolds, P. S. (2002). Fur does not fly, it floats: buoyancy of pelage in semi-aquatic mammals. *Aquat. Mamm.* **28**, 103–112.

Flynn, M. R. and Bush, J. W. M. (2008). Underwater breathing. *J. Fluid Mech.* Submitted.

Fogg, G. E. (1948). Adhesion of water to the external surfaces of leaves. *Faraday Disc. Chem. Soc.* **3**, 162–166.

Furstner, R., Barthlott, W., Neinhuis, C. and Walzel, P. (2005). Wetting and self-cleaning properties of artificial superhydrophobic surfaces. *Langmuir* **21**, 956–961.

Gao, L. and McCarthy, T. J. (2006). A perfectly hydrophobic surface ($\theta_a/\theta_r = 180^\circ/180^\circ$). *J. Am. Chem. Soc.* **128**, 9052–9053.

Gao, L. and McCarthy, T. J. (2007). How Wenzel and Cassie were wrong. *Langmuir* **23**, 3762–3765.

Gao, X. and Jiang, L. (2004). Water-repellent legs of water striders. *Nature* **432**, 36.

Gifford, W. A. and Scriven, L. E. (1971). On the attraction of floating particles. *Chem. Eng. Sci.* **26**, 287–297.

Gittelman, S. H. (1975). Physical gill efficiency and winter dormancy in pigmy backswimmer, *Neoplea striola* (Hemiptera: Pleidae). *Ann. Entomol. Soc. Amer.* **68**, 1011–1017.

Glasheen, J. W. and McMahon, T. A. (1996a). A hydrodynamic model of locomotion in the basilisk lizard. *Nature* **380**, 340–342.

Glasheen, J. W. and McMahon, T. A. (1996b). Size dependence of water-running ability in basilisk lizards *Basiliscus basiliscus*. *J. Exp. Biol.* **199**, 2611–2618.

Glasheen, J. W. and McMahon, T. A. (1996c). Vertical water entry of disks at low Froude numbers. *Phys. Fluids* **8**, 2078–2083.
Gorb, N. S. (1998). The design of the fly adhesive pad: distal tenent setae are adapted to the delivery of an adhesive secretion. *Proc. R. Soc. Lond. B* **265**, 747–752.
Gorb, N. S. (2008). Chapter in this issue. *Adv. Insect Physiol.*
Grant T. (1995). *The platypus: a unique mammal*. Sidney: University of New SouthWales Press Ltd.
Gryzbowski, B. A., Bowden, N., Arias, F., Yang, H. and Whitesides, G. M. (2001). Modeling of menisci and capillary forces from the millimeter to the micrometer size. *J. Phys. Chem. B* **105**, 404–412.
Gu, Z. Z., Uetsuka, H., Takahashi, K., Nakajima, R., Onishi, H., Fujishima, A. and Sato, O. (2003). Structural color and the lotus effect. *Angew. Chem. Int. Ed.* **42**, 894–899.
Hadley, N. F. (1978). Cuticular permeability of desert tenebrionid beetles: correlations with epicuticular hydrocarbon composition. *Insect Biochem.* **8**, 17–22.
Hadley, N. F. (1979). Wax secretion and color phases of the desert tenebrionid beetle *Cryptoglossa verrucosa* (LeConte). *Science* **293**, 367–369.
Hadley, N. F. (1981). Cuticular lipids of terrestrial plants and arthropods: a comparison of their structure, composition, and waterproofing function. *Biol. Rev.* **56**, 23–47.
Hagemann, J. (1910). Beitrige zur kenntnis von corixa. *Zool. Jahrb. Abt. Anat. Ontog. Tiere.* **30**, 373–2685.
Harpster, H. T. (1944). The gaseous plastron as a respiratory mechanism in *Stenelmis quadrimaculata* Horn (Dryopidae). *Trans. Amer. Micro. Soc.* **63**, 1–26.
Hazlett, R. D. (1990). Fractal applications: wettability and contact angle. *J. Coll. Interf. Sci.* **137**, 527–533.
Hebets, E. A. and Chapman, R. F. (2000). Surviving the flood: plastron respiration in the nontracheate arthropod *Phrynus marginemaculatus* (Amblypygi; Arachnida). *J. Insect Physiol.* **46**, 13–19.
Heckman, C. W. (1983). Comparative morphology of arthropod exterior surfaces with the capability of binding a film of air underwater. *Int. Revue. Ges. Hydrobiol.* **68**, 715–736.
Herminghaus, S. (2000). Roughness-induced non-wetting. *Europhys. Lett.* **52**, 165–170.
Hinton, H. E. (1969). Respiratory systems of insect egg shells. *Annu. Rev. Entomol.* **14**, 343–368.
Hinton, H. E. (1976). Plastron respiration in bugs and beetles. *J. Insect Physiol.* **22**, 1529–1550.
Hinton, H. E. and Jarman, G. M. (1976). A diffusion equation for tapered plastrons. *J. Insect Physiol.* **22**, 1263–1265.
Holdgate, M. W. (1955). The wetting of insect cuticle by water. *J. Exp. Biol.* **32**, 591–617.
Holloway, P. J. (1970). Surface factors affecting the wetting of leaves. *Pestic. Sci.* **1**, 156–163.
Hoppe, J. (1911). Die atmung von Notoencta glauca. *Zool. Jb. Abt. Allg. Zoo.* **31**, 189–244.
Hoskins, W. M. (1940). Recent contributions of insect physiology to insect toxicology and control. *Hilgardia* **13**, 307–386.
Howard, R. W. (1993). Cuticular hydrocarbons and chemical communication in insect lipids. In: *Insect Lipids: Chemistry, Biochemistry, and Biology* (eds Stanley-Samuelson, D. W. and Nelson, D. R.), pp. 179–226. Lincoln, NE: University of Nebraska Press.

Hu, D. L. and Bush, J. W. M. (2005). Meniscus-climbing insects. *Nature* **437**, 733–736.
Hu, D. L. and Bush, J. W. M. (2008a). The hydrodynamics of water-walking arthropods: Part 1. Experiments. *J. Fluid Mech.* To be submitted.
Hu, D. L. and Bush, J. W. M. (2008b). The hydrodynamics of water-walking arthropods: Part 2. Theory. *J. Fluid Mech*. To be submitted.
Hu, D. L., Chan, B. and Bush, J. W. M. (2003). The hydrodynamics of water strider locomotion. *Nature* **424**, 663–666.
Hungerford, H. B. (1919). The biology and ecology of aquatic and semiaquatic Hemiptera. *Kans. Univ. Sci. Bull.* **11**, 1–328.
Hurst, H. (1941). Insect cuticle as an asymmetrical membrane. *Nature* **147**, 388.
Hurst, H. (1948). Asymmetrical behaviour of insect cuticle in relation to water permeability. *Disc. Faraday. Soc.* **3**, 193–210.
Imms, A. D. (1906). *Anurida (a springtail). LMBC Mem. XIII Typical British Marine Plants and Animals*. London: Williams & Norgate.
Israelachvili, J. (1992). *Intermolecular and Surface Forces*, 2nd edn New York: Academic Press.
Janssens, F. (2005). Checklist of the Collembola of the world: Note on the morphology and origin of the foot of the Collembola. http://www.Collembola.org/publicat/unguis.htm
Jenkins, L. and Donald, A. (1999). Condensation of water droplets onto individual fibres for contact angle measurement in the ESEM. *Langmuir* **15**, 7829–7835.
Joanny, J. F. and de Gennes, P. G. (1984). A model for contact angle hysteresis. *J. Chem. Phys.* **81**, 552–562.
Johansson, L. C. and Norber, U. M. L. (2001). Lift-based paddling in diving grebe. *J. Exp. Biol.* **240**, 1687–1696.
Johnson, R. E. and Dettre, R. H. (1964). Contact angle hysteresis I. Study of an idealized rough surface. In: *Contact Angle, Wettability, and Adhesion* (ed. Fowkes, F. M.), Advances in Chemistry Series, Vol. 43, pp. 112–135. Washington, DC: American Chemical Society.
Joseph, P., Cottin-Bizonne, C., Benoît, J. M., Ybert, C., Journet, C., Tabeling, P. and Bocquet, L. (2006). Slippage of water past superhydrophobic carbon nanotube forests in microchannels. *Phys. Rev. Lett.* **97**, 156104.
Journet, C., Moulinet, S., Ybert, C., Purcell, S. T. and Bocquet, L. (2005). Contact angle measurements on superhydrophobic carbon nanotube forests: effect of fluid pressure. *Europhys. Lett.* **71**, 104–109.
Kellen, W. R. (1956). Notes on the biology of *Halovelia marianarum* Usinger in Samoa (Veliidae: Heteroptera). *Ann. Entomol. Soc. Am.* **52**, 53–62.
Keller, J. B. (1998). Surface tension force on a partly submerged body. *Phys. Fluids* **10**, 3009–3010.
Kim, H.-Y. and Mahadevan, L. (2006). Capillary rise between elastic sheets. *J. Fluid Mech.* **548**, 141–150.
Knoll, M. (1935). Aufladepotentiel und sekundäremission elektronenbestrahlter körper. *Z. Tech. Phys.* **16**, 467–475.
Kousik, G., Pitchumani, S. and Renganathan, N. G. (2001). Electrochemical characterization of polythiophene-coated steel. *Prog. Org. Coat.* **43**, 286.
Kovac, D. and Maschwitz, U. (1999). Protection of hydrofuge respiratory structures against detrimental microbiotic growth by terrestrial grooming in water beetles. *Entomol. Gen.* **24**, 277–292.
Kralchevsky, P. A. and Denkov, N. D. (2001). Capillary forces and structuring in layers of colloid particles. *Curr. Opin. Coll. Interf. Sci.* **6**, 383–401.

Krantz, G. W. and Baker, G. T. (1982). Observations on the plastron mechanism of *Hydrozetes* sp. (Acari: Oribatida: Hydrozetidae). *Acarologia* **23**, 273–277.
Krivosheina, M. G. (2005). The plastron is a universal structure that ensures breathing of dipteran larvae both in the water and in the air. *Doklady Bio. Sci.* **401**, 112–115.
Kühnelt, W. (1928). Über den bau des insektenskelettes. *Zool. Jb. (Anat.)* **50**, 219–278.
Lafuma, A. and Quéré, D. (2003). Superhydrophobic states. *Nat. Mater.* **2**, 457–460.
Lamoral, B. H. (1968). On the ecology and habitat adaptations of two intertidal spiders, *Desis formidabilis* and *Amaurobioides africanus* Hewitt at 'The Island' (Kommetjie, Cape Peninsula), with notes on the occurrence of two other spiders. *Ann. Natal. Mus.* **20**, 151–193.
Lau, K., Bico, J., Teo, K., Milne, W., McKinley, G. and Gleason, K. (2003). Superhydrophobic carbon nanotube forest. *Nano Lett.* **3**, 1701–1705.
Lauga, E. and Brenner, M. P. (2004). Evaporation-driven assembly of colloidal particles. *Phys. Rev. Lett.* **93**, 238–301.
Lee, W., Jin, M. K., Yoo, W. C. and Lee, J. K. (2004). Nanostructuring of a polymeric substrate with well-defined nanometer-scale topography and tailored surface wettability. *Langmuir* **20**, 7665–7669.
Liew, K. M., Wong, C. H. and Tan, M. J. (2005). Buckling properties of carbon nanotube bundles. *Appl. Phys. Lett.* **87**, 041901.
Liu, H., Zhai, J. and Jiang, L. (2006). Wetting and anti-wetting on aligned carbon nanotube films. *Soft Matter.* **2**, 811–821.
Lodge, R. A. and Bhushan, B. (2006). Wetting properties of human hair by means of dynamic contact angle measurement. *J. Appl. Polymer Sci.* **102**, 5255–5265.
Lou, S.-T., Ouyang, Z.-Q., Zhang, Y., Li, X.-J., Hu, J., Li, M.-Q. and Yang, F.-J. (2000). Nanobubbles on solid surface imaged by atomic force microscopy. *J. Vac. Sci. Technol. B* **18**, 2573–2575.
Manoharan, V. N., Elsesser, M. T. and Pine, D. J. (2003). Dense packing and symmetry in small clusters of microspheres. *Science* **301**, 483–487.
Mansfield, E. H., Sepangi, H. R. and Eastwood, E. A. (1997). Equilibrium and mutual attraction or repulsion of objects supported by surface tension. *Philos. Trans. R. Soc. Lond. Ser. A* **355**, 869–919.
Matsuda, K., Watanabe, S. and Eiju, T. (1985). Real-time measurement of large liquid surface deformation using a holographic shearing interferometer. *Appl. Optics.* **24** (24), 4443–4447.
McHale, G., Aqil, S., Shirtcliffe, N. J., Newton, M. I. and Erbil, H. Y. (2005). Analysis of droplet evaporation on a superhydrophobic surface. *Langmuir* **21**, 11053–11060.
McMahon, T. A. and Bonner, J. T. (1985). *On Size and Life*, p. 211. New York: Scientific American Library.
Miller, P. L. (1964). Possible function of haemoglobin in *Anisops*. *Nature* **201**, 1052.
Min, T. and Kim, J. (2004). Effects of hydrophobic surfaces on skin-friction drag. *Phys. Fluids* **16**, 55–58.
Minsky, M. (1953). Neural-analog networks and the brain-model problem. Ph.D. thesis, Princeton University Press, Princeton, NJ.
Minsky, M. (1988). Memoir on inventing the confocal scanning microscope. *Scanning* **10**, 128–138.
Miyamoto, S. (1955). On a special mode of locomotion utilizing surface tension at the water-edge in some semiaquatic insects. *Kontyû* **23**, 45–52.

Mock, U., Förster, R., Menz, W. and Rühe, J. (2005). Towards ultrahydrophobic surfaces: a biomimetic approach. *J. Phys.: Condens. Mat.* **17**, S639–S648.
Moore, W. (1921). Spreading and adherence of arsenical sprays. *Minnesota Agric. Exp. Sta. Tech. Bull.* **2**, 1–50.
Mordvinov, Y. E. (1976). Locomotion in water and the indices of effectiveness of propelling systems for some aquatic mammals. *Zool. Zh.* **55**, 1375–1382. (in Russian).
Nadkarni, G. and Garoff, S. (1992). An investigation of microscopic aspects of contact angle hysteresis: pinning of the contact line on a single defect. *Europhys. Lett.* **20**, 523.
Neinhuis, C. and Barthlott, W. (1997). Characterization and distribution of water-repellent, self-cleaning plant surfaces. *Ann. Bot.* **79**, 667–677.
Nicolson, M. M. (1949). The interaction between floating particles. *Proc. Camb. Phil. Soc.* **45**, 288–295.
Noble-Nesbitt, J. (1963). Transpiration in *Podura aquatica* L. (Collembola, Isotomidae) and the wetting properties of its cuticle. *J. Exp. Biol.* **40**, 681–700.
Nutman, S. (1941). The function of the ventral tube in *Onychiurus armatus* (Collembola). *Nature* **148**, 168–169.
O'Kane, W. C., Westgate, W. A., Glover, L. C. and Lowry, P. R. (1932). Studies of contact insecticides. V. The performance of certain contact agents on various insects. *Tech. Bull. NH Agric. Exp. Sta.* **51**, 1–20.
Oliver, J. F., Huh, C. and Mason, S. G. (1977). Resistance to spreading of liquids by sharp edges. *J. Colloid Interf. Sci.* **59**, 568–581.
Onda, T., Shibuichi, S., Satoh, N. and Tsujii, K. (1996). Super-water-repellent fractal surfaces. *Langmuir* **12**, 2125–2127.
Öner, D. and McKarthy, T. J. (2000). Ultrahydrophobic surfaces. Effects of topography length scales on wettability. *Langmuir* **16**, 7777–7782.
Otten, A. and Herminghaus, S. (2004). How plants keep dry: a physicist's point of view. *Langmuir* **20**, 2405–2408.
Ou, J., Perot, B. and Rothstein, J. P. (2004). Laminar drag reduction in micro-channels using ultrahydrophobic surfaces. *Phys. Fluids* **16**, 4635–4643.
Pal, R. (1951). The wetting of insect cuticle. *Bull. Ent. Res.* **51**, 121–139.
Parker, A. R. and Lawrence, C. R. (2001). Water capture by a desert beetle. *Nature* **414**, 33–34.
Patankar, N. A. (2004). Transition between superhydrophobic states on rough surfaces. *Langmuir* **20**, 7097–7102.
Perez-Goodwyn, P. and Fujisaki, K. (2007). Sexual conflicts, loss of flight, and fitness gains in locomotion of polymorphic water striders (*Gerridae*). *Entomol. Exper. Appli.* In press.
Perez-Goodwyn, P. J. (2007). *Functional surfaces in biology,* chap. Anti-wetting surfaces in Heteroptera (Insecta): Hairy solutions to any problem. Dordrecht: Springer. In press.
Persson, B. (2003). On the mechanism of adhesion in biological systems. *J. Chem. Phys.* **118**, 7614–7621.
Philip, G. D., Matthews, D. and Seymour, R. S. (2006). Diving insects boost their buoyancy bubbles. *Nature* **441**, 171.
Pike, N., Richard, D., Foster, W. A. and Mahadevan, L. (2002). How aphids lose their marbles. *Proc. R. Soc. Lond. B* **269**, 1211–1215.
Plateau, J. (1873). *Statique Expérimentale et Théorique des Liquides Soumis aux Seules Forces Moléculaires*. Paris: Gauthier-Villars.
Quéré, D. (2002). Fakir droplets. *Nat. Mater.* **1**, 1415.

Rabinovich, Y. I., Esayanur, M. S. and Moudgil, B. M. (2005). Capillary forces between two spheres with a fixed volume liquid bridge: theory and experiment. *Langmuir* **21**, 10992–10997.
Rahn, H. and Paganelli, C. V. (1968). Gas exchange in gas gills of diving insects. *Respir. Physiol.* **5**, 145–164.
Rayleigh, L. (1879). On the instability of jets. *Proc. Lond. Math. Soc.* **10**, 413.
Reimer, L. (1998). *Scanning Electron Microscopy: Physics of Image Formation and Microanalysis*. Berlin: Springer.
Reyssat, M., Pépin, A., Marty, F., Chen, Y. and Quéré, D. (2006). Bouncing transitions in microtextured materials. *Europhys. Lett.* **74**, 306–312.
Ribak, G., Weihs, D. and Arad, Z. (2005). Water retention in the plumage of diving great cormorants *Phalacrocorax carbo sinensis*. *J. Avian Biol.* **36**, 89–95.
Rijke, A. M. (1970). Wettability and phylogenetic development of feather structure in water birds. *J. Exp. Biol.* **52**, 469–479.
Ross, S. and Becher, P. (1992). The history of the spreading coefficient. *J. Colloid Int. Sci.* **149**, 575–579.
Rovner, J. S. (1986). Spider hairiness: air stores and low activity enhance flooding survival in inland terrestrial species. In: *Acta X International Congress of Arachnology Jaca/Espana*, 123–129.
Rowlinson, J. S. and Widom, B. (1982). *Molecular Theory of Capillarity*. Mineola, New York: Dover Publications, Inc.
de Ruiter, L., Wolvekamp, H. P. and van Tooren, A. J. (1951). Experiments on the respiration of some aquatic insects (*Hydrous piceus* L., *Naucoris cimicoides* L., and *Notonecta glauca* L.). *Acta Physiol. et Pharmacol. Neerl.* **1**, 657–659.
Sabbatovskii, K. G., Dutschk, V., Nitschke, M. and Grundke, F. S. K. (2004). Properties of the teflon AF1601S surface treated with the low-pressure argon plasma. *Colloid J.* **66**, 208–215.
Saliternik, Z. (1942). The macroscopic differentiation of anopheline eggs according to their pattern on the surface of the water. *Bull. Entomol. Res.* **33**, 221.
Schildknecht, H. (1976). Chemical ecology — a chapter of modern natural products chemistry. *Angew. Chem. Int. Ed. Engl.* **15**, 214–222.
Scriven, L. E. and Sternling, C. V. (1970). The Marangoni effects. *Nature* **187**, 186–188.
Shirtcliffe, N. J., McHale, G., Newton, M. I., Perry, C. C. and Pyatt, F. B. (2006). Plastron properties of a superhydrophobic surface. *Appl. Phys. Lett.* **89**, 104–106 (2 pages).
Shuttleworth, R. and Bailey, G. L. (1948). Spreading of a liquid over a rough solid. *Disc. Faraday Soc.* **3**, 16–22.
Silberglied, R. and Aiello, A. (1980). Camouflage by integumentary wetting in bark bugs. *Science* **207**, 773–775.
Slodowska, A., Woźnak, M. and Matlakowska, R. (1999). The method of contact angle measurements and estimation of work of adhesion in bioleaching of metals. *Biol. Proc. Online* **1** (3), 114–121.
Snyder, B. A., Aston, D. E. and Berg, J. C. (1997). Particle-drop interactions examined with an atomic-force microscope. *Langmuir* **13**, 590–593.
Spence, J. R., Spence, D. H. and Scudder, G. G. (1980). Submergence behavior in *Gerris*: underwater basking. *Am. Midl. Nat.* **103**, 385–391.
Steinmann, T., Casas, J., Krijnen, G. and Dangles, O. (2006). Air-flow sensitive hairs: boundary layers in oscillatory flows around arthropods appendages. *J. Exp. Biol.* **209**, 4398–4408.
Stelmashenko, N. A., Craven, J. P., Donald, A. M., Terentjev, E. M. and Thiel, B. L. (2001). Topographic contrast of partially wetting water droplets in environmental scanning electron microscopy. *J. Microsc.* **204**, 172–183.

Stratton, G. E., Suter, R. B. and Miller, P. R. (2004a). Evolution of water surface locomotion by spiders: a comparative approach. *Biol. J. Linn. Soc.* **81** (1), 63–78.

Stratton, G. E., Suter, R. B. and Miller, P. R. (2004b). Taxonomic variation among spiders in the ability to repel water: surface adhesion and hair density. *J. Arachnol.* **32**, 11–21.

Straus-Durckheim, H. (1828). *Considérations générales sur l'anatomie comparée des animaux articulés, auxquels on a joint anatomie descriptive du Hanneton vulgaire (Melolontha vulgaris)*, p. 435. Paris, Strasbourg, Bruxelles: F.G. Levrault.

Stride, G. O. (1955). On the respiration of an aquatic African beetle, *Piotamodytes tuberosus* Hinton. *Ann. Entomol. Soc. Am.* **48**, 344–351.

Taylor, R. L., Verran, J., Lees, G. C. and Ward, A. J. (1998). The influence of substratum topography on bacterial adhesion to polymethyl methacrylate. *J. Mater. Sci. Mater. Med.* **9**, 17–22.

Thibaud, J. M. (1970). Biologie et écologie des Collemboles, Hypogastruidae, édaphiques et Cavernicoles. *Mém. Mus. Natl. Hist. Nat. Nouvelle Sér. A* **61**, 83201.

Thorpe, W. H. (1950). Plastron respiration in aquatic insects. *Biol. Rev.* **25**, 344–390.

Thorpe, W. H. and Crisp, D. J. (1947a). Studies on plastron respiration I. The biology of *Apelocheirus* [Hemiptera, Aphelocheiridae (Naucoridae)] and the mechanism of plastron rentention. *J. Exp. Biol.* **24**, 227–269.

Thorpe, W. H. and Crisp, D. J. (1947b). Studies on plastron respiration II. The respiratory efficiency of the plastron in *Apelocheirus*. *J. Exp. Biol.* **24**, 270–303.

Thorpe, W. H. and Crisp, D. J. (1947c). Studies on plastron respiration III. The orientation responses of *Apelocheirus* [Hemiptera, Aphelocheiridae (Naucoridae)] in relation to plastron respiration; together with an account of specialized pressure receptors in aquatic insects. *J. Exp. Biol.* **24**, 310–328.

Thorpe, W. H. and Crisp, D. J. (1949). Studies on plastron respiration IV: plastron respiration in the Coleoptera. *J. Exp. Biol.* **25** (3), 219–261.

Torre-Bueno, J. R. (1907). On *Rhagovelia obesa* Uhler. *Can. Entomol.* **39**, 61–64.

Vaknin, Y., Gan-Mor, S., Bechar, A., Ronen, B. and Eisikowitch, D. (2000). The role of electrostatic forces in pollination. *Plant Syst. Evol.* **222**, 133–142.

Vella, D., Lee, D.-G. and Kim, H.-Y. (2006a). Sinking of a horizontal cylinder. *Langmuir* **22**, 2972–2974.

Vella, D. and Mahadevan, L. (2005). The "Cheerios effect". *Am. J. Phys.* **73**, 817–825.

Vella, D., Metcalfe, P. D. and Whittaker, R. J. (2006b). Equilibrium conditions for the floating of multiple interfacial objects. *J. Fluid Mech.* **549**, 215–224.

Vincent, J. F. V. and Wegst, U. G. K. (2004). Design and mechanical properties of insect cuticle. *Arthrop. Struct. Dev.* **33**, 187–199.

Vlasblom, G. V. (1970). Respiratory significance of physical gill in some adult insects. *Comp. Biochem. Physiol.* **36**, 377–385.

Vogel, S. (2006). Living in a physical world. VIII. Gravity and life in water. *J. Biosci.* **30** (3), 309–322.

Wagner, P., Furstner, R., Barthlott, W. and Neinhuis, C. (2003). Quantitative assessment to the structural basis of water repellency in natural and technical surfaces. *J. Exp. Bot.* **54**, 1295–1303.

Wagner, P., Neinhuis, C. and Barthlott, W. (1996). Wettability and contaminability of insect wings as a function of their surface sculpture. *Acta Zool.* **77**, 213–225.

Walsh, M. J. (1990). Riblets. In: *Viscous Drag Reduction in Boundary Layers* (eds Bushnell, D. M. and Hefner, J. N.), Progress in Astronautics and Aeronautics,

Vol. 123, pp. 203–261. Washington, DC: American Institute of Aeronautics and Astronautics, Inc.
Walther, P. and Muller, M. (1997). Double-layer coating for field-emission cryo-scanning electron microscopy-present state and applications. *Scanning* **19**, 343–3488.
Wenzel, R. N. (1936). Resistance of solid surfaces to wetting by water. *Ind. Eng. Chem.* **28**, 988–994.
West, T. (1982). The foot of the fly; its structure and action: elucidated by comparison with the feet of other insects. *Trans. Linn. Soc. Lond.* **23**, 393–421.
White, F. M. (1994). *Fluid Mechanics*. New York: McGraw-Hill, Inc.
Whitesides, G. and Grzybowski, B. (2002). Self-assembly at all scales. *Science* **295**, 2418–2421.
Wigglesworth, V. B. (1933). The physiology of the cuticle and of ecdysis in *Rhodnius prolixus* (Triatomidae, Hemiptera); with special reference to the function of the oenocytes and of the dermal glands. *Q. J. Microsc. Sci.* **76**, 269–318.
Wigglesworth, V. B. (1945). Transpiration through the cuticle of insects. *J. Exp. Biol.* **21**, 97–114.
Wigglesworth, V. B. (1950). *The Principles of Insect Physiology*. London: Methuen.
Wigglesworth, V. B. (1979). The physiology of insect cuticle. *Annu. Rev. Entomol.* **2**, 37–54.
Wigglesworth, V. B. (1984). *Insect Physiology*, pp. 1–17. London: Chapman and Hall.
Wilcoxon, F. and Hartzell, A. (1931). Some factors affecting the efficiency of contact pesticides. I. Surface forces as related to wetting and tracheal pentration. *Contr. Boyce. Thompson Inst.* **3**, 1–12.
Wu, C. W., Kong, X. Q. and Wu, D. (2007). Micronanostructures of the scales on a mosquito's legs and their role in weight support. *Phys. Rev. E.* **76**, 017301 (4 pages).
Yi, U.-C. and Kim, C.-J. (2004). Soft printing of droplets pre-metered by electrowetting. *Sens. Actuat. A* **114**, 347354.
Yoshimitsu, Z., Nakajima, A., Watanabe, T. and Hashimoto, K. (2002). Effects of surface structure on the hydrophobicity and sliding behavior of water droplets. *Langmuir* **3**, 5818–5822.
Young, T. (1805). An essay on the cohesion of fluids. *Phil. Trans. Roy. Soc. Lond. A* **95**, 65–87.
Zeng, C., Bissig, H. and Dinsmore, A. D. (2006). Particles on droplets: from fundamental physics to novel materials. *Solid State Comm.* **139**, 547–556.
Zhang, X., Tan, S., Zhao, N., Guo, X., Zhang, X., Zhang, Y. and Xu, J. (2006). Evaporation of sessile water droplets on superhydrophobic natural lotus and biomimetic polymer surfaces. *Chem. Phys. Chem.* **7**, 2067–2070.
Zheng, Y., Gao, X. and Jiang, L. (2007). Directional adhesion of superhydrophobic buttery wings. *Soft Mater.* **3**, 178–182.
Zisman, W. A. (1964). Relation of equilibrium contact angle to liquid and solid constitution. In: *Contact Angle, Wettability and Adhesion; The Kendall Award Symposium Honoring William A. Zisman* (ed. Fowkes, F. M.), Advances in Chemistry Series, Vol. 43, p. 6. Washington, DC: American Chemical Society.